Investigating the effects of spatial confinement on multicellular morphogenesis

Sebastian Vasilis Hadjiantoniou

A thesis submitted to the Faculty of Graduate and Postdoctoral Studies in partial fulfillment of the requirements for the degree of

Doctoral of Philosophy in Biology

Ottawa-Carleton Institute for Biology

University of Ottawa

Ottawa, Canada

January 29th, 2018

ABSTRACT

It has long been established that the physical properties of the cell's surrounding microenvironment has the ability to impose its influence on a range of cell processes. Morphology, differentiation, and proliferation have all been shown to be sensitive to the mechanical cues inherent within the extracellular matrix. Although significant advancements in microfabrication and cell mechanics have been made, questions regarding how physical interactions guide biological systems in three dimensions remain unanswered. By utilizing cocultured systems and microfabricated channeled topographies, we reveal that the three dimensional nature of the environment is capable of driving cell patterning. Contact guidance is the phenomenon by which cells will orient themselves along the geometric patterns of a substrate. Much of its research has focused on the nano/micro scale of two dimensional topographies, affecting alignment along grooves. We have revealed that contact guidance has the ability to impose far more complex cellular behaviour in three dimensional systems. Furthermore, by modulating the elements of confinement surrounding cells, we directed the balance of binding forces between cells and substrate leading to significantly different cell type dependent morphologies. By then altering the geometry of the topography, we revealed the ability to induce cell type separation in cocultured systems. These concepts led to the subsequent discovery that confinement induces three dimensional spheroidal growth of embryonic stem cells. These results reveal that the element of confinement not only influences patterning in three dimensions but guides the fundamental early stages processes essential to all life.

STATEMENT OF ORIGINALITY

I certify that, to the best of my knowledge, the research data and contents of this thesis are entirely original. Any copyrighted material, ideas, techniques or work included in this thesis are fully acknowledged in accordance with the standard referencing practices. Research and manuscript preparation were prepared under the supervision of Dr. Andrew Pelling in the Center for Interdisciplinary Nanophysics Laboratories in the Department of Physics and Biology at the University of Ottawa.

Manuscripts in this thesis

Chapter 4 is an adaptation of:
Hadjiantoniou, S.V., Tahvildari. R., Ignacio, M., Najahi Sohi, Ali., Godin, M., Pelling, A.E. "Exploiting contact guidance to trap cells in three-dimensions" (Manuscript In progress)

Chapter 2 is an adaptation of:
Hadjiantoniou, **S.V**., Leblanc-Latour, M., Ignacio, M., Slater G.W., Pelling, A.E "Spontaneous phase separation of cocultured cell mixtures in vitro." Scientific Reports (2016) (Manuscript ID: SREP-17-47313) (First Revision)

Chapter 5 is an adaptation of:
Hadjiantoniou, **S.V**., Sean. D., Ignacio, M., Godin, M., Slater G.W., Pelling, A.E. "Physical Confinement Signals Regulate the Organization of Stem Cells in Three Dimensions."J Roy Soc Interface, 16, 20160613, (2016)

Chapter 3 is an adaptation of:
Leclerc, A., Tremblay, D., **Hadjiantoniou, S**., Bukoreshtliev, N.V., Rogowski, J.L., Godin, M. & Pelling, A.E. "Three Dimensional Spatial Separation of Cells in Response to Microtopography." Biomaterials 34, 8097, (2013)

Conferences & Workshops:

- Hadjiantoniou, S.V, Pelling. A.E. “The Effects of Confinement on Embryonic Stem Cell Spherogenesis in Engineered Three Dimensional Microenvironments” Ottawa-Carleton Institute Symposium, Ottawa, Ontario, 2014 (Talk)

- Hadjiantoniou, S.V, Pelling, A.E. “Mechanically Induced Embryonic Stem Cell Differentiation” Cell Dynamics Workshop, Keen, Ontario, 2013 (Talk)

- Hadjiantoniou, S.V, Pelling, A.E. “ The Role of Confinement in Embryonic Stem Cell Development”, Cell Dynamics Workshop, Keen, Ontario, 2012 (Poster)

OTHER CONTRIBUTIONS

Whilst completing the research in preparation for this thesis, I have also made contributions towards publications of other members of the Pelling lab and external groups within the physics department (Dr. Ravi Bhardwaj).

Contributions to other manuscripts:

- Haase. K., Macadangdang. J.K.L., Edrington. C.H., Cuerrier. C.M., **Hadjiantoniou. S**., Harden, J.L.. Skerjanc, I.S. & Pelling, A.E. "Extracellular Forces Cause the Nucleus to Deform in a Highly Controlled Anisotropic Manner." Scientific Reports 6, 21300, (2016)

- Alshehri. A., **Hadjiantoniou. S**., Hickey. R., Al-Rekabi. Z., Harden. J., Pelling. A.E., Bhardwaj. R. "Selective Cell Adhesion on Femtosecond Laser Microstructured Polydimethylsiloxane." Biomed Mater 11, 015014, (2016)

- Deepak, K. L. N, Alshehri. A. M., **Hadjiantoniou. S. V.**, Marquez. D., Scaiano. J.C., Pelling. A., and Bhardwaj. V. R., "High Density Data Storage In Transparent Plastics Using Femtosecond Laser Microstructuring." *OSA Publishing*, 7475, (2015)

- **Hadjiantoniou, S.V**, Guolla, L. & Pelling, A.E. "Mechanically Induced Deformation and Strain Dynamics in Actin Stress Fibres." Commun Integr Biol 5, 627, (2012)

STATEMENTS OF CONTRIBUTIONS

I, Sebastian Hadjiantoniou, contributed to the majority of the work performed for the completion of this thesis. This includes cell culture, molecular biology, microfabrication design, microfabrication, confocal microscopy techniques, image and statistical analysis. I have first authored 4 papers, of which three are presented in this thesis (Chapters 2, 4,6) including all revisions. I also co-supervised all undergraduate work performed by Cory Lefevbre and Alex Leclerc in their respective papers.

Fellow lab members and external researchers have also contributed to this work. Professor Andrew Pelling has contributed to the direction and revision of all manuscripts within this thesis (Chapter2-5). Dr. Maxime Ignacio and Dr. David Sean (assisted by Maxime Leblanc-Latour), under supervision of Professor Gary Slater, has significantly contributed to chapters 2 and 4 by modeling the observed biological results into physical simulations. Undergraduate student Alex Leclerc, with the guidance of post-doc student Dominique Trembley performed significant work on the initial discoveries of the patterning phenomenon (Chapter 3) including microfabrication, cell culture and experimental design. Radin Tahvildari, under supervision of Professor Michel Godin, performed microfabrication reflowing techniques to create the elliptical topographies used in Chapter 4. Ryan Hickey performed AFM measurement for durotaxis analysis in Chapter 4.

ACKKNOWLEDGMENTS

It has been a journey. One whose regular turns, occasional obstacles and inevitable cliffs would have never been surmounted had it not been for the undying support of loved ones and peers.

Firstly, I'd like to thank Andrew Pelling, not only for handing me such a life changing opportunity, but for the years of mentorships that have developed my skills as a scientist and a person. He is an incessant reminder of what one can achieve if you fearlessly look past accepted dogma and explore the power of ideas.

To Panos, whose relentless optimism and culinary skills was the perfect counter balance to the many long hours spent in the dungeon (aka microscope room). Most importantly however, he has been a companion with whom I could explore the scientific unknowns of every day life. Our "curiosity" podcast has been the source of my rejuvenated love for science and an accomplishment I hold as dearly as this thesis.

To Max, for expanding my horizons into the world of a physicist's mind, as dangerous as that may be… Our "walk and talks" were often the source of new lines of thought and has undoubtedly been the reason for the discoveries within this thesis. His European flair and charisma always managed to make me feel "at home".

To the entire pelling crew for simply being awesome. No matter where you are or what you're doing, the people you surround yourself with will always make or break the adventure. Except for maybe Dan.

To my brother Alex, who to me serves as the model of what passion, charm and talent can achieve. His support has been the foundation for my survival over the years of which I can't thank him enough.

To Anne, who has been the founding pillar to my academic success. I cannot begin to describe how thankful I am for the endless years of understanding, guidance and support.

A maman, pour qui je ne cesserai jamais de surpasser mes limites pour m'assurer de ta fierté. Mon succès est le resultat de tes efforts implacables. Je t'aime.

Lastly, to my father, whose unquestioned belief in my success expected nothing less. It is because of you, that I am. Let the next chapter begin…

TABLE OF CONTENTS

LIST OF ABBREVIATIONS

- ATP - Adenosine Triphosphate
- CAM - Cellular Adhesion molecule
- DAH - Differential Adhesion Hypothesis
- DMEM - Dulbecco's Modified Eagle's medium
- DMSO - Dimethylsiloxane
- $\in_{cc}$ - Cell-Cell Energy
- $\in_{cs}$ - Cell-Substrate Energy
- EB - Embryoid Body
- ECM - Extracellular Matrix
- ESC - Embryonic Stem cells
- F-actin - Actin filament
- FA - Focal Adhesion
- FAK - Focal Adhesion Kinase
- FBS - Fetal bovine serum
- FC - Focal Complexes
- GAP - GTPase-activating Protein
- GEF - Guanine nucleotide Exchange Factor
- GFP - Green Fluorescent Protein
- ICM - Inner Cell Mass
- IF - Intermediate filament
- I_g - Globular Isotropy
- I_p - Planar Isotropy
- K-S - Kolmogorov-Smirnov
- KMC - Kinetic Monte Carlo
- LIF - Leukemia Inhibitory Factor
- LSCM - Laser Scanning Confocal Microscope
- M - Molar Mass
- MDCK - Madin Darby Canine Kidney
- mESC - Mouse Embryonic Stem Cell
- Mt - Microtubule
- MTOCs - Microtubule Organizing Center
- NIH3T3 - Embryonic Mouse Fibroblast
- Pax - Paxillin
- PBS - Phosphate Buffered Saline
- PDMS - Polydimethylsiloxane
- ROCK - Rho associated protein Kinase
- TX - Triton X-100

LIST OF FIGURES

LIST OF TABLES

CHAPTER 1 | INTRODUCTION

Since the very inception of cell theory and its definition as a single autonomous unit of life, laid the most important observation that started it all, confinement. As Robert Hooke placed a thin slice of cork under the microscope for the very first time he observed compartmentalized spaces, reminding him of the cells of a monastery. Whether it be the cell wall of plant tissue or embryonic stem cells growing within the inner cell mass of the trophoblast, confinement has ubiquitously guided cell morphogenesis. It imposes its influence by altering the physical properties of the surrounding microenvironment. These properties affect the most basic biological mechanisms from paracrine signaling to cellular migration. Like any dynamically responsive system, it possesses sensory modalities capable of transducing and interpreting external information. This cell sensing mechanism is responsible for constantly surveying changes in the local microenvironment such as substrate stiffness, topography and confinement. Interestingly, the former have been and continue to be extensively studied, but the modulating effects of confinement and the methods by which the cells sense remain to be fully elucidated. There are several excellent general reviews on cell sensing, which to some extent reflects the authors' personal research interests and expertise. The following review will explore the anatomy of the cell, the key molecular proteins that permit cell sensing, and the governing mechanisms that influence cell morphogenesis.

1.1 THE CELL, IN A FILAMENT NUTSHELL

To the chemist, the cell is a consortium of interacting peptides contained within an amphipathic lipid bilayer; to the engineer, a flexible semi-permeable vessel containing a heterogeneous liquid mixture; to the physicist, an open system out of equilibrium. The inherent interdisciplinary nature of the cell requires us to expand our definition of what once was simply described as the structural, functional and biological unit of all organisms[1]. In another example of evolution's form fits function, the mammalian cell abides by no single distinct morphology. Instead, depending on the inherent cell type

and its physiological function, it adapts to the vastly different two-dimensional and three-dimensional microenvironments in which it resides[2]. Despite their differences, all cells are supported by a structural network of interlinking filaments, designated as the cytoskeleton[1,3]. Its role is to carry out three main biological functions: to create a structural environment to spatially organize the contents of the cell; to act as the intermediary link between the physical and biochemical stimuli of the external microenvironment; and to orchestrate the synchronous generation of forces that enable cell shape and migration[4].

To achieve this, it consists of three major biopolymers: microtubules (MTs; 25nm), intermediate filaments (IFs; 8–12nm wide) and actin filaments (F-actin; 7nm wide)[4,5]. Between them, it is their mechanical stiffness, their dynamics of assembly, and the molecular motors they interact with[4] that formalize the architecture and function of the cytoskeleton.

As the stiffest, MTs contain two monomer subunits (α,β-tubulin) that assemble in a head-to-tail fashion. As such, the rates of polymerization events that occur to form long protofilament strands are polarized with the "plus end" assembling faster than the "minus end". Thirteen of these protofilaments link to form the hollow MT that will serve as a highway platform for intracellular traffic. At the "minus end", adjacent to the nucleus, lies the microtubule organizing centers. They act as capping proteins and anchors to MTs, permitting the anterograde and retrograde transport of intracellular cargo through kinesin and dynein motor proteins[3,6,7]. This method of active transport produces extremely rapid intercellular communication between the nucleus and the leading edge. Despite being described as a motor, kinesin doesn't actually generate forward force. Instead, it leans forward momentarily to favor forward diffusion of the freed leg which eventually hydrolyzes a single adenosine triphosphate (ATP) molecule producing 5pN of force over an 8nm step[6,8]. Impressively, this form of transport can reach speeds of up to 2μm/s, suggesting the potential for cell wide communication in under a minute[7].

As the least stiff, IF are molecularly different to other biopolymers as they form staggered α-helical anti-sense coiled-coil tetramer dimers[1]. Since these dimers bind in an anti-sense formation, the filaments lack polarity and are incapable of supporting directional movement and molecular motor proteins. Although there exists five subtypes of IFs, lamins (type V) have been the focus of most research. Located within the inner nuclear membrane, their low stiffness/high elasticity mechanical properties make them ideal at resisting tensile forces compared to compressive ones. In addition to their structural role[9–11], lamins are connected to chromatin and the external actin cytoskeleton via LINC complexes[12]. As such, they have been observed to play a major role in gene expression, DNA replication/repair, chromatin organization and transcriptional response[13–16].

As a single filament strand, F-actin is far less rigid than MTs. However, due to its highly organized assembly and the high concentration of crosslinking molecules (such as α-actinin and filamin), it is capable of constructing various forms of bundled networks that support the entire structural integrity of the cell. F-actin are highly polarized polymers, consisting of two parallel protofilaments that twist around each other in a helical formation[1]. Similarly to MT, their polymerization occurs far more rapidly at the barbed end (plus) than the pointed end (minus). This distinctive property of the filament regulates its growth by creating a thermodynamically driven nucleation process[17,18]. Fluctuations in this concentration create two phases of actin assembly: elongation and steady state. Elongation of the actin filament occurs by surpassing a critical concentration of monomeric actin subunits, which causes higher levels of polymerization at the plus end[17,19,20]. This is most notably observed during migration as the cell extends its filopodial extrusions in the effort to explore its surroundings. Despite driven through Brownian forces, assembly is promoted with the help of polymerization proteins known as profilin and formin[18,21]. These proteins work in tandem to support the nucleation and elongation phases of actin. Their importance on actin stress fibers have been well documented and are further explored in chapter 5 of this thesis. During steady state, the rate of actin polymerization is equally balanced by actin disassembly,

which creates a phenomenon known as "actin treadmilling"[17,19,20]. This permits the cytoskeleton to be in a constant state of structural remodeling, allowing it to quickly adapt to external stimuli. Perhaps the most important proponent of actin is the interlinking motor protein non-muscle myosin (myosin II)[22,23]. Utilizing the opposing polarities between parallel actin fibers, myosin II generates contractile forces by "walking" towards each fibers respective plus-end. This creates stressed actin fibers under tension through out the cytoskeleton which the cell then uses to regulate it's own structural morphology and movement.

The importance of actin and myosin however, far exceeds that of its structural role in the cell. As a transductive link, it is involved in converting the physical properties of the external microenvironment into biochemical signaling cascades[3,5,21,24,25]. The following will explore how it achieves this and the key proteins involved at the various stages of transduction.

1.2 The path to cell sensing

In *vivo*, cells are part of an extensive composition of tissues, each of which encounter a wide variety of forces. Examples of this are widespread: Vascular endothelial cells endure fluid shear forces and circumferential distention due to the pulsatile nature of blood pressure[26]. Epithelial cells are subjected to uniform tensile strain mediated through intracellular adherens junctions[27]. These forces act as mechanical cues that are constantly relaying pivotal information back to the cell, which in turn, allows it to respond by modifying its cytoskeleton[28], altering gene expression[29–31], promoting migration[32] and proliferation[33].

The development of a series of novel techniques capable of measuring sub-cellular mechanical forces propelled what would soon become the field of mechanobiology. The very first discovery of force generation in non-muscle cells was observed when elastic silicone was utilized as an adherable cellular substrate[34]. Surface wrinkling of the substrate clearly demonstrated a pulling force towards the cell. This was

the basis for what would eventually become traction force microscopy, whereby fluorescent beads within the gel would track dynamic cellular forces in real time[35]. Following this, the use of microcontact printing demonstrated how cell morphology and adherable surface area was critical for growth and proliferation[36]. But it wasn't until the development of magnetic twisting techniques that integrin transmembrane proteins and associated intracellular protein complexes known as focal adhesions (FA) were revealed as key players. By magnetically twisting peptide coated beads adhered to integrins, the applied stress to the cell surface resulted in a direct cytoskeletal stiffening. Disrupting F-actin resulted in the abolishment of the transmitted force[28]. Together, these seminal studies shifted the scientific community's attention and put a spotlight on the importance of mechanobiology and the key molecular proteins involved in mechanotransduction.

Integrins are transmembrane heterodimers that sit at the interface between the cell and the extracellular matrix (ECM). On the extracellular side, their 24 isoforms of α & β-subunits are responsible for formalizing adherent connections to the interlocking mesh of fibrous proteins and glycosaminoglycans (e.g. collagen, fibronectin, laminin). On the cytosolic side, lies the multiprotein complex known as the focal adhesion. FAs are dynamic actin–integrin links, the formation and maturation of which are driven by feedback from spatial and temporal interactions between the actin cytoskeleton, and integrin based molecular clusters of increasing complexity[37]. In their initial conformational state as focal complexes (FC) (precursor to mature FA), they are not reliant on mechanical tension to induce assembly[37]. Their complex consists of Talin[38], Tensin[39] and eventually Vinculin[40], all of which play an essential roles in assembly. Talin and tensin acts as anchoring proteins, connecting the actin filaments directly to the integrin β-subunit. In addition, they also permit the recruitment of vinculin, which initiates the maturation phase of the focal adhesion. Vinculin not only promotes the clustering of elementary nanocomplexes which solidifies the integrin-cystoskeleton link but also triggers the aggregation of integrin receptors[41]. The subsequent maturation of this focal complex occurs through consistent mechanical force stimulation that

originates from the extracellular milieu or from actomyosin mediated contractility. It is these locally applied tensile forces that induce a conformational change in the protein structure of vinculin[42,43] that renders newly accessible binding motifs to surrounding supportive proteins. These proteins: Src, p130Cas, Focal adhesion kinase (FAK) and Paxillin (Pax) constitute the formation of a mature FAs. It is important to note that the molecular nature of this transition is still enigmatic as several studies report diversity in the protein structure and phosphorylation dynamics of FAs[44–47]. This diversity has been shown to correlate with the positional location of the cell, revealing insights into the role and evolution of their maturation. As the cell moves forward, FC are quickly assembling and disassembling at the leading edge of the lamellipodium. As migration continues, the lamellipodium forms into the lamella, which is the transitionary zone where FCs undergo maturation[48]. At this stage, FAs are localized at the termini of actin stress fibers where they experience a continuous pulling force through myosin II contraction[49–51], which they then transmit externally to the ECM through associated integrins[48,52]. Purely based on thermodynamic principles, the application of a tensile force to an aggregate of protein subunits would promote the growth of the aggregate in the direction of the force[19,53]. This is because elastic stresses induced via pulling forces decrease the chemical potential of the aggregate molecule compared to nonassembled cytoplasmic molecules[54]. As a result, molecular interactions increase on stressed aggregates and promote self-assembly. As such, focal adhesions are an interconnected network of mechanosensory units that respond to mechanical forces in a uniformly orchestrated manner.

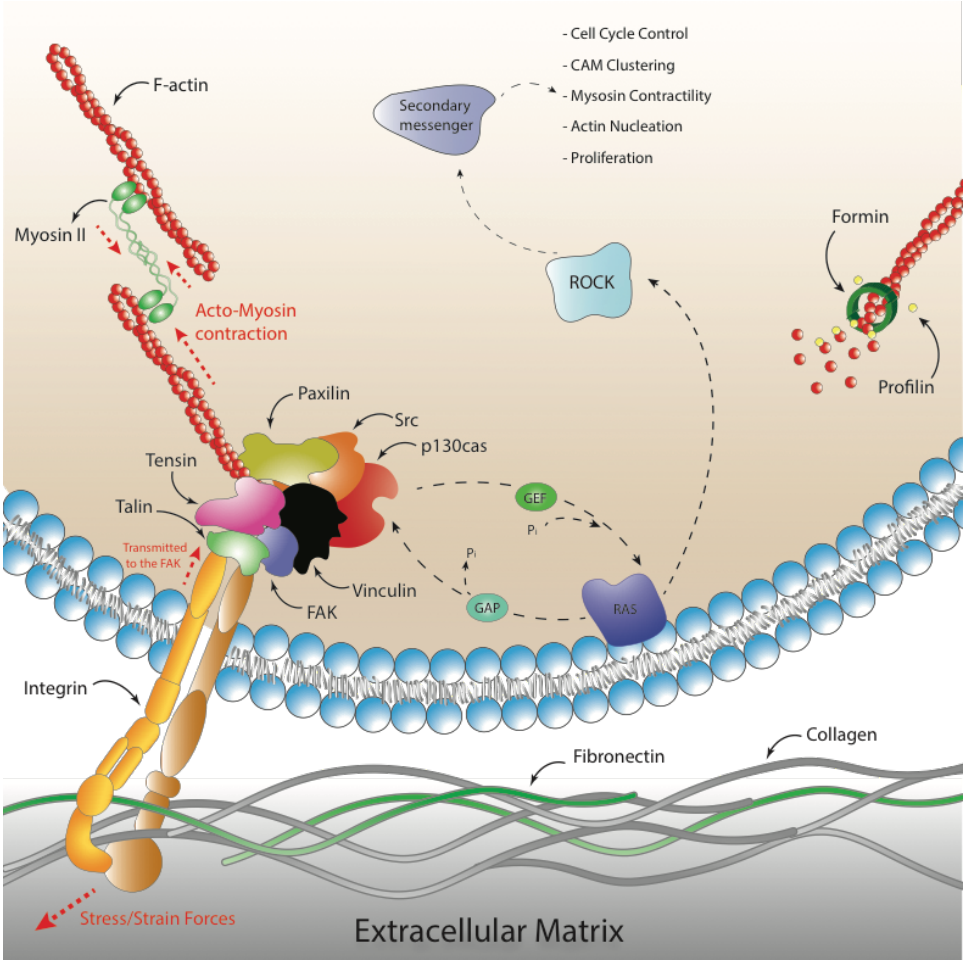

FIGURE 1.1 MECHANOTRANSDUCTION AND MECHANOSENSING AT A GLANCE
Cells adhere to the extracellular matrix (fibronectin, collagen) through transmembrane proteins (integrins). Connected to integrins on the cytosolic side are focal adhesion complexes which are composed of: Talin, Tensin, Paxilin, Src, p130cas, Vinculin, Fak. Talin and Tensin serve as anchoring proteins that bind the integrin transmembrane protein to actin filaments. These filaments are part of the actin-myosin complex that is capable of inducing tensional forces through Myosin II contraction. These forces, in addition to external forces originating from the ECM, cause conformational changes in the focal adhesion complex that promote the recruitment of Vinculin to induce maturation. Vinculin subsequently promotes the recruitment of Paxilin, Src, p130cas and FAK who are responsible for transducing tensional forces into biochemical signals. This occurs through regulated phosphorylation of RAS by Guanine Exchange Factor (GEF) and GTPase-activating proteins (GAP). Activation of RAS promotes the activation of a high level-signaling regulator (ROCK). As a master regulator, ROCK induces pleotropic activation of multiple signaling molecules that influence an extensive array of cell processes, from local actin nucleation to the regulation of gene expression.

This transduction mechanism however, between myosin II contraction and integrin based molecular complexes, is merely the foundation of a much larger signaling complex (Fig 1.1). Intertwined within FA proteins FAK, p130cas and pax are sets of master regulating proteins that control every aspect of cytoskeletal functioning. Known

as the small Rho family of GTPases, consisting primarily of Rho, Rac[55] and CDC42, their governance oversees everything from localized integrin clustering[56] to orchestrating large scale would healing[57]. Rho GTPases cycle between an active GTP-bound and inactive GDP-bound conformation that is regulated by two proteins. Guanine nucleotide exchange factors (GEFs) activate GTPase by catalyzing the exchange of GDP to GTP whilst GTPase-activating proteins (GAPs) inactivate it by increasing the intrinsic GTP hydrolysis rate[58,59]. Modulation of GEF and GAP is mediated through FA proteins FAK, p130cas and paxillin as a result of mechanically induced conformational changes[37,60]. Despite the pleiotropic effect of this activation, one GTPase among the many has revealed itself to be quintessential in the regulation of actin polymerization dynamics, myosin contractility, integrin complex formation and cellular adhesion molecule (CAM) clustering[61–63]. This protein, Rho-associated protein kinase (ROCK), directly and indirectly modulates the activation and inhibition of an extensive list of key mechanotransduction proteins. As such, its inhibition through the exposure of Y-27632 drug is widely used within the following chapters of this thesis to assess the involvement of mechanosensing on the behavior of cells in microfabricated channeled topographies.

1.3 THE INFLUENCE OF THE PHYSICAL MICROENVIRONEMENT ON THE CELL

It was over 100 years ago that Harrison revealed that surface topography had the ability to dictate cell morphology and behavior[64]. By plating neuronal cells on spider web fibers he observed that their axonal processes would preferential migrate and align along them. This was later confirmed by Weiss and colleagues and coined the term “contact guidance”[65]. With the advent of soft lithography and microfabrication technologies, the field of cell biology was presented with the tools to explore new avenues of cell-substrate interaction. The design and development of different geometries and length scales have revealed the microenvironment’s ability to influence cell morphology, migration, proliferation and even differentiation.

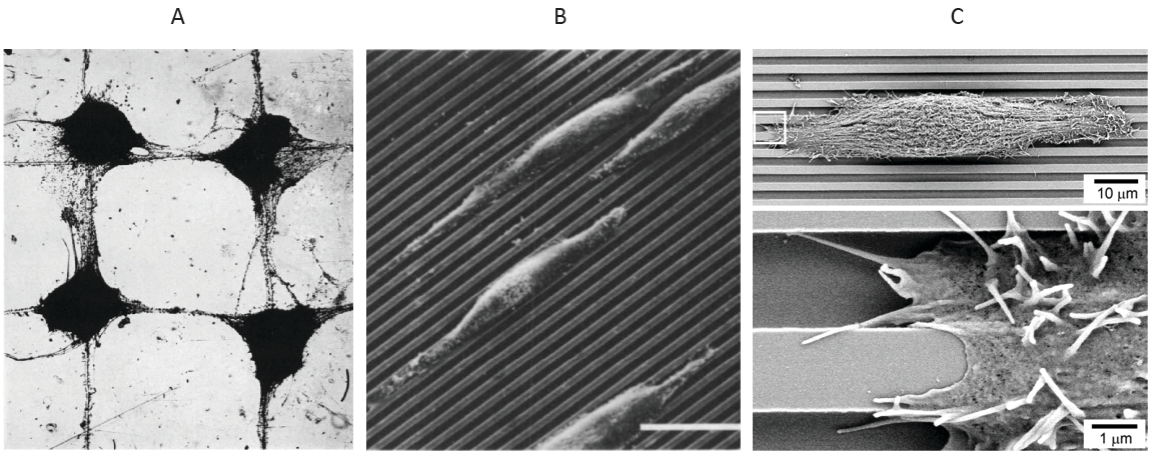

FIGURE 1.2 ADVANCES IN CONTACT GUIDANCE RESEARCH WITH MICROFABRICATION
A) Initial demonstrations of contact guidance shown by culturing neuronal cells on a freshly scratched glass surface[65]. B) Epithelial cells plated on a microfabricated grooved substrates 6μm wide and 2μm[66]. C) SEM images of cell cultured on microfabricated channels with their lamellipodia extending from the ridges to the grooves[67].

The most commonly engineered substrates utilized to test the effects of surface topography on morphology are arrays of parallel nanogrooves or nanoridges (75-1000nm). Interestingly, contact guidance cues from these substrates compel multiple cell types including endothelial cells[68–70], fibroblasts[71–75] and smooth muscle cells[76], to preferentially elongate and orient along the direction of the nanogrooves[77–83]. Cells that adhere to this topography demonstrate localized focal adhesion aggregation and actin fiber alignment along the ridges of the grooves. However, this behavioral response is intrinsically dependent on the geometric parameters of the topography that include groove width[68,70,72,74,84], ridge width[67,68,70,85,86] and groove height[66,67,69,74,85]. Depending on the cell type, altering the density, spacing or orientation of these topographic features can have a significant influence on the morphological response of the cells. For instance, growing NIH3T3 cells on a gradient of nanoridges with varying groove widths led to increased cell polarity towards denser patterns. These polarized cells displayed aligned actin stress fibers and vinculin positive focal adhesions scaled with the width of the underlying nanoridges[67]. Conversely, greater grooves widths induced more randomly distributed focal adhesions and consequently displayed no distinct cell polarity.

In the effort to mechanistically explain how cell respond to substrate topography, multiple theories have been proposed. No single theory fully elucidates the complexity of contact guidance, but together, they provide insight into a functional mechanism. The mechanical restriction theory proposed by Dunn and Heath[87] suggests that depending on the geometric properties of the microenvironment, cells are mechanically restricted from forming filopodial extrusions. If the groove width is larger than the cell's ability to overcome it via a filipodial bridge, polarization and elongation occurs along the ridges. The "focal adhesion theory" suggests that cellular orientation occurs as a result of FA maximizing their surface area. A narrow ridge presents a confined surface area that a cell will respond to by maximizing its adhered surface along the ridge. Conversely, a wide ridge promotes non localized FA maturation, allowing stress fibers to form in an isotropic manner[88]. The "discontinuity theory" by Curtis and Clark states that sharp edges (e.g. ridge) triggers localized actin condensation and consequently FA formation. Furthermore, during migration, actin filament bundles spanning from the nucleus to the lamella possess rigid mechanical properties that would bear unfavorable bending loads at the discontinuity. The cell responds by orienting itself so as to minimize mechanical stress.

The mechanisms of cellular migration have been extensively well documented. But the underlying influence by which the ECM acts as a guiding force remains to be fully understood[89]. Contrary to flat substrates where cells will migrated in a "random walk" formation, nanotopographies induce guided cell motility[90–92]. An example of this was shown in neutrophils whereby migration speeds were fastest when grooved substrates were spaced between 5-10μm apart[93]. This was suggested to have implications for immune surveillance in addition to wound repair when the ECM architecture is disrupted and subsequently repaired. Topography however, isn't the only property of the microenvironment that affects cell migration. It's been shown that by modulating the stiffness of a substrate, one can alter cell phenotypes. In a study by Weaver and colleagues, a non-malignant cell line (MCF10a) was cultured on an artificial ECM with a stiffness moduli resembling those of breast cancer and resulted in malignant

behavior including increased cell migration[94].

Micro-scaled patterned substrates have been used to demonstrate the correlation between adhesion and proliferation[82,95–97]. Cells cultured on a series of randomized adherent nano-islands of varying heights demonstrated altered proliferation rates. The higher the island, the lower the observed proliferation rate. Continued reduction in island height eliminated the discrepancy between a textured substrate and a flat surface and resulted in increased adhesion and subsequently higher proliferation[79]. Perhaps even more interesting than this is the spatial resolution at which cells respond differently. Culturing cells on surfaces with nanoscale roughness demonstrated that even alterations of less than 2nm affected cell proliferation[98,99]. The effects of maximizing cell adherence may explain, in part, why cells proliferate at much greater rates in vitro than in native in vivo microenvironment[100].

Engineered substrates have also begun to reveal the effect of surface topography on stem cell differentiation. As process that was once thought to be primarily dictated by biochemical cues, differentiation is highly influenced by the physical properties of the microenvironement[101–105]. This has been demonstrated with nanogratings of 250nm line widths that can align actin stress fibers and induce an upregulation of neurogenic and myogenic differentiation markers[103]. In addition to being highly sensitive to the surface topographies, stem cells are also highly sensitive to substrate stiffness. In a seminal study by Engler et al., mesenchymal stem cells were seeded on engineered substrates that mimicked the mechanical stiffness's of various tissues in vivo. In a demonstration of biomechanical mimicry, cells differentiated into neurons, muscle and bone in response to soft (0.1-1kPa), medium (8-17kPa) and stiff (25-40kPa) substrates respectively[106].

1.4 Embryonic stem cell growth in confinement

Embryonic stem cells (ESCs) are characterized by their unique ability to proliferate indefinitely whilst being able to differentiate into any cell type [107,108]. Their

manipulation for directed cell differentiation has been a topic that has been widely studied [109–111]. Traditionally, inducing differentiation has been achieved through chemical cocktails of signaling factors which have led to the upregulated expression of desired genes [112]. This however, has shown to present limitations due to inconsistent non-uniform differentiation [113,114]. More recently, attention has been directed to understanding the influence of the physical properties of the microenvironment on stem cell fate. It has now been established that controlling the in vitro mechanical properties of the substrate (elasticity) allows one to direct stem cell fate [106]. ESCs emerge during the development of the embryo at the blastocyst stage, 4 days post coitum. With the formation of the blastocyst, a fluid filled cavity with an inner cell mass emerges. ESCs are located within this inner cell mass of the blastocyst. The conditions of their growth are unique as the fluid filled cavity of the blastocoel forces the cells to proliferate under a high degree of spatial confinement [112] (Fig 1.3).

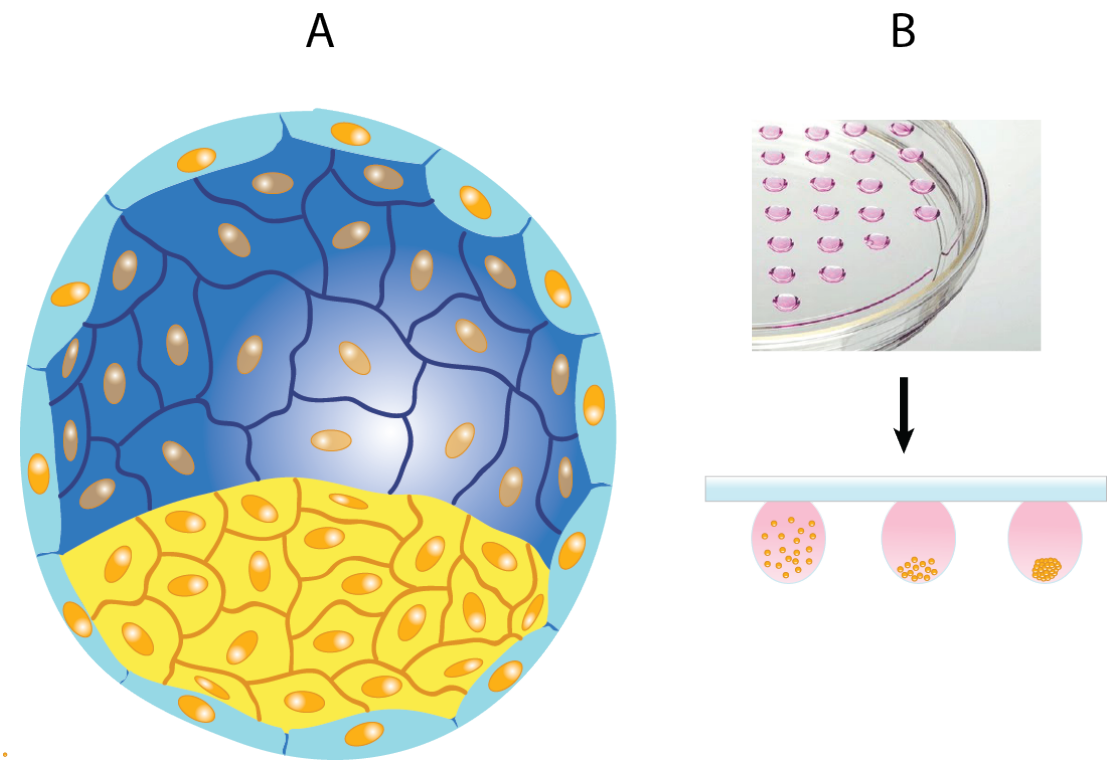

FIGURE 1.3 EMBRYONIC STEM CELLS IN VIVO & VITRO

A) Diagrammatic representation of the blastocyst, demonstrating the proliferation of embryonic stem cells (inner cell mass) under confined conditions. The trophoblast is the encapsulating embryonic layer that will become the placenta further into development. B) Hanging drop tissue culture method whereby 800 cells/ 20µl of media are plated on a petri dish that is then inverted so as to let the droplets hang. Cells are left to aggregate and proliferate for 2 days to induce spheroid formation. Once developed, they are plated onto a flat collagen coated surface and allowed to differentiate. (Adapted from [115])

Traditional culturing of ESCs commences with the cells being plated on a feeder layer of fibroblast cells. Fibroblasts release leukemia inhibitory factor (LIF), which is a cytokine that prevents stem cell differentiation. After the feeder layer dies, a LIF supplement is added to all subsequent passages to maintain pluripotency. To initialize differentiation, cells are plated within an inverted hanging drop, mimicking in vivo confinement properties, and permitting three dimensional cellular proliferation [116]. The confinement within the drop results in the formation of a large (approx. diameter range of 500µm) multi-cellular mass that is roughly spherical and known as an embryoid body (EB) [117]. Standard ESC differentiation protocols then require the EB to be plated onto flat tissue culture plates. The EBs are maintained under defined media conditions in order to promote the commitment of ESCs towards particular lineages and fates [117]. This process can take several days or weeks to complete and often the EB is observed to begin flattening and spreading out as the flat surface offers no degree of confinement allowing committed cells to migrate freely. This differs significantly from the in vivo environment, where cells proliferate and differentiate in a highly confined three-dimensional space.

Numerous studies have attempted to manipulate the growth of ESCs into aggregates mimicking the geometry of their microenvironment. Examples of this have been shown with triangular or cylindrical microwells, which create an isotropic confinement forcing the cells to acquire the shape of the microwell [118]. Furthermore, by using hollow sphere microwells (Fig 1.4), they were capable of inducing consistent ESC spheroids possessing an EB morphology. By varying the diameter of the microwells, they were able control the size of the spheroids and induce different differentiation lineages,

demonstrating a direct correlation between microenvironmental confinement and the transcriptional regulation of the cell [119].

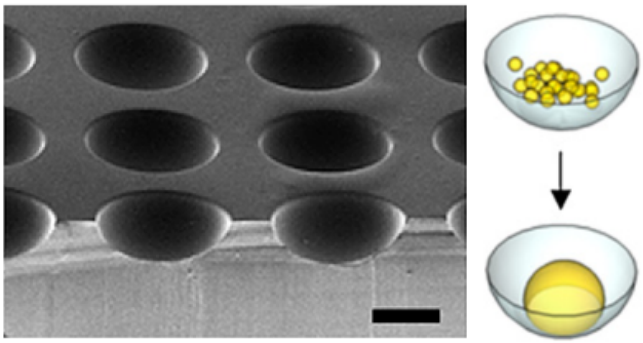

FIGURE 1.4 MICROFABRICATED PDMS TOPOGRAHPIES FOR EMBRYONIC STEM CELLS
Examples of microfabricated PDMS concave microwells employed to assess the influence of 3d topography on embryonic stem cells. (Scale bars 500µm, adapted from [119])

1.5 UNDERSTANDING CELL-CELL INTERACTIONS THROUGH COCULTURED SYSTEMS

In the early 20th century, significant interest began to form around understanding the mechanism of embryonic development. Morgan first noticed the polarity of organisms and that regeneration in worms occurs at different rates depending on the location of the severing. He postulated that the mechanism of regeneration is influenced by gradients of "formative substances"[120]. Fifty years later, Turing[121] proposed the reaction-diffusion hypothesis, also known as the morphogen gradient model, which has become the staple for explaining spatio-temporal organization in complex biological systems. Simply put, two or more signaling molecules with different diffusion properties that react by auto- and cross-catalyzing or inhibiting their production can generate spatial patterns of morphogen concentration[122]. This simple yet encompassing biological model to cell organization applies not only to embryogenesis but the myriad of actively regulated systems including the immune system[123–125], tumerogenesis[126–128], and neural networks[129–132]. Co-cultured systems

have since been used to understand the complex cell-cell interactions between different cell populations. By culturing multiple cell types in the same microenvironment, one could simplify the complexities of an in vivo system to a single isolated interaction. These experiments provided further insights into the exact signaling molecules being diffused via paracrine release inducing guided migration towards or away from target areas[133–136].

However, despite the comprehensiveness of the reaction-diffusion hypothesis, it lacked the ability to fully explain observed patterns of morphogenesis in vivo and vitro. One particular study presented by Holtfreter and colleague propelled a new paradigm for embryogenic sorting. Amphibian embryonic cells were isolated during their initial gastrulation stages and disassociated into single cells. These cells were then mixed and re-suspended onto an agar-coated petri dish to prevent adhesion. They observed that cells had not only re-aggregated together, but had reacquired their positional embryonic location with respect to one another. Following this observation, Steinberg et al.[137–139] proposed the differential adhesion hypothesis that brought forward thermodynamic principle to cell sorting. He suggested that different cells possessed different adhesive binding affinities towards one another and that sorting occurred as a result of minimizing the interfacial free energies of the system[140]. The binding affinities he referred to were later revealed to be the various 24 integrin and >80 cadherin CAM isoforms expressed on the cell surface. Depending on the cell type and cellular event, different configurations of CAMs will be present on the surface of the cell. These configurations lead to relative intensities of intercellular adhesion, which served as a set of morphological determinants creating highly organized cellular patterns through passive or active motility. Despite cocultured systems being ubiquitously used to study the effects of molecular gradients on cell interactions, their use in examining binding affinities has been less explored. Through the use of microfabricated topographies, significant strides can be made in revealing how binding affinities influence cells grown in three dimensions.

1.6 Conclusion

The cell possesses a complex cytoarchitecture that is highly sensitive to the geometric and mechanical properties of its milieu. Seeing as these physical properties are capable of directing migration, proliferation and differentiation, progress in the field will depend on revealing how microenvironmental features induce these responses. The advent of microfabrication has given us the tools to systematically test cells under different topographical conditions. However, these conditions have remained largely two-dimensional, ignoring the potential effects of confined three-dimensional space. Furthermore, their added simplicity of monocultured systems simplifies the in vivo complexities of different cell-cell interaction. The following thesis is a compendium into the effects of three dimensional confined topographies and their influence on cellular behaviour.

1.7 Motivation and approach

In chapter 2, we begin by establishing an understanding of the interactions between cocultured cells in flat two dimensional topographies. This initial experiment is critical to formalizing a baseline of cellular behaviour in cocultured systems. We hypothesize that in simple two dimensional topographies, cell interactions and patterning are driven through physical binding energies arising from cellular adhesion molecules. To test this, MDCK and NIH3T3 cells are fluorescently dyed to enable cell type differentiation during subsequent imaging and seeded onto flat PDMS. After 48hrs incubation, confocal imaging, which permits three dimensional image capture, is used to acquire a complete rendering of the cocultured system. We subsequently perform a systematic inhibition of mechanosensing proteins to assess the involvement of biological mechanisms in the displayed coculture behaviour. We hope to observe a consistent behavioral pattern that is unaffected by the inhibition of biological mechanisms. If this cocultured system is in fact driven by physical binding energies, we'll be able to reproduce it within a Monte Carlo simulation model. Ascertaining an

understanding of these interactions in two dimensions will allow us to subsequently introduce more complex three dimensional systems.

In chapter 3, we introduce a channeled three dimensional topography within our cocultured system. Having previously identified the patterning of behaviour on flat substrates, we hypothesize that adding a confined channeled geometry will promote more complex biological driven behaviour. To test this, MDCK and NIH3T3 cells are seeded onto a series of microfabricated PDMS channels of varying widths. They're incubated for 48hrs and imaged with the confocal microscope. Based on the varying channel widths, we hope to reveal the effects of different levels of confinement on cellular behaviour. This would suggest that the confinement properties of three dimensional microenvironments have the ability to induce altered behaviour and promote biologically driven mechanisms in cocultured interactions.

In chapter 4, we explore the mechanisms behind the distinct patterning migration observed from introducing channeled topographies into cocultured systems. NIH3T3 cells appear to demonstrate an active migration to the top of the channels where they then remain. We hypothesize that the distinct channeled geometry is guiding migration through a phenomenon known as contact guidance. To test this, we begin by revealing the threshold height of the channel at which the patterning phenomenon occurs. We subsequently alter that channel through reflow techniques which create curved edges rather than acute 90°angles. This removes the effect of contact guidance whilst maintaining all other channel parameters. We hope to acquire an understanding of how manipulating the substrate geometry and directly influence cell patterning and behaviour. Revealing this would have far outreaching applications in biomaterial science and bioengineering.

In chapter 5, we introduce ESCs into our confined channeled topographies. ESCs are natively found within the trophoblast, which is a highly confined geometric space. Because of this, altering the level of confinement by varying the channel widths should have highly influential effect on the growth and morphology of the cells. We

hypothesize that high levels of confinement through small channel widths will induce altered morphological growth. To assess this, we seeded ESCs into channeled topographies of varying channel widths. After 48hrs incubation, cells with imaged via confocal microscopy. Inhibition studies were also performed to ascertain the potential involvement of mechanosensing proteins such as Rock, Myosin and Formin. We hope to identify a confinement threshold at which ESCs begin to respond differently and to reveal whether this mechanism is biologically or physically driven. This, of course, would have extensive applications in understanding how stem cells grow in vitro and perhaps help direct future studies towards harnessing their potential.

This body of work and the results they infer demonstrate the potential of what further exploration into the influence the physical microenvironment on the cell can achieve.

Chapter 2 | Manuscript

Patterned cell type separation in cocultured cell mixtures *In vitro*

Sebastian V. Hadjiantoniou[1], Maxime Leblanc-Latour[2], Maxime Ignacio[2], Cory S. Lefevbre[1], Gary W. Slater and Andrew E. Pelling[1,2,3]

[1]*Department of Biology, Gendron Hall, 30 Marie Curie*
[2]*Department of Physics, 598 King Edward*
[3]*Institute for Science, Society and Policy, Desmarais Building, 55 Laurier Ave. East*

Submitted June 6th 2017 to Soft Matter

Motivation & Objectives |

It has been proposed by Steinberg et al. that the organization of cells during embryogenesis is not only the result of morphogen gradients but can be guided through purely physical interactions. In the attempt to understand the interaction of cells in a simplified in vitro system, we cocultured different cell types and observed the mechanisms of patterning. We utilize a Monte Carlo simulation to demonstrate how this patterning can be achieved through modulating the relative binding interactions in the system.

2 | SPONTANEOUS PHASE SEPARATION OF COCULTURED CELL MIXTURES IN VITRO

2.1 ABSTRACT

During Embryogenesis, cells undergo constant organizational remodeling. Biochemical and biophysical guidance cues act in tandem to guide migration and morphogenesis into distinct cellular patterns. It has been shown that various cell types will express different configurations of cellular adhesion molecules known as cadherins and integrins. Cocultured *in vitro* experiments have focused on revealing the extensive genetic expression profiles that modulate embryogenesis whilst overlooking the physical cell-cell and cell-substrate interactions that influence organization. We demonstrate that NIH3T3 and MDCK cells undergo a spontaneous cell type separation when cocultured *in vitro.* By means of a Monte Carlo simulation model, we have been able to qualitatively replicate the observed phenomenon through physical binding energies. Cells with different cell-cell and cell-substrate binding undergo spontaneous cell type separation due to the minimization of interfacial free energy within the system. Our model suggests that cell-cell and cell-substrate binding could play a critical role in cell organization and is capable of cell type separating different populations of cells in vitro.

2.2 INTRODUCTION

At the heart of embryogenesis lies an extensively complex list of cues which drive the cohesive formation of organized tissue[21]. Efforts to elucidate these governing mechanisms have resulted in identifying two key proponents in development: differentiation and cellular organization. Differentiation is ultimately controlled through highly regulated transcriptional activity[141]. On the other hand, explaining the mechanisms of cellular organization has required the examination of the mechanisms that impact cell-cell and cell-substrate interactions. It is for this reason that Steinberg et al. [137–139] proposed the differential adhesion hypothesis (DAH), which suggests that

morphogenetic sorting forms through tissue interfacial free energies arising from cellular adhesive interactions[140]. In other words, cells possess cellular adhesion molecules (CAMs) known as integrins and cadherins, responsible for cell-substrate and cell-cell binding, respectively. Depending on the cell type and cellular event, different configurations of CAMs will be present on the surface of the cell. These configurations lead to relative intensities of intercellular adhesion, which serve as a set of morphological determinants creating highly organized cellular patterns through passive or active motility. The physical phenomenon of adopting the lowest free energy configuration was originally shown in a study whereby amphibian embryonic cells were disassociated, mixed, and subsequently allowed to re-associate. The outcome showed a spherical reformation with cells that re-aggregated into their embryonic position[138]. More recent studies have shown similar examples of the influential effects of differential cell to cell vs cell to substrate adhesion. Mouse embryonic stem cells were seeded into channeled topographies whereby after 48hrs, the cells demonstrated preferential cell-cell adhesion and formed spherical embryoid bodies rather than flat island-like aggregates commonly seen in flat two dimensional culture vessels[142].

Despite the clear multicellular environment of native tissue, co-cultured systems, whereby multiple cell types are cultured together in vitro, have primarily focused on analyzing changes in gene expression[143–146]. For example, some progress has been made at characterizing the relationship between carcinoma and stromal cells as cell-cell communication has been considered to play an important role in triggering cancerogenesis[147–149]. Many of these coculture systems however prefer a paracrine-only interaction by utilizing separated adherable membranes[143]. Although this method elucidates potential biochemical influences, it prevents any physical cell-cell interaction from occurring. As such, cells may display patterned growth that would be solely attributed to reaction-diffusion mechanisms while completely ignoring the effects of differential adhesion. Other studies have explored differential adhesion via synthetic biology strategies. By utilizing the L-929 murine fibroblast cell line which expresses no known cadherins and displays no aggregation when placed in hanging drops, Steinberg

et al. were able to modulate exogenous cadherin expression to induce predictable patterned formations[150]. Similar results were obtained by Cachat et al., whereby aggregated spheroids displayed cell partitioning (termed phase separation) depending on cadherin expression patterns[151]. Despite the extensive work via synthetic biological approaches to demonstrating cadherin based differential adhesion, utilizing endogenously expressed cadherin based sorting has yet to be demonstrated.

In this thesis, we use unaltered cell lines in coculture and demonstrate spontaneous cell type separation in mixtures of two distinct cell types on flat two dimensional topographies. To achieve this, we specifically selected two distinct cell types with different endogenously expressed cadherin profiles. NIH3T3 fibroblasts are highly motile, transiently adherent cells whilst MDCK epithelial cells form strong cell-cell tight junction bonds. In vitro, these cocultured cells quickly underwent a cell type separation. MDCK cells randomly dispersed, eventually forming a monolayer on the substrate whilst NIH3T3s slowly aggregated into patterned formations. We also illustrate how selectively inhibiting signaling cascades that modulate binding affinities between cells and substrate resulted in statistically different cellular patterning formations. To observe the potential patterning that could be achieved though purely physically driven forces, we developed a kinetic Monte Carlo computer simulation model of our experimental system. By mapping cell-cell and cell substrate adhesion into binding energies and minimizing the interfacial free energies between cells, our model was able to replicate our in vitro coculture results. This simulation only supports the notion of force driven organization and is limited compared to the vast complexities of biological systems. Its purpose is to serve as an illustrative model that suggests the potential possibilities of physically driven systems. Taken together, our study suggests how highly influential differential adhesion can be in mixtures of cells in-vitro. Moreover, even when key biological mechanisms that dictate the morphology and sensory perception of the cell are inhibited, fundamental biophysical interactions are capable of driving cell type dependent separation.

2.3 RESULTS

2.3.1 THE ROLE OF THE CYTOSKELETON IN COCULTURED CELL TYPE SEPARATION

To explore the behavioural interaction between cells, NIH3T3 and MDCK cells were co-cultured for 48 hrs. NIH3T3 fibroblasts and MDCKs epithelial cells were preloaded with a green and red fluorescent cell tracker, respectively, permitting visual differentiation during imaging. As can be seen in Fig 2.1A, there is a clear cell type separation of fibroblast cells (green) compared to the epithelial cells (red). To assess the involvement of key cytoskeletal proteins, we systematically performed the same set of experiments with selective inhibitory drugs. At a concentration of 10 μM, Y-27632, Blebbistatin and SMIFH2 were each added to their respective samples seeded with ~25000 cell/cm^2 for 48 hrs. As shown in Fig 2.1A, inhibition of actin contractility (Blebbistatin) and actin polymerization (SMIFH2) had no effect on the behavioural interaction of both cell types in coculture. Inhibition of cytoskeletal signaling cascades (Y-27632) however presented more definable changes in patterns of cellular formation. Whilst MDCK epithelial growth remained widely dispersed in the form of a monolayer, NIH3T3s aggregated into larger islands connected via strands of cells. Further LSCM analysis reveals that there is in fact a monolayer of MDCK cells below the patterned NIH3T3s (Fig 2.1B). These results are in contrast to NIH3T3 and MDCK cells cultured in isolation in which they formed a mesh-like network or a monolayer, respectively, as has been long established and observed[152] (Fig 2.4).

In order to quantify and assess this visual cell patterning (Fig 2.1C), a Kolmogorov-Smirnov (K-S) test was used. This includes performing a quadrat analysis to compare the cell frequency distribution to a random Poisson distribution by measuring the absolute, largest difference between cumulative frequencies, designated as the D statistic-value which has been described in detail previously[151]. Briefly, the D statistic-value is a dimensionless parameter that allows one to quantitatively determine if a cell population is randomly distributed ($D < 0.136$) or not ($D > 0.195$). In coculture, the D statistic value for MDCKs was 0.11±0.02 ($p>0.05$, $n=7$), indicating that the distribution is

not statistically different from a random spatial distribution. As expected, NIH3T3s cells have a much higher D value of 0.22±0.04 ($p<0.05$, $n=7$), confirming that their distribution is patterned and suggesting that there is a governing mechanism controlling their aggregation.

Quadrat analysis indicates a significant patterning difference in NIH3T3s with a D statistic value of 0.37±0.04 ($p<0.01$, $n=8$) when cultured with Y-27632 compared to the untreated. Despite the observed changes in patterning with Y-27632, NIH3T3 cells demonstrated only minor variation in their patterning behaviour with D values of 0.24±0.04 ($p>0.05$, $n=8$) and 0.28±0.04 ($p>0.05$, $n=9$) for Blebbistatin and SMIFH2, respectively. MDCKs however demonstrate relatively no patterning change among any of the selective inhibitions with a consistent D value of 0.9-1.1 (Fig 2.1C).

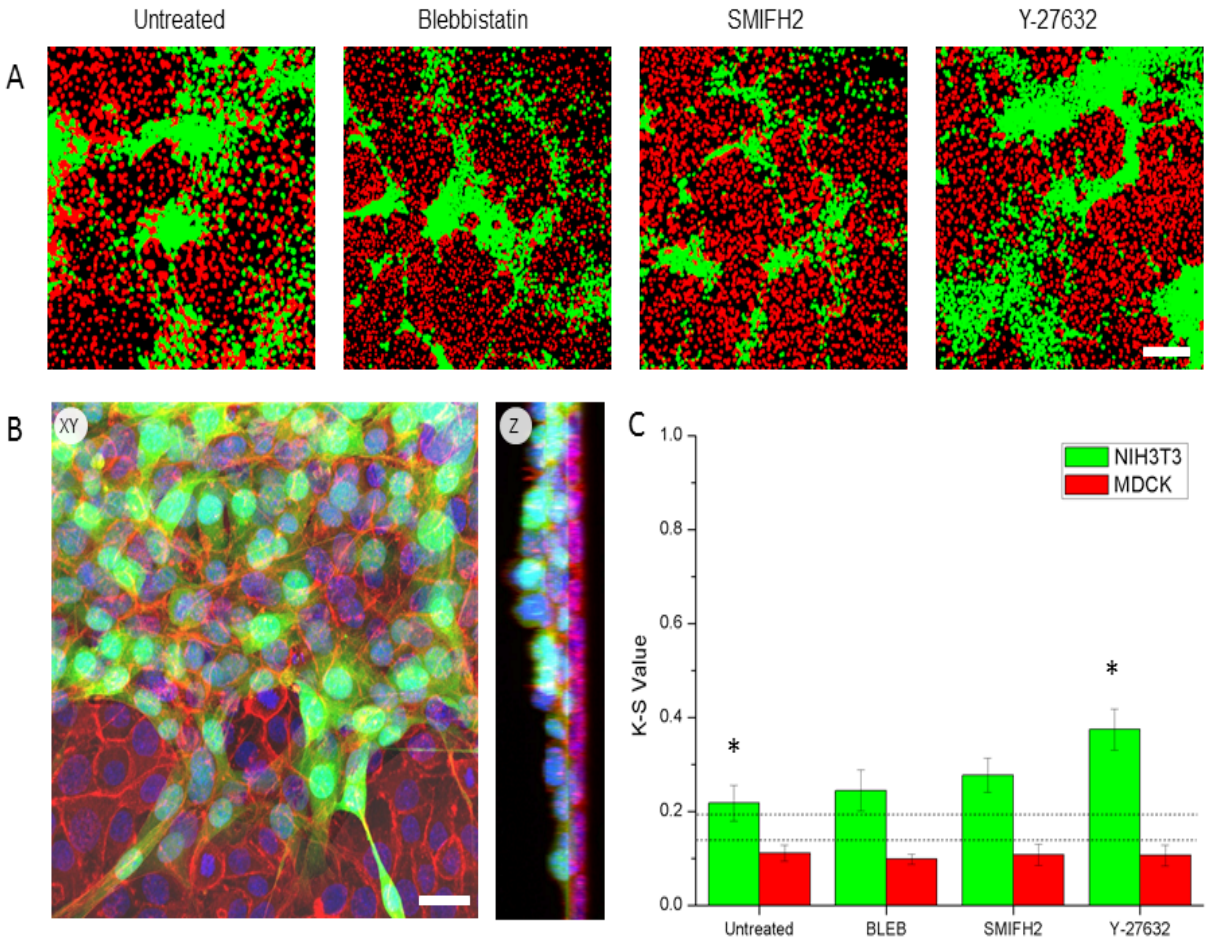

FIGURE 2.1 COCULTURED NIH3T3 AND MDCK ON FLAT SUBSTRATES

(A) NIH3T3 (green) and MDCKs (red) co-cultured and seeded onto a flat substrates for 48 hrs. Images have been thresholded to amplify the contrast between cell types. Distinct patterns of cell type separations are apparent in all conditions. (B) Orthogonal view of NIH3T3 (green) and MDCK (red) co-cultured on a flat substrate. Z projection rendering of confocal stacks reveals the layered patterning as NIH3T3s directly on a monolayer sheet of MDCK cells. (Scale bar = 25μm) (C) Kolmogorov-Smirnoff test analyzing the presence of patterned behavior in both cell types. The lower (0.136) and higher (0.195) critical values (dotted lines) correspond to the confidence threshold for which the null hypothesis of a random distribution can be rejected. Therefore, above indicates patterned formation whilst below suggests random cell dispersion. In all cases, NIH3T3s display patterned cell behavior whilst MDCKs present a random cellular distribution pattern. Statistically significant ($p<0.05$) results were found when comparing untreated cells to ROCK inhibited (Y-27632) patterning. Scale bar = 200μm

2.3.2 Cell substrate binding affinity in cocultured cells

Based on these results, we hypothesized that Y-27632 treated cells underwent inhibition of cell-substrate adhesion leading to increased aggregation and cell type separation. To test this hypothesis, we performed a flow assay[153] with a cocultured system confined within a microchannel (Fig 2.2 A,B). At a shear stress of 0.2 Pa, untreated NIH3T3s adhered significantly more than Y-27632 treated cells with 58% ±0.09 of cells remaining compared to only 29% ±0.07 ($p<0.05$, $n = 3$) after 30 minutes (Fig 2.2 C,D). When increasing the flow to a maximum shear stress of 3 Pa, 40% ±0.12 of untreated cells remained attached compare to 23% ±0.05 after treatment with Y-27632. It is important to note that under all conditions, 100% ±0.00 ($p>0.05$, $n=3$) of MDCK cells remained unaffected. This result further confirms that the cell-substrate binding affinity of MDCKs is significantly higher than that of NIH3T3s.

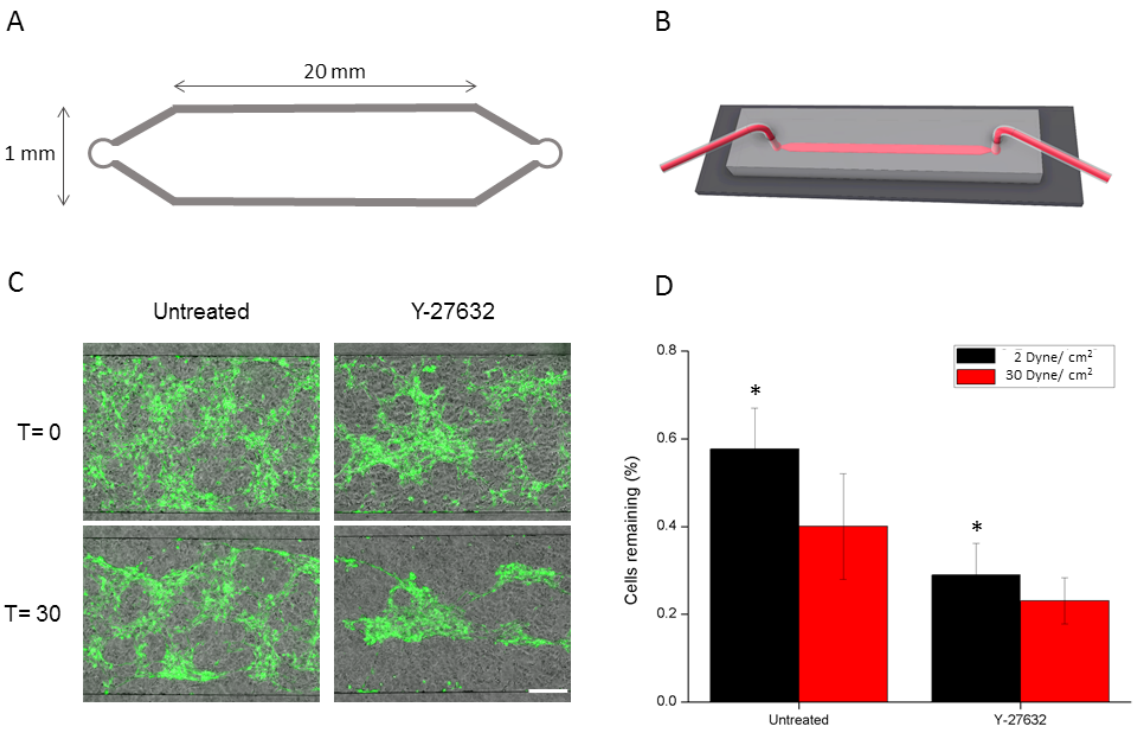

FIGURE 2.2 FLOW ADHESION ASSAY OF COCULTURED NIH3T3S AND MDCKS.
(A) Flow chamber design dimensions, L= 20mm, W= 1mm and H=160µm. (B) Graphical rendering of PDMS mold inverted and bound onto a glass slide with microfluidic tubing inserted into the 0.75mm inlets. Typical adhesion assay where cells were exposed to shear stress over a period of 30 min. Cells were counted before and after flow to quantify changes in cell-substrate adhesion strength (scale bar = 250 µm). (A) NIH3T3s (green) and MDCKs (phase) before (T=0) and after (t=30) 1µl/s of flow (2 dynes/cm2). (B) Ratio of cells remaining on the glass substrate after exposing to a shear stress of 2 & 30 Dyne/cm2 over a period of 30 min. There is a significant difference between the untreated and Y27632 treated cells ($p<0.05$).

2.3.3 Simulating Patterned Adhesion

It has been well established that different cell types express their own combinations of cell adhesion molecules (CAMs)[154,155]. Through specific integrin isoforms and cadherin binding, differential adhesion energies can form complex cell patterning[156–158]. To assess whether the experimentally observed phenomenon of cell type dependent separation between NIH3T3s and MDCKs is achievable through differential adhesions alone, we developed a computer simulation model. Our Kinetic Monte Carlo simulation utilizes properly chosen binding energies between cells ($\varepsilon_{11}, \varepsilon_{12}, \varepsilon_{22}$) and substrate ($\varepsilon_{1S,}\varepsilon_{2S}$) to model the various interactions taking place

during cell migration (Table 1). This simulation is not meant to fully represent the biological complexities present in vitro, but to ascertain whether the cell type separation observed in vitro can be obtained through purely physical interactions. When simulating co-cultures on flat two dimensional topographies the results display the same cell type separation phenomenon to cells cultured in vitro (Fig 2.3A). Simulated co-cultures with the chosen NIH3T3 (ε_{11}=1.05, ε_{1S}=0.5) and MDCK (ε_{22}=4, ε_{2S}=5), (ε_{12}=1.5) energy parameters $_{were}$ found to replicate the in vitro observations. NIH3T3 patterning was statistically significant with a K-S D value of 0.26±0.01 ($p<0.05$, n=5) (Fig 2.3B). Simulated MDCKs also showed identical cell dispersion to that observed in vitro, with a D value of 0.10±0.02 ($p>0.05$, n=5).

After identifying the binding parameters that replicate in vitro observations, we modulated them in accordance to the known biological effect of Y-27632. By merely decreasing the binding energy of NIH3T3 substrate adhesion ($\varepsilon_{1S)}$ from 0.5 to 0.3, we observed the same K-S D value of 0.33 ± 0.02 ($p<0.05$, n=5) as in vitro experiments. Many of the key observations made in vitro were also observed in our simulations. For instance, MDCKs adhere and form strong cell-substrate and cell-cell bonds whilst NIH3T3s migrate until they have contacted an adjacent cell of the same type. Over time, they form large island like aggregates (25μm high, corresponding to ~2-3 cells) positioned above the monolayered MDCK cells (Fig 2.3A). To compensate for the simulation model not taking into account cell duplication, we performed the same set of experiments with the addition of thymidine (2mM). As a deoxynucleoside, thymidine causes cell cycle arrest and is often utilized for cell synchronization[159]. Fig 2.5A demonstrates that co-cultured cells under cell cycle arrest display the same patterning effect shown in mitotically active cells. KS test (Supplementary Fig 2.5B) quantitatively shows a statistically significant pattern in NIH3T3 cells (D value = 0.35±0.04, $P<0.05$, N= 3) whilst MDCK cells remain randomly dispersed (D value = 0.11±0.02, $P> 0.05$, N=3).

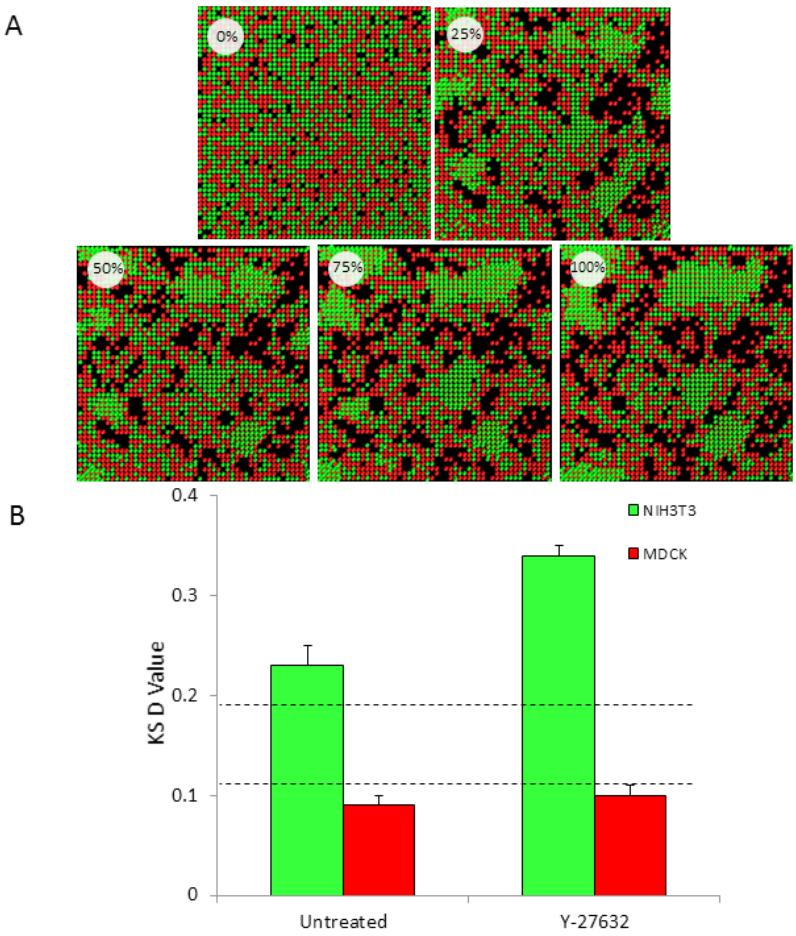

FIG. 3 SIMULATION OF CO-CULTURED CELLS UTILIZING THE DIFFERENTIAL ADHESION MODEL OF PATTERNING.

A kinetic Monte Carlo simulation whereby cells undergo stochastic diffusion and interact with one another based on their binding energy parameters. These parameters (ε_{11} , ε_{22} , ε_{12} , ε_{1s} , ε_{2s}) represent the cell-cell and cell-substrate adhesion of NIH3T3s/MDCK and have been modeled accordingly. (A) Timelapse sequence of rendered simulation for NIH3T3s (green) and MDCKs(red) co-cultured onto a flat substrate. Similarly, to experimental results, the differences in adhesion energies between cell types create a two layered cell phase separation whereby MDCKs are widely dispersed on the bottom whilst 3T3s display aggregated islands on top. (B) Kolmogorov-Smirnoff test analyzing the presence of patterned behavior in both cell types. The lower (0.136) and higher (0.195) critical values (dotted lines) correspond to the confidence threshold for which the null hypothesis of a random distribution can be rejected. Therefore, above indicates patterned formation whilst below suggests random cell dispersion. Simulated NIH3T3s on two dimensional substrates display patterned cell behavior whilst MDCKs present a random cellular distribution pattern.

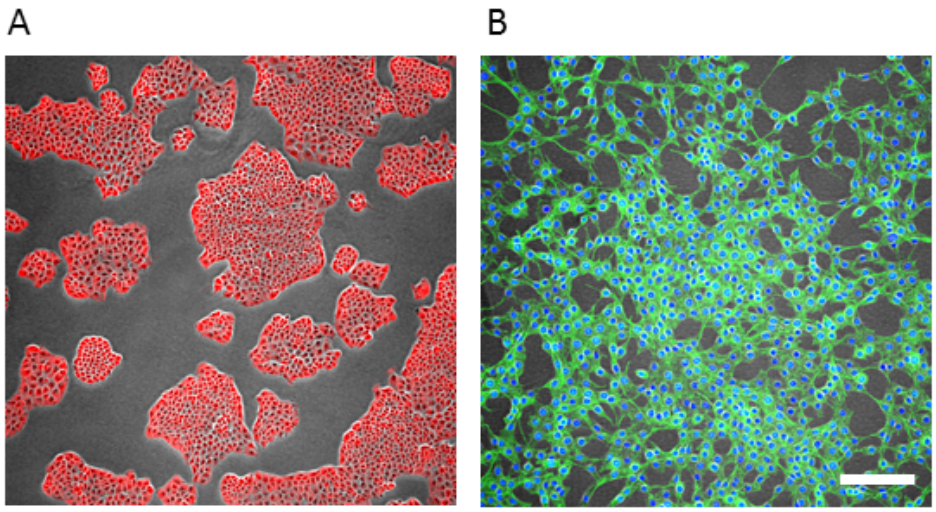

FIGURE 2.4 TYPICAL GROWTH PATTERNS OF MONO CULTURED CELLS IN VITRO.
(A) MDCK cells (red; Actin) develop into island like aggregates until eventually creating a monolayered epithelial sheet, formed through tight cell-cell junctions and strong cell-substrate adherence. (B) NIH3T3 cells (green; Actin) equidistantly space themselves to form an intricate mesh dependent upon cell-cell adheren junctions and transient cell-substrate binding. (Scale bar = 50µm)

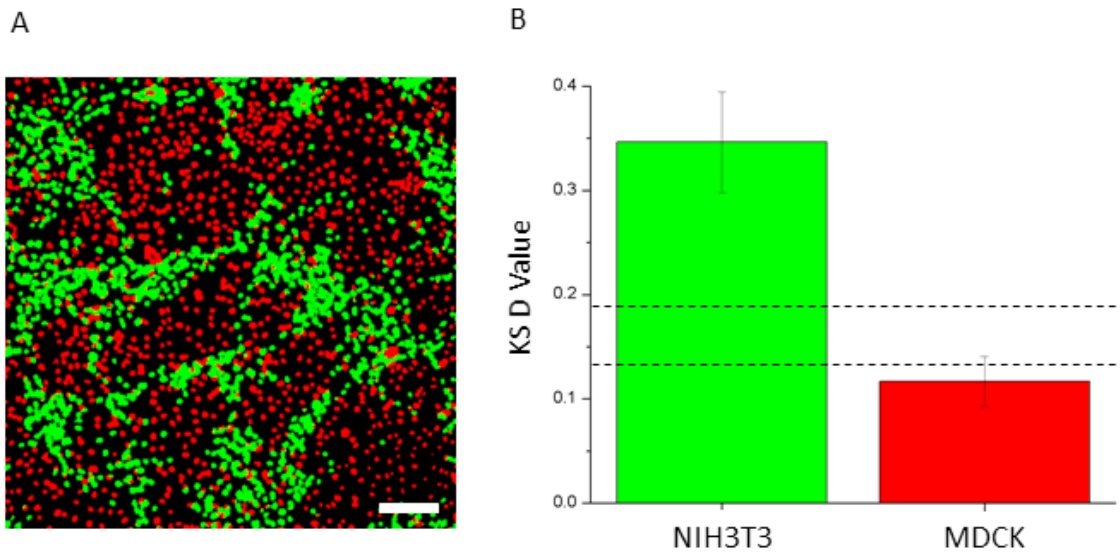

FIGURE 2.5 COCULTURED NIH3T3S AND MDCKS ON A FLAT SURFACE MITOTICALLY INHIBITED VIA THYMIDINE.

(A) NIH3T3s were pre-loaded with CellTracker Green CMFDA dye for 30 minutes prior to experiments. Cells were then mixed (1:1) and deposited at twice the seeding density (~ 50 000 cell/cm2 each) of channeled experiments with thymidine (2mM) for 48hrs. Samples were then fixed and stained with DAPI and imaged on the confocal microscope. NIH3T3s (green) and MDCKs (red) display the same cell type separation as mitotically active cells. Scale bar = 200µm. (B) Kolmogorov-Smirnoff test analyzing the presence of patterned behaviour in both cell types. The lower (0.136) and higher (0.195) critical values (dotted lines) correspond to the confidence threshold for which the null hypothesis of a random distribution can be rejected. Results reveal that inhibition of mitosis has no effect in coculture as only NIH3T3s display patterning.

2.4 DISCUSSION

Although identified as the inherent governing mechanisms for cell patterning[2,122,139,157,160], the differential adhesion and the morphogen gradient models remain experimentally bifurcated. Experiments focusing on cocultured systems have rarely permitted cells to not only biologically interact but to physically interact as well. In this study, we utilize a simple co-culturing strategy with cell types expressing different cadherin subtypes to examine cell patterning formation.

To investigate this phenomenon, we cocultured NIH3T3 fibroblasts and MDCK epithelial cells onto two dimensional flat topographies. After 48hrs incubation, the initial melange of cells had undergone a distinct cell type separation creating a two-layered system. The first layer was a well dispersed epithelial monolayer of MDCKs. The second layer, on the other hand, was a complex structure of aggregated NIH3T3s throughout the system. As can be seen in Fig 2.1A, this aggregating behaviour is unlike their normal growth pattern (Fig 2.4B), which usually forms large meshes consistent with connective tissue. The morphology and behaviour of MDCK cells however appears unaffected in coculture. To further simplify the patterning system from the dynamic biological complexities presented by cell proliferation, we plated a high density 1:1 mixture of cells types with the addition of a mitosis inhibitor. Mitosis inhibited cocultures (Fig 2.5) demonstrate the exact same cell patterning which suggests that this cell type separation does not evolve from cell division. To further investigate the potential influence of biological mechanisms in this cell type separation phenomenon, we performed a set of cytoskeleton inhibition experiments. Preventing myosin II contraction which has been shown to be a key protein in migration and tissue architecture demonstrated a slight change in altered patterning behaviour however this was not statistically significant ($p>0.05$). The same is true for when inhibiting de novo forming actin polymerization. Two hypothesis can be inferred from these results. First, the spontaneous patterning observed in coculture is not actively guided via migration,

as this would require a properly functioning cytoskeleton. Studies have shown how exposure to Blebbistatin and SMIFH2 causes substantially decreased migration in addition to lowering focal adhesion turnover[161–163]. Secondly, although inhibition of actin contraction and polymerization did occur through myosin II and formin, compensatory mechanisms mitigated the overall effects on cell organization. Cross-talk between effector pathways and feedback inhibition is ubiquitous in normal signal transduction. When signaling is blocked, regulatory loops can up-regulate parallel pathways to compensate, permitting the cellular response to be dynamic and adaptive[164]. It is for this reason that the statistically different results observed with Y-27632 inhibition are highly revealing of the mechanisms at play. ROCK is a high level pleotropic regulator of multiple signaling pathways mediating cytoskeleton reorganization[165], stress fiber formation[166], cell contraction and cell polarization[61]. Its inhibition results in a widespread downregulation of the various direct and indirect pathways regulating the cytoskeleton[61]. The increase in cell patterning suggests that cytoskeletal involvement is unlikely and that some other governing mechanism is driving the observed effect.

It has been established that ROCK is involved in the maturation of focal adhesions (FA). These FA are multiprotein complexes serving as transmembrane links between the extracellular matrix and the actin cytoskeleton. During the initial stages of adhesion, FA maturation involves a sequential cascade of compositional changes[167]. ROCK, on the other hand, promotes FA maturation through tension induced conformational changes[168]. This conformation change allows the recruitment of key proteins including talin, paxillin and vinculin into the FA complex. As a result, the cell is capable of forming mature adhesion sites strengthening their cell-substrate binding affinity. Inhibiting ROCK via Y-27632 may sufficiently reduce cell-substrate affinity in NIH3T3s, causing cells to depend more highly on their cell-cell binding properties for adhesion. This is supported by our computer simulation results which showed that the impact of Y-27632 can be reproduced simply by lowering the cell-substrate adhesion

from 0.5 to 0.3: modulating this binding adhesion induced an increase in the cell type separation of cocultured cells as observed in vitro.

ROCK has also been shown to be intimately involved in the regulation of cadherin ligation in epithelial cells[169]. As an epithelial cell line, MDCKs possess the E-cadherin superfamily of cellular adhesion molecules. These transmembrane glycoproteins mediate specific cell-cell adhesion, functioning as key molecules in the morphogenesis of a variety of organs[170,171]. E-cadherins are not passively distributed on the surface of the plasma membrane, but rather localize at cell-cell contacts in response to adhesion. This focalizing mechanism is dependent on functionally linked cytoplasmic regulators, of which ROCK is involved[169]. During adhesion, two distinct patterns of cadherin clusters form, fine punctate and larger streak-like macroclusters. Inhibition of ROCK activity preferentially abolishes the macroclusters which form the termini for prominent actin bundles which resemble the rapid loss of E-cadherin from cell-cell contacts[172,173] This is crucial as it has been shown that E-cadherins can heterotypically bind to N-cadherins during epithelio–fibroblast contact but that these links are highly transient[174]. As epithelial cells strongly form their cell-substrate bonds, they spread and occupy the entire cell-surface interface causing NIH3T3s to phase separate above. Consequently, fibroblasts are highly dependent on the E-N cadherin heterotypic binding to allow adherence. By inhibiting ROCK, the E-cadherin focalizing mechanism that promotes cell-cell contacts is downregulated, resulting in poor adhesion between cell types. As such, NIH3T3s become highly dependent on their homotypic N-cadherin binding and form larger patterned aggregates.

This result is in accordance with previously observed homophilic type binding which favors thermodynamically stable patterns[138,139,150,171]. Cells present a higher affinity to other cells that share their unique cadherin subfamily configuration. This differential adhesion leads to a system with lower interfacial free energy[138,160,171]. It is the differential adhesive strength of these binding affinities that we hypothesize creates a two layered cell type separation.

To test whether this two-dimensional patterning phenomenon could result from a minimization of interfacial free energies between binding affinities, we developed a kinetic Monte Carlo simulation. Binding parameters were chosen by translating the homotypic, heterotypic and substrate adhesion forces into relative binding energies. MDCKs' cell-cell and cell-substrate binding are significantly stronger than the transient bonds that NIH3T3s transiently break in order to migrate[174]. Based on this, we have simulated a co-cultured system whereby cellular movement is solely driven by differential binding affinities. The result is a two layered system in which there is a distinct partition between cell types (Fig 2.3). Cell type 1 (MDCK) are dispersed and remain adjacently adhered to the substrate whilst cell type 2 (NIH3T3) form aggregates layered above. The simulated cell patterning is similar to what the experimental results showed, which suggests that differential adhesion may be sufficient to dictate cellular organization patterning.

It is not surprising that complex cellular organizational processes such as embryogenesis and tissue repair are governed by mechanisms that exceed any single model of migration. The results shown here however suggest that in cocultured systems, cell-cell and cell-substrate binding affinities are highly influential in dictating cell morphogenesis. We hypothesize that there is a constant interplay between physical forces and biological signaling cues within the microenvironment. Together, they inform the cell's sensory perception of its surroundings and dictate cellular behaviour. The future lies in further elucidating the balance of this interplay and to more comprehensively understand the mechanisms by which they function.

2.5 MATERIALS AND METHODS

2.5.1 CELL CULTURE AND DRUG STUDIES

NIH3T3 mouse fibroblast cells (ATCC® CRL-1658™) and Madin Darby Canine Kidney (MDCK) epithelial cells were cultured in high glucose DMEM containing 10% Fetal

Bovine Serum (FBS) and 1% penicillin/streptomycin antibiotics (all from Hyclone). The cells were cultured at 37 °C and 5% CO2 in 100 mm dishes. Monoculture experiments were performed by seeding ~20 000 cells/cm^2 on tissue culture treated petri dishes for 48 hrs. Cocultures of NIH3T3 and MDCK cells were thoroughly mixed and seeded at equal densities of ~10 000 cells/cm^2 and subsequently imaged in the same manner as monoculture experiments. Inhibition studies of ROCK (Y-27632; 10 µM in dH_2O, Sigma, Catalogue #Y0503), Myosin II (Blebbistatin; 10 µM in DMSO, Sigma, Catalogue #B0560) and mDia (SMIFH2; 10 µM in DMSO, Sigma, Catalogue #S4826) were all performed by exposing both cell types for the 48 hrs incubation time period.

2.5.2 Immunofluorescence staining and microscopy

Coculture experiments were performed by pre-loading NIH3T3s and MDCKs with CellTracker Green CMTPX dye (Invitrogen, Catalogue #C34552) and CellTracker Red CMFDA dye (Invitrogen, Catalogue #C7025), respectively. After a 48 hr incubation period, the dyes were removed and the cells were rinsed three times with DMEM. Cells were then trypsinized and plated on the microchanneled grooves as describe in section 2.2. After 48hrs, cells were fixed with 3.5% paraformaldehyde and stained with Dapi (Invitrogen, Catalogue #D1306).

Monoculture experiments were fixed after 48hrs incubation with 3.5% paraformaldehyde and permeabilized with Triton X-100 at 37°C. Cells were stained for actin using phalloidin Alexa Fluor 488 & 546 (Invitrogen, Catalogue # A12379 & #A22283) and DNA was stained using DAPI. A full protocol has been published previously [175]. Samples were then mounted using Vectashield (Vector Labs) and a #1 coverslip placed on top. Samples were then inverted and imaged with a Nikon Ti-E A1-R high-speed resonant laser scanning confocal microscope (LSCM) with a phase contrast 10x NA0.3 objective or a DIC 60x NA1.2 water immersion objective. For high resolution three dimensional image capture of cocultured cells, NIH3T3 GFP (Cedarlane, #AKR-214) were used with MDCKs and subsequently fixed, stained and imaged as described above.

2.5.3 Parallel Plate Flow Assay

A polydimethylsiloxane (PDMS) microfluidic flow chamber, 1000 mm in width, 160 µm in height and 20 mm long, was produced using standard microfabrication techniques. Liquid-state 1:10 ratio PDMS was poured on the master and cured for 2 hours at 70°C. Inlets and outlets, 0.75 mm in diameter, were punched at both ends of the chamber. The PDMS layer was bonded to a standard glass microscope slide after being plasma treatment (50 W for 30 sec), creating an enclosed channel. The entire chamber was submerged in media and cells were then pipetted at a seeding density of ~4 million/ml each. Cells were cultured inside the chamber overnight. Y-27632 (10 µM) was added to the cells prior to seeding so as to expose the cells until the flow assay. The cells were exposed to an average flow of 1µl/s, for 30 min, which corresponded to a shear stress at the wall of the chamber of 0.2 Pa [42]. The flow rate was then increased to 13 µl/s (3 Pa) for an additional 15 min. Images were captured every 5 minutes from the same region of interest before, during and after exposure to shear stress.

2.5.4 Image and statistical analysis

A Kolmogorov-Smirnoff (K-S) test was performed for each study case in order to determine if they exhibited patterned formation. Analysis consisted of partitioning the image samples into 100 quadrats, whereby the number of each cell type per quadrat was recorded and the corresponding cumulative distribution function was calculated (F_{exp}) [176]. The absolute maximum difference D compares F_{exp} and the cumulative distribution function of a Poisson distribution ($F_{Pois.}$):

$$[1]\quad D=\left|max\left(F_{exp}\right)-max\left(F_{pois.}\right)\right|$$

Each D was computed independently for epithelial cells (type 1) and fibroblast cells (type 2) in the *in vitro* experiments and simulation model. For a value of D above 0.195, we rejected the null hypothesis of a random distribution at a 99.9% confidence threshold, and concluded that the cells exhibit a patterning. For a D value below 0.136 (corresponding to the 95% confidence threshold), we concluded that the cells were

randomly distributed. The reader can consult cachet et al.[151] for further details . All statistical analyses were carried out using *ImageJ*. In addition to the K-S distribution test, we quantified the cell type separation of the two cell types in the computational simulation.

2.5.4 Kinetic Lattice Monte Carlo Simulations

Through the use of Kinetic lattice Monte Carlo (KMC) simulations[177,178], we have modeled the morphological "evolution" of a binary system with $N = N_1 + N_2$ cells initially deposited on a two dimensional (2D) flat substrate, where the $N_1$and N_2type cells are analogous to NI3T3s and MDCKs, respectively, used in both the untreated and Y-27632 *in vitro* experiments. Each cell occupies a three dimensional (3D) cubic lattice site of volume $a^3 = 1$. Initially, each lattice site on the surface has a 0.95 uniform probability of being occupied by a cell of type 1 or type 2 (0.475 each) and a 0.05 probability of being unoccupied (in our case, an unoccupied lattice space is analogous to a cell media element). We used a simulation box of volume $V = L_X \cdot L_Y \cdot L_Z$ (50·50·10) with lateral periodic boundary conditions in x and y. For boundary conditions in z, the position z = 0 represents the flat substrate whilst a sufficiently large L_z was chosen to ensure that no cell touch the upper boundary condition during the simulation.

Cells may only move to a first nearest-neighbor free lattice site[179] (corresponding to a lattice site being occupied by cell media), such that two cells cannot simultaneously occupy the same site. However, cell motion can only be accepted if the moving cell remains in the vicinity of either another cell or the substrate (vicinity is defined as being a first- or a second -nearest neighbor); in other words, cells are not allowed to swim freely in solution.

Cells of type i, where *i*=1,2, can form bonds with cells of the same type (homotypic binding energy: ε_{ii}) or of the other type (heterotypic bond energy: ε_{if} with $i \neq j$). We also account for the interactions between the cells and the substrate (substrate binding energies: ε_{is}) and we set the interaction energy with the surrounding media at

zero[180]. Moreover, one does not treat the substrate energy since it has no internal degree of freedom. For each cell *i*, we define an energy barrier to be overcome to complete a move, $E_b = n_{i1}\varepsilon_{i1} + n_{i2}\varepsilon_{i2} + n_{is}\varepsilon_{is}$, where n_{ij} (j = 1,2) are the number of first neighbors of each type. Given this energy barrier, each cell is assigned a transition rate given by

$$[2]\ \Gamma = \omega_0 e^{\frac{-E_b}{E_m}},$$

which only depends on the initial energy configuration, a constant attempt frequency ω_0 and the typical energy of biological fluctuations E_m [181]. The latter characterizes cell motility driven by cytoskeleton motion (E_m is equivalent, from a thermodynamic perspective, to the thermal energy $(k_B T)$. As defined by [3], the transition rates allow to reach the equilibrium state which corresponds to a configuration with a minimum surface/interface energy[182,183]. The reader can consult[178,182] for further details on the KMC algorithm used.

2.5.5 KMC PARAMETERS

All the energy parameters are expressed in E_m units. The values of the binding energies were chosen in order to semi-quantitatively reproduce the experimental observations, in both untreated and Y-27632 experiments. We assumed that the binding energies between homotypic cells are comparable to E_m. MDCK cells (type 2) are known to strongly interact with the substrate and form a 2D monolayer. Based on this, the binding energies have to be chosen in order to verify $\varepsilon_{2s} > \frac{\epsilon_{22}}{2}$ and $\varepsilon_{2s} \gg E_m$, $\varepsilon_{2s} \gg E_B$. On the other hand, NIH3T3 cells (type 1) can form homotypic 3D clusters on the substrate and over the MDCKs. This condition suggests that the binding energies have to be chosen to verify that $\frac{\varepsilon_{11}}{2} \gg \varepsilon_{1s}$, $\varepsilon_{12} \geq \varepsilon_{1s}$ and $\varepsilon_{2s} > \frac{\varepsilon_{12}}{2}$. To simulate the effect of the ROCK inhibition, we used the untreated parameters as a set baseline and lowered ε_{1s} to replicate the inhibitory effects of Y-27632. Finally, to be consistent with the DAH whereas cell type separation is expected between cell type with non-equal

binding energies, we must verify that $\varepsilon_{12} < \frac{\varepsilon_{11}+\varepsilon_{22}}{2}$. Numerical values are shown in Table 1.

TABLE 2.5.5.1: PARAMETER VALUES FOR THE BINDING ENERGIES. SUBSCRIPT I REFERS TO CELL TYPE 1 AND 2, S TO A SUBSTRATE LATTICE SITE"

Binding energy	Values (in units of E_m) Untreated / Y-27632
ε_{11}	1.05 / 1.05
ε_{22}	4 / 4
ε_{12}	1.5 / 1.5
ε_{1s}	0.5 / 0.3
ε_{2s}	5 / 5

2.6 ACKNOWLEDGEMENTS

S.H. was supported by the Queen Elizabeth II Graduate Scholarship in Science and Technology. A.E.P. gratefully acknowledges generous support from the Canada Research Chairs program. This work was also supported by the Natural Sciences and Engineering Research Council of Canada (NSERC) Grant No. RGPIN/046434-2013 to G.W.S and RGPIN/355535 to A.E.P. We would also like to acknowledge the University of Ottawa for their generous support.

Chapter 3 | Manuscript

Three dimensional spatial separation of cells in response to microtopography

Alexandre Leclerc[1], Dominique Tremblay[1], Sebastian Hadjiantoniou[1], Nickolay V. Bukoreshtliev[1], Jacob L. Rogowski[1] , Michel Godin[1,2], Andrew E. Pelling[1,2,3]

[1]Department of Physics, MacDonald Hall, 150 Louis Pasteur
[2]Ottawa-Carleton Institute for Biomedical Engineering, Colonel By Hall, 161 Louis Pasteur
[3]Department of Biology, Gendron Hall, 30 Marie Curie,
[4]Institute for Science, Society and Policy, Simard Hall, 60 University, University of Ottawa

Submitted June 15th 2013 to Biomaterials

Published July 27th 2013, V 34. (8097-8104)

Motivation & Objectives |

Having previously identified the influence that physical binding affinities can have in cocultured flat topographies, we introduce complex three dimensional confined geometries to the system. We modulate the levels of confinement in the effort to understand the effects it imposes on the cell behavior.

My 3rd authorship here is because the research for this paper had begun shortly before my arrival to the lab. This work led to the development of chapters 4 and was complementary to my work in chapter 2. As such, it is a pivotal part of this thesis.

3 | THREE DIMENSIONAL SPATIAL SEPARATION OF CELLS IN RESPONSE TO MICROTOPOGRAPHY

3.1 ABSTRACT

Cellular organization, migration and proliferation in three-dimensions play a critical role in numerous physiological and pathological processes. Nano- and micro-fabrication approaches have demonstrated that nano- and micro-scale topographies of the cellular microenvironment directly impact organization, migration and proliferation. In this study, we investigated these dynamics of two cell types (NIH3T3 fibroblast and MDCK epithelial cells) in response to microscale grooves whose dimensions exceed typical cell sizes. Our results demonstrate that fibroblasts display a clear preference for proliferating along groove ridges whereas epithelial cells preferentially proliferate in the grooves. Importantly, these cell type dependent behaviors were also maintained when in co-culture. We show that it is possible to spatially separate a mixed suspension of two cell types by allowing them to migrate and proliferate on a substrate with engineered microtopographies. This ability may have important implications for investigating the mechanisms that facilitate cellular topographic sensing. Moreover, our results may provide insights towards the controlled development of complex three-dimensional multi-cellular constructs.

3.2 INTRODUCTION

The physical properties of the cellular microenvironment play a crucial role in governing numerous critical physiological and pathological pathways[5,184–186]. In vivo, cells are exposed to and reside in an intricate mesh of proteins known as the extracellular matrix (ECM)[187]. It is well known that complex physical and biochemical interactions between cells and their ECM regulate differentiation, proliferation and migration [5,101,185,186,188]. Moreover, the physical properties of the ECM, such as matrix topography and mechanical properties, also play a major role in modulating cell biology [66,100,189–193]. In the laboratory, cells are traditionally cultured on flat two-dimensional

surfaces. In comparison to the in vivo matrix microenvironment, these surfaces often lack the complex nano- and micro-scale topographies found in vivo. Indeed, engineered substrates with tunable nano- and micro-scale topographies are now becoming extensively employed in many studies [100,194]. Substrate topography can be modulated in numerous ways, including altering surface roughness through chemical or plasma treatments to creating long-range ordered features with micro- and nano-scale fabrication approaches[194].

Cellular responses to nanoscale topographies have been extensively studied and may have the potential in aiding elucidation of complex control mechanisms involved in many biological pathways[195]. Fabricated nanoscale grooves, holes and pillars arranged in ordered patterns or in spatial gradients have all been employed to study cellular responses to topography[100,189,196]. Importantly, as these structures are far smaller than typical cell size, an individual cell will be exposed to many features at any given time. It has been observed that cells display an exquisite sensitivity to nanoscale changes in aspect ratio, density and spacing of these features, often in a cell-type dependent manner[193]. For example, nanoscale grooves will affect the alignment and migration dynamics of many cell types (such as fibroblasts, neurons and smooth muscle cells)[100,104,196]. This is a process known as contact guidance[197] and has been observed in response to both micro- and nano-scale topographic features. In vivo, migration is extremely important in many physiological and pathological processes (such as cancer metastasis, wound healing and embryogenesis) and is highly sensitive to the nanotopography of the ECM [100,189,192]. In addition to cell morphology and migrations, nanoscale grooves also modulate subcellular organization of the cytoarchitecture as well as numerous signaling pathways[23,198,199]. In several cases, cell proliferation has also been observed to display sensitivity to substrate topography in many cell types[200–203]. Finally, during very complex processes, such as stem cell differentiation, it is becoming clear that stem cell fate is influenced by the integration of a multitude of nanotopographical, physical and biochemical cues[101–103,105,199].

In contrast to previous work investigating the role of topographical cues smaller than the typical length scale of a cell, a large number of studies have employed substrates with microscale topographies[66,69,192,194,200,204–206]. In many studies, surfaces containing grooves whose geometries (depth, width and ridge width) can vary in a range of less than 10μm to greater than 100μm have been employed to demonstrate effects on cell alignment, migration and organization. Importantly, as the groove sizes become larger than a typical cell, this allows for the appearance of several phenomena. Cells not only align with the direction of the grooves, but have also display bridging behavior. Bridging behavior occurs when fibroblast preferentially migrate and proliferate along groove ridges to form bridges from one ridge to another or between the bottom of the groove and the top of a ridge[204,205]. Moreover, bridging also occurs when cells form a connection between the bottom of the groove and the top of a ridge[205]. This type of behavior is very much dependent on the geometric properties of the grooves and in the case of fibroblasts, at least three distinct geometric regimes of behavior have been characterized[205].

Here, we microfabricated a series of 50μm deep grooves with increasing widths (25, 50, 100 and 500μm) and 100μm wide ridges. In contrast to previous studies, we compared the influence of these substrates on two distinct cell types (NIH3T3 fibroblast and MDCK epithelial cells). NIH3T3 cells are highly motile and lack the strong cell-cell coupling and tight junctions found in MDCK cells. Therefore, we hypothesized that the two cell types may display distinct responses to substrate topography. Cells were cultured on the grooved substrates and were examined after 4, 24, 48 and 72 h of culture. At each time point we quantified the three-dimensional cellular alignment and organization for each cell type on each substrate. Finally, as multiple cell types are found in close contact in vivo, we also grew co-cultures of cells on the substrates. This approach allowed us to examine the influence of contact guidance in a mixture of fibroblast and epithelial cells.

3.3 RESULTS

3.3.1 MICROFABRICATED SUBSTRATES WITH MICROSCALE TOPOGRAPHY FOR CELLULAR CONFINEMENT

In this study, the effects of micron scale surface topography and confinement on cell localization were investigated with PDMS substrates. Substrates were fabricated using standard soft lithography procedures (Fig 3.1A-E). In all cases cells were seeded onto substrates that possessed a surface topography with 50µm deep grooves and 100µm wide ridges (Fig 3.1F). The ridges were spaced at defined pitch to create 25, 50 or 100µm grooves. In this context, cells are exposed to confinement geometries that are ~2-10 times larger than the typical length scale of an individual cell. Cells were then imaged 4, 24, 48 and 72h after seeding to investigate how microscale confinement affects cellular localization. In contrast to previous studies, here we investigated the response of two cell types (NIH3T3 fibroblast and MDCK epithelial cells) alone or in coculture. These cell types were specifically chosen, as NIH3T3 fibroblasts are highly motile[51,161], whereas MDCK epithelial cells are strongly interacting, forming strong cell-cell contacts and stable monolayers[207,208]. For the purposes of this study, we defined localization in the grooves if cells were found on the bottom or sidewall surfaces occurring between the ridges (Fig 3.1E). Conversely, localization on ridges was defined as cells being found on the top 100µm ridge surface (Fig 3.1F). In both cases, minutes after seeding, cells were always found to sink to the bottom of the grooves, simply due to their higher density than the surrounding medium. In this initial state, cells were easily confined to the grooves by the 50µm ridge height. Cells were then placed in a culture incubator and examined at the time points described above. The 4-h time point was found to be the earliest time at which cell surface interactions were strong enough to allow for reproducible staining and imaging.

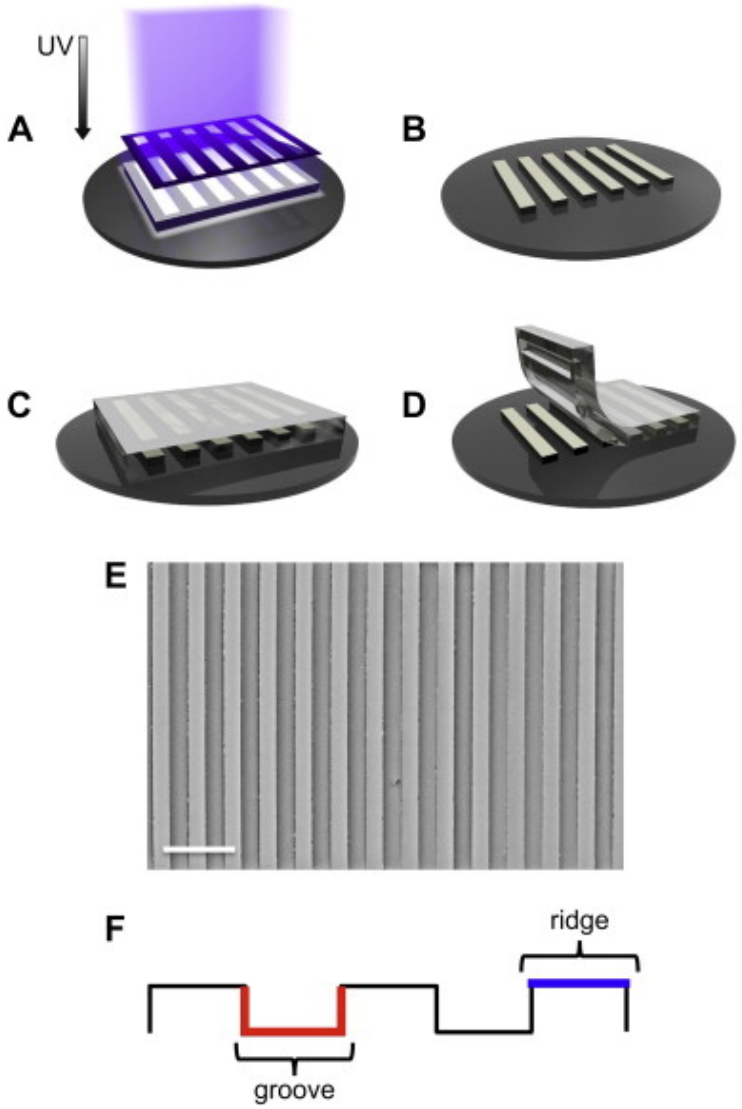

FIGURE 3.1 MICROFABRICATION OF MICROSCALE GROOVES IN PDMS.
(A) After spin coating a 50 µm thick SU8 photoresist onto a silicon wafer, UV light is shone through a mask to crosslink exposed areas. (B) After developing the wafer, un-crosslinked SU8 is removed leaving behind rectangular features. (C) PDMS is poured over the features and cured. (D) The PDMS is then peeled from the substrate and the substrate microtopography is then functionalized with collagen. (E) A top-down SEM image of the PDMS substrate reveals the structure of a typical microtopography with 100 µm grooves and ridges. (F) For the purposes of this study we defined cells as in a 'groove' (red region) or on a 'ridge (blue region), as shown in the schematic. (For interpretation of the references to colour in this figure legend, the reader is referred to the web version of this article.)

3.3.2 CELL TYPE DEPENDENT RESPONSES TO MICROSCALE CONFINEMENT

At each time point, cellular actin and nuclei were fluorescently labeled and imaged with laser scanning confocal microscopy (LSCM). LSCM images provide information on the three dimensional location of individual cells in the microscale features. In this study, we quantified the number of cells found on the ridges or within the grooves. A total of n = 3 independent substrates were prepared for each groove width and 3 randomly chosen regions were imaged on each sample with LSCM. Therefore, we counted cell locations in a total of 9 images for each groove width and each cell type. NIH3T3 cells display a clear response to surface topography for all groove widths (Fig 3.2A-C). In all cases, we have falsely coloured the actin of cells found within the grooves (red) and on the ridges (green) in order to provide a visual reference. NIH3T3 cells are found to be highly localized within the grooves after 4 h of culture time, however, by 48 h, cells have migrated specifically to the ridges and become highly confluent. It is clear that after 48 h of culture, NIH3T3 cells display a clear preference to the ridge surfaces. Very few cells are found within the grooves even though the ridges are highly crowded. In some cases cells were observed to form ridge-to-ridge ridges over grooves, consistent with previous studies[204,205]. On the other hand, a vastly different response is observed in MDCK cells (Fig 3.3A-C). Consistent with the NIH3T3 cells, MDCK cells are found in large numbers in the grooves after only 4 h of culture. However, after 48 h of culture, MDCK cells continue to be found in the grooves in high proportions and at high density, whereas only a small fraction of cells are found on the ridges by 48 h. Clearly, these two cell types display distinct responses to confinement in microscale geometries.

Using the nuclei to count cells, we calculated the ratio of the number of cells growing on the ridges to the number of cells growing in the grooves, as a function of time, for all substrate geometries. The Ridge/Groove ratio reveals that after ~24 h of culture, the majority of NIH3T3 cells are found preferentially on the ridges (Ridge/Groove ratio > 1) on substrates with 25µm and 50µm wide grooves in

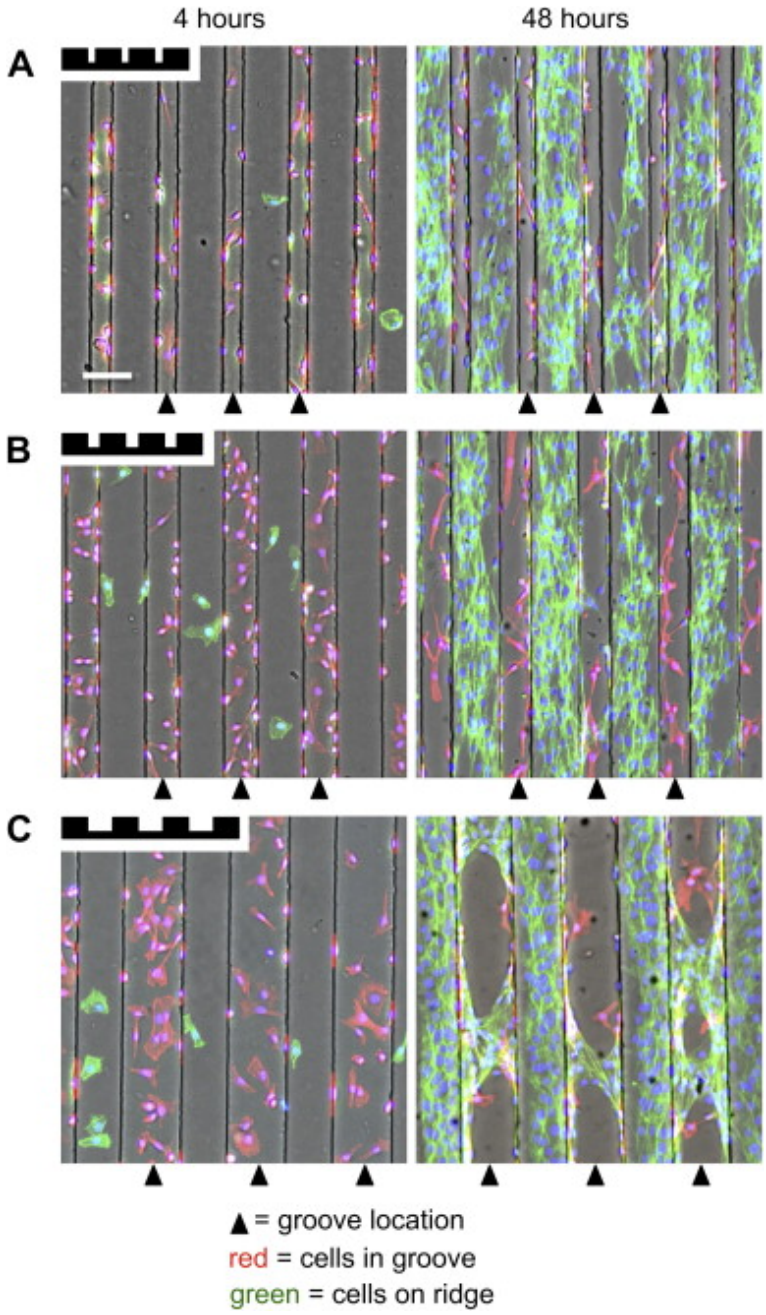

FIGURE 3.2 CULTURED NIH3T3S ON CHANNELED PDMS TOPOGRAPHIES.
NIH3T3 cells were cultured on the (A) 25 µm, (B) 50 µm and (C) 100 µm wide grooves for 4, 24, 48 and 72 h, subsequently stained for actin and cell nuclei and imaged the LSCM. Nuclei are shown in blue and actin is coloured red for cells growing within the grooves and coloured green for cells growing on the ridges (triangles indicate the grooves). Images are shown for cells cultured for 4 and 48 h. Triangles indicate the bottom surface of the grooves. Scale bar in (A) = 100 µm and applies to all. NIH3T3 cells display a clear preference for migrating and proliferating on the ridges.

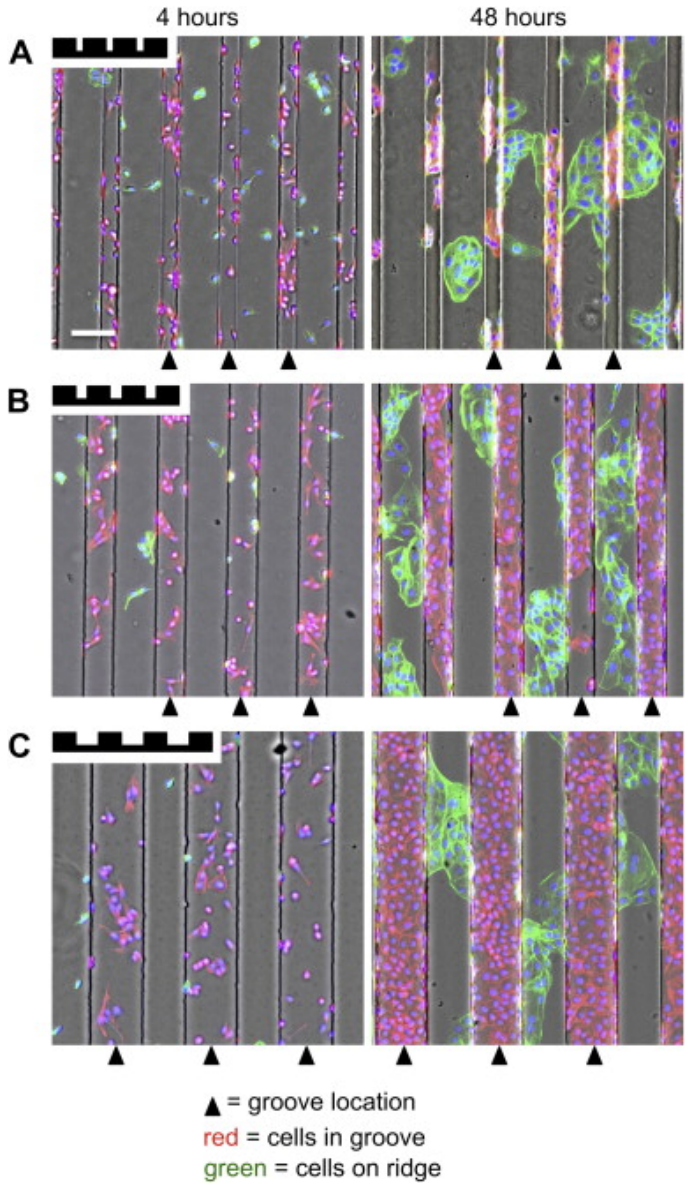

FIGURE 3.3 CULTURED MDCKS ON CHANNELED PDMS TOPOGRAPHIES

MDCK cells were cultured on the (A) 25 mm, (B) 50 mm and (C) 100 mm wide grooves for 4, 24, 48 and 72 h, subsequently stained for actin and cell nuclei and imaged the LSCM. Nuclei are shown in blue and actin is coloured red for cells growing within the grooves and coloured green for cells growing on the ridges (triangles indicate the grooves). Images are shown for cells cultured for 4 and 48 h. Triangles indicate the bottom surface of the grooves. Scale bar in (A) ¼ 100 mm and applies to all. MDCK cells display a clear preference for migrating and proliferating within the grooves. (For interpretation of the references to colour in this figure legend, the reader is referred to the web version of this article.) ridges

comparison to the 100µm grooves (Fig 3.4A). After 48 h of culture a statistically significant difference appears when comparing the Ridge/Groove ratio between the 100µm and the 25µm grooves ($p < 0.01$) but not the 50µm grooves ($p > 0.9$). However, by the 72h time point, the Ridge/Groove ratio approaches w2 in all cases with no significant dependence on groove width ($p > 0.2$ in all cases). In contrast, MDCK cells display a different response to microscale topography when compared to NIH3T3 cells. In all cases, the Ridge/Groove ratio slowly approaches 1 over the 72h time course (Fig 3.4B). However, cells cultured on the 25µm grooves approach 1 more rapidly and become significantly different from the 50µm and 100µm grooves by 48 h of growth ($p < 0.05$ in both cases). Similar to the NIH3T3 cells, there is no statistically significant dependence of the Ridge/Groove ratio on groove width ($p > 0.2$ in all cases). Importantly, when NIH3T3 cells are cultured on substrates where the groove width is increased to 500µm, cells no longer display any preference for migrating and proliferating on the ridges (Fig 3.4C). Unsurprisingly, MDCK cells are still found within the 500µm grooves (Fig 3.4D). Finally, when cells were allowed to propagate until covering the entire surface (~120 h of growth), two distinct morphologies were observed. NIH3T3 (Fig 3.5A, B) and MDCK (Fig 3.5C,D) cells growing to confluence on the 50µm grooves and are representative of the morphologies observed on the 25 and 100µm grooves. In the case of MDCK cells, a complete cell monolayer formed after 120h and covered the entire grooved substrate. The monolayer was observed to match the surface topography with cells observed along all surfaces of the grooves and ridges. Conversely, NIH3T3 cells were first observed to grow to confluence along the ridges, eventually forming bridges. After 120h of culture cells were observed to completely fill the grooves.

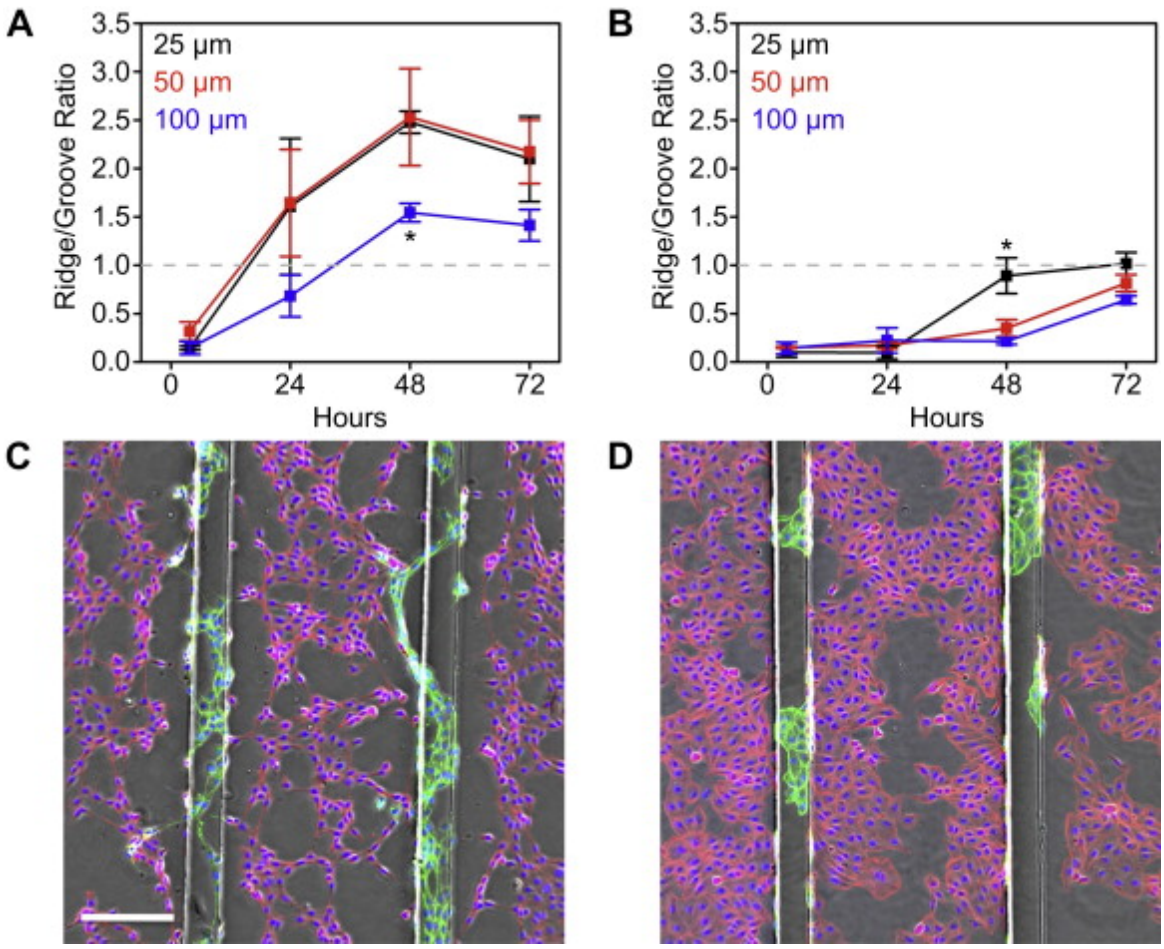

FIGURE 3.4 RIDGE TO GROOVE RATIOS OVER 72HRS OF NIH3T3S AND MDCKS.

The number of cell growing within the grooves or on the ridges was determined and a Ridge/Groove ratio was calculated for the 25µm (black), 50µm (red) and 100µm (blue) wide grooves. (A) The Ridge/Groove ratio for NIH3T3 cells demonstrates that the cells rapidly move to the ridges. By 48 h the Ridge/Groove ratio is significantly (*) higher for the 25 and 50µm grooves compared to the 100µm grooves. (B) The Ridge/Groove ratio for MDCK cells demonstrates that the cells preferentially localize within the grooves. By 48 h, the Ridge/Groove ratio is significantly (*) higher for the 25µm grooves compared to the 50 and 100µm grooves. (C) NIH3T3 and (D) MDCK cells cultured on 500µm wide grooves for 48 h (scale bar = 250µm and applies to both images). Nuclei are shown in blue and actin is coloured red for cells within the grooves and green for cells are on the ridges. (For interpretation of the references to colour in this figure legend, the reader is referred to the web version of this article.)

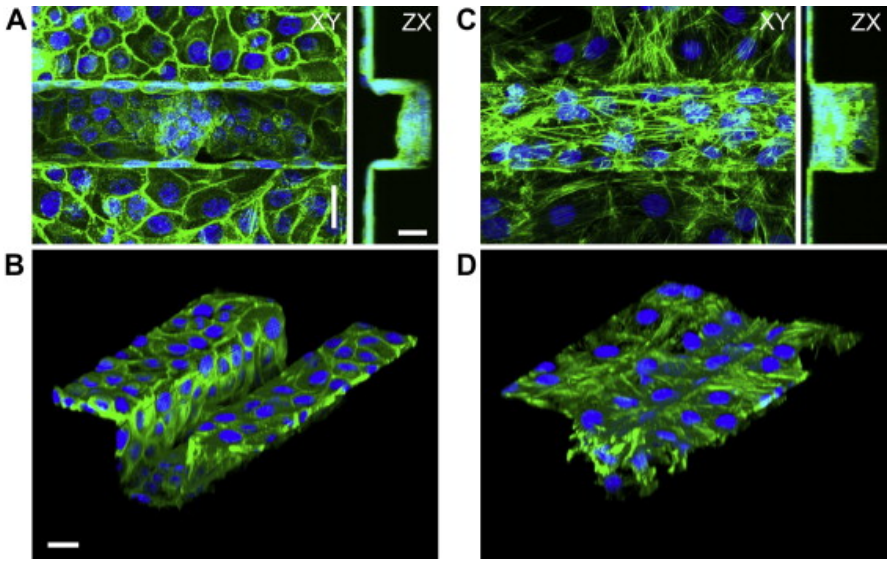

FIGURE 3.5 ORTHOGONAL AND PERSPECTIVE IMAGES OF NIHT3S CULTURE IN CHANNELED TOPOGRAPHIES.

Images of actin (green) and nuclei (blue) for (A, B) MDCK and (C, D) NIH3T3 cells after growing for 120 h on 50µm wide grooves (scale bars = 25µm and apply to all, results are representative of all groove sizes). MDCK cells for a continuous two-dimensional sheet, closely matching substrate topography whereas NIH3T3 cells fill the grooves and completely cover the substrate. This behaviour is clearly observed in the three-dimensional rendering of the LSCM data in (B) and (D). (For interpretation of the references to colour in this figure legend, the reader is referred to the web version of this article.)

3.3.3 CELLULAR ALIGNMENT IN MICROSCALE GROOVES

In order to quantify cellular alignment, we characterized the orientation of cell nuclei computationally by first calculating the angle (q) formed between the long axis of each elliptical nucleus and the groove direction. We then calculated the degree of alignment by using an approach commonly employed when characterizing the preferred directionality in liquid crystals. The average value of the second order Legendre polynomial was calculated using the orientation of each nucleus in a field of view [38]:

$$S = \langle \frac{3cos^2\Theta - 1}{2} \rangle$$

In a given population of cells, S will approach 0 if they are randomly oriented with respect to the groove direction. Conversely, S will approach 1 if there is a strong degree of alignment between the groove direction and the cells. Finally, if the cells are aligned perpendicular to the groove direction, S will approach -0.5. Therefore, S

provides a quantitative measure of the degree of alignment parallel or perpendicular to the groove direction or if the cell population lacks significant alignment. NIH3T3 or MDCK cells were allowed to proliferate on 25, 50, 100 and 500μm wide grooves for 48 h at which point the cells were fixed and stained. A total of n = 3 independent substrates were prepared for each groove width and 3 randomly chosen regions were imaged on each sample with LSCM. Therefore, an average order parameter was calculated from cells in a total of 9 images for each groove width and each cell type (Fig 3.6). NIH3T3 cells displayed a strong degree of alignment ($S = 0.80 \pm 0.04$), with no significant dependence on the 25, 50 and 100μm grooves ($p > 0.6$ in all cases). On the other hand, MDCK cells displayed a smaller degree of alignment ($S = 0.58 \pm 0.04$) compared to NIH3T3 cells ($p < 0.01$ in all cases), with no significant dependence on groove widths ($p > 0.3$ in all cases). Finally, NIH3T3 and MDCK cells cultured on grooves of 500μm displayed a statistically significant decrease in alignment compared to the 25, 50 and 100μm grooves ($S = 0.30 \pm 0.03$ and 0.36 ± 0.03, respectively, $p < 0.01$ in all cases) with no cell-type dependence ($p > 0.7$)

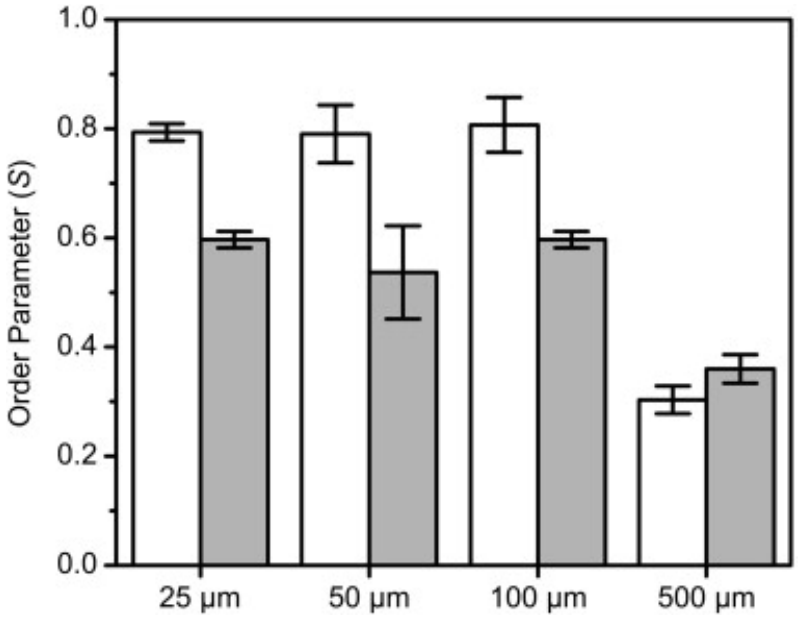

FIGURE 3.6 ORDER PARAMETER INDICATING CELLULAR ALIGNMENT ALONG CHANNELS
An order parameter (S) was calculated for NIH3T3 (white bars) and MDCK (grey bars) using cell nuclei as indicators of orientation with respect to the groove direction. An order parameter approaching 1 indicates a high degree of parallel alignment between cells and the groove direction. Conversely, an order parameter approaching 0 indicates a high degree of perpendicular alignment between cells and the groove direction. On the 25, 50 and 100µm grooves, both cell types display a strong degree of alignment with the groove direction. Conversely, alignment was significantly diminished on the 500µm grooves.

3.3.3 CONFINEMENT GUIDANCE IN CO-CULTURES

To further investigate the cellular response to confinement, we co-cultured NIH3T3 and MDCK cells and exposed them to substrates with defined microscale topography. In all cases, NIH3T3 cells were pre-loaded with a green fluorescent cell tracker dye prior to co-culture and prior to imaging, all cell nuclei were labeled with the DNA specific Hoechst 33342. This approach allowed us to positively identify individual cells as either NIH3T3 or MDCK. Imaging reveals that even in the presence of a co-culture, the majority of cells continued to display a clear preference for growing on the ridges or in the grooves. Phase contrast and fluorescence imaging reveals that after 48 h of co-culture on 100µm wide grooves, NIH3T3 cells display a clear preference to migrate and grow on the ridge surfaces (Fig 3.7A). At the same time, MDCK cells are clearly observed in the grooves (Fig 3.7B). This is in contrast to co-cultured cells grown on flat

PDMS surfaces. In this case NIH3T3 and MDCK cells are observed to distribute heterogeneously (Fig 3.7C).

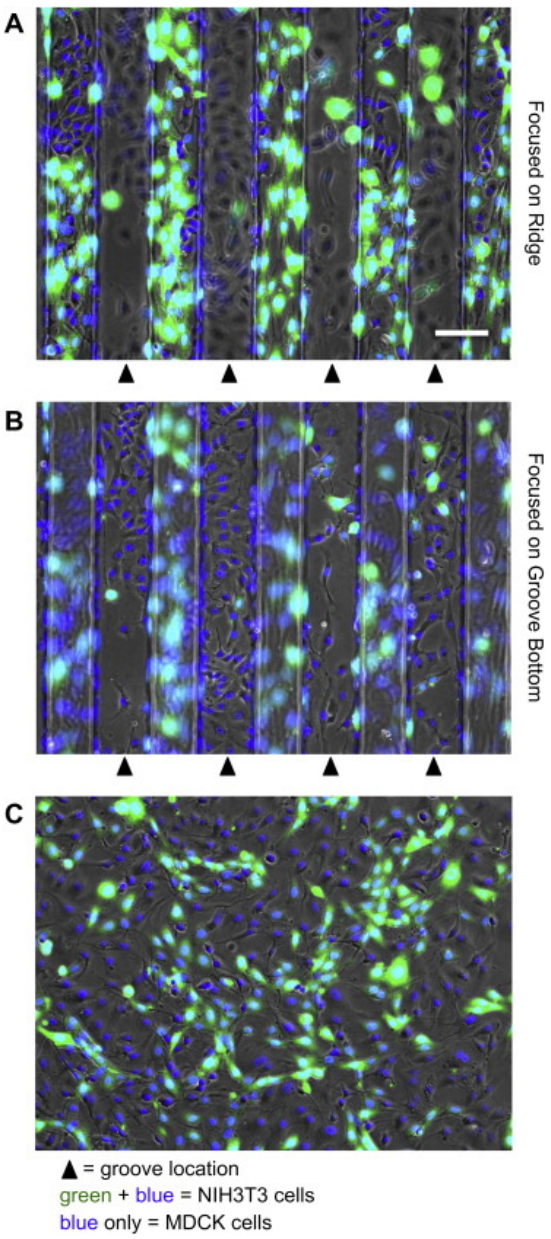

FIGURE 3.7 CO-CULTURED NIH3T3S AND MDCKS ON THREE DIMENSIONAL AND FLAT SURFACES.

NIH3T3 cells (green with blue nuclei) and MDCK cells (blue nuclei only) were placed in co-culture and imaged after 48 h (triangles indicate the grooves). Data shown were recorded on 100µm grooves but is representative for all groove widths. Phase contrast images were recorded when the microscope was focused on the (A) ridges and (B) bottom surfaces of the grooves and reveals a spatial separation of both cell types (scale bar = 100 µm and applies to all). When co-cultured cells are grown on a flat PDMS surface cells are heterogeneously distributed and no alignment or separation is visible. (For interpretation of the references to colour in this figure legend, the reader is referred to the web version of this article.)

3.4 DISCUSSION

Physical cues in the cellular microenvironment such as substrate topography and mechanical properties have a significant role in regulating physiological and pathological processes [5,101,184–186]. In addition, it has also been shown that flat substrates patterned with ECM proteins can be used to control cell shape, alignment, proliferation and differentiation[131,193,201,206]. Recently, cells exposed to either microscale grooves or microscale lines of fibronectin were observed to align along the presented patterns[206]. However, when a substrate of grooves fabricated in one direction was overlaid with lines of fibronectin in the orthogonal direction, cells were observed to preferentially align with the grooves. Therefore, surface topography is an extremely strong cue in regulating living cells, even overcoming the influence of surface patterns of ECM protein[206] and might even be used as a means of characterizing cellular signaling pathways[195]. Indeed, it has been demonstrated that libraries of substrate topographies can be employed to reveal previously unknown cellular responses to substrate topography[175].

In this study, we examined the influence of microscale topography on the three-dimensional spatial organization and alignment of NIH3T3 fibroblasts and MDCK epithelial cells. PDMS substrates were fabricated with grooves of varying widths (25, 50 and 100μm) and constant depth (50μm) and ridge width (100μm). NIH3T3 fibroblasts displayed a clear preference for proliferating on the ridges, consistent with previous studies[204,205]. On the other hand, MDCK epithelial cells preferentially proliferated inside the grooves, a result that has not been observed previously to our knowledge. However, nanoscale grooves are well known to exhibit contact guidance on cultured epithelial cells[100,192,209]. In all cases, our substrates were functionalized with collagen and it is well known that aligned collagen fibers, both in vivo and in vitro, can lead to preferential cellular alignment, migration and contact guidance[100,192,209]. Here, we can rule out collagen-induced contact guidance, as the collagen is likely randomly bound to our substrates after using standard functionalization protocols. In addition, in both cases

cellular alignment was lost on the substrates with 500µm grooves. Alignment was quantified by calculating an order parameter which was shown to vary from ~0.8 to ~0.6 (fibroblasts and epithelial cells respectively) on the 25, 50 and 100µm grooves to ~0.3 on the 500µm grooves. Co-cultured cells on flat collagen-functionalized PDMS substrates did not display any preferential alignment. Therefore, it can be reasonably assumed that microtopography, rather than collagen functionalization, produces the observed contact guidance in our study.

We also quantified the preferential three-dimensional spatial localization of cells by simply counting how many were found on the ridge or anywhere within the groove, at each time point, on all substrates. The surface area available to the cells is significantly different on the ridges versus in the grooves. The ridges have a surface area of 1.5 cm 100µm ±0.015 cm^2 whereas each groove in this study has a surface area of ~0.019, ~0.023 and 0.030 cm^2. If the higher available surface area in the grooves played a major role in cell organization, the observed Ridge/Groove ratio would consistently be less than 1 in all cases. This was clearly not the case when examining NIH3T3 cells. However, this was the case in MDCK cells at all time points and for all groove widths. The Ridge/Groove ratio is initially ~0.2 in the first 24 h before rapidly approaching 1 whereas the Ridge/Groove surface area ratio varies from 0.5 to 0.8. Therefore, within the first 24h of culture, MDCK cells display preferential proliferation within the grooves that cannot be simply explained by an increase in surface area. However, once MDCK cells have proliferated to the point where they can no longer remain confined in the groove, they migrate out and begin proliferating on the ridge surface. At this point the Ridge/Groove ratio approaches 1 and this may simply be a result of the surface area occupied by the cells on each surface. Indeed, MDCK cells were observed to form complete two-dimensional sheets of cells that closely followed substrate topography with no tendency to form multicellular aggregates within the grooves during the timescale of our experiment. In contrast, when allowed to proliferate to confluence over 5 days, NIH3T3 cells were first observed to preferentially grow on the ridges and at later times (>3 days) would form large aggregates within the grooves.

In order to examine the influence of topography on the spatial localization of the cells, we co-cultured both cell types on the grooved substrates. In this case, fibroblasts were pre-loaded with a live cell cytoplasmic green fluorescent dye prior to co-culture. Prior to imaging, all cells were loaded with a blue fluorescent live cell dye specific to DNA. Therefore, during imaging, fluorescent green cells with blue fluorescent nuclei could be positively identified as fibroblasts. On the other hand, cells with blue-fluorescent nuclei alone could be positively identified as epithelial cells. In this case, it was clear after 48 h of proliferation, that cells still displayed a preferential localization on the ridges or in the grooves. However, we note that the separation is not 100% complete. However, despite numerous cell-cell interactions and possible effects associated with the release of cellular factors and signaling molecules, substrate topography still had a major influence on migration and organization. NIH3T3 cells maintained a preferential alignment and organization on the ridges while MDCK cells were still preferentially found in the grooves. Importantly, when cells were cocultured on a flat PDMS surface they were organized in a heterogeneous manner after 48 h of proliferation.

There is currently significant interest in using the characteristic of nano- and micro-textured surfaces to control, direct and modulate cell behaviors. Although many studies have revealed that cells are clearly sensitive to substrate topography, the exact underlying molecular mechanism responsible for their ability to sense and respond to topographic cues is still not well understood. It is now clear the regulation of acto-myosin contractility, and perhaps cellular traction forces, form part of the sensing mechanism[23,69,199]. In addition, topography also has a significant impact on the organization, dynamics and regulation of structures involved in coupling the cell to its microenvironment, such as integrins, focal adhesions and the cytoskeleton[23,69,199]. It was recently postulated that one of the forces driving fibroblasts to localize on the ridge of microgrooves is the local oxygen gradient[204]. However, the results on epithelial cells appear to contradict this possibility, assuming their oxygen requirements are similar to fibroblasts. Moreover, in our experiments, several millimeters of liquid exist above the

substrate surface and it is unlikely that any change in oxygen concentration in the 50µm distance between the bottom of the grooves and the ridge will be significant enough to drive the migration of the cells.

We hypothesize that one of the main driving forces that results in the differential response of fibroblasts and epithelial cells is likely cell function. Fibroblasts are highly motile cells and in comparison to epithelial cells, tend to lack the same degree of strong cell-cell coupling and the presence of tight junctions[208,210]. Therefore, we postulate that there would be less physical confinement on the ridges and therefore promote migration. Conversely, in a more physically confined environment, cell-cell contacts are more likely to form thereby inhibiting migration away from the growing cell sheet and promoting proliferation within the groove. Although this explanation does not provide any mechanistic insight, it is supported by the Ridge/Groove ratio data. In the case of fibroblasts, the Ridge/Groove ratio on 100µm wide grooves does not increase as rapidly as the 25 and 50µm grooves. In this case, the 100µm grooves are just as wide as the ridges, however the degree of confinement within the 50µm deep well appears to drive migration out of the groove and onto the ridge. Conversely, epithelial cells are forced onto the ridge as they quickly fill the 25µm grooves in comparison to the 50 and 100µm grooves. The wider 50 and 100µm grooves allow for prolonged cell proliferation within the grooves before being forced out onto the ridges. Therefore, although substrate topography can act as a stronger environmental cue than substrate biochemistry[206], clearly cell function and physiology play an equally important role in dictating the response to topographic information in the microenvironment.

3.5 CONCLUSION

This study has revealed that topographic cues can lead to the three dimensional spatial separation of two cell types. Fibroblasts displayed a clear preference for migrating and proliferating on the ridges of microscale grooves whereas epithelial cells preferentially migrated and proliferated in the microscale grooves. Importantly, the cell-type dependent behavior observed here is also maintained when fibroblasts and

epithelial cells were co-cultured. Physical confinement also appears to be playing an important role in driving cell-type dependent responses to microtopographies. This is consistent with previous work demonstrating that confinement and encapsulation of cells in engineered three dimensional hydrogels can drive their organization and fate. The ability to pattern and organize at least two distinct cell types in three-dimensions may have important implications for investigating the mechanisms of cellular organization and proliferation. Moreover, the phenomena described here may find utility in the development of biomaterials that can direct the complex three dimensional growth and behaviour of cells in complex artificial tissue constructs.

3.6 MATERIALS AND METHODS

3.6.1 SUBSTRATE FABRICATION

Master substrates were created with standard soft photolithography techniques on silicon wafers (Universitywafers.com, USA). The wafers were cleaned with a Piranha wet etch solution (3:1 sulphuric acid:hydrogen peroxide), followed by immersion in de-ionized water and subsequent dehydration by baking at 200°C for 30min. SU-8 2015 photoresist (Microchem, USA) was then spin coated to a uniform film thickness of 50µm. A master mold was created by transferring photomask patterns to the photoresist according to the photoresist manufacturer's protocol. The photomask consisted of separate 2.25 cm^2 square regions each containing 1.5 cm long black lines, spaced every 100µm. The widths of the lines varied in each region and were either 25, 50 or 100µm. Polydimethylsiloxane (PDMS) substrates with defined topographies were created by pouring a 1:10 solution of curing agent:elastomer (Sylgard 184, Ellsworth Adhesives) over the photoresist master. The PDMS was allowed to crosslink in a convection oven at 80 C for 3 h. A schematic of the substrate fabrication process is shown in Fig 3.1. To functionalize the PDMS substrates, they were air plasma treated at 30 W for 30 s to generate hydroxyl groups. The substrates were then immediately coated with 5 mg/cm^2 rat-tail collagen I (Gibco), incubated at room temperature for 1 h

and then rinsed in PBS. Scanning electron microscopy (SEM) of gold-coated PDMS substrates were acquired with a JEOL JSM-7500F FESEM.

3.6.2 Cell culture

NIH3T3 mouse fibroblast cells and Madin Darby Canine Kidney (MDCK) epithelial cells were cultured in high glucose DMEM containing 10% Fetal Bovine Serum (FBS) and 1% penicillin/streptomycin antibiotics (all from Hyclone). The cells were cultured at 37 C and 5% CO2 in 100µm dishes. For experiments, functionalized PDMS substrates were placed into 35µm diameter dishes and the cells were seeded at a density of 20,000 cells/cm^2. Cells were grown at 4, 24, 48 or 72 h before inspection. For co-culture experiments, an equal number of NIH3T3 and MDCK cells were thoroughly mixed and then seeded and imaged in the same manner as mono-culture experiments.

3.6.3 Immunofluorescence staining, live cell staining and microscopy

Cells cultured on PDMS substrates were fixed with 3.5% paraformaldehyde and permeabilized with Triton X-100 at 37 C. Cells were stained for actin using phalloidin conjugated to Alexa Fluor 546 (Invitrogen) and DNA was stained using DAPI (Invitrogen). A full protocol has been published previously [33]. Samples were then mounted using Vectashield (Vector Labs) and a #1 coverslip placed on top of the PDMS substrate. The sample was inverted and then imaged with confocal microscopy. In co-culture NIH3T3 cells were pre-loaded with the live cell dye CellTracker Green CMFDA (Invitrogen) following manufacturer protocols and cultured with MDCK cells for 4 or 48 h. After the allotted time in culture, all cells were loaded with live cell nuclear stain, Hoechst 33342 (Invitrogen). In some cases co-cultures were imaged live with a Nikon Ti-E inverted phase contrast and fluorescence microscope with a long working distance 40 objective or they were fixed (but not permeabilized) and mounted in Vectashield. Fixed samples were imaged on a Nikon Ti-E A1-R high-speed resonant laser scanning confocal microscope (LSCM) with a phase contrast 10 NA0.3 objective or a DIC 60 NA1.2 water immersion objective. Bare PDMS substrates were also imaged with Scanning Electron Microscopy (SEM).

3.6.4 IMAGE AND STATISTICAL ANALYSIS

All images were analyzed with ImageJ. Cell nuclei were manually counted in order to quantify the numbers of cells proliferating in the grooves or on the ridges. The degree of cell alignment with respect to the groove direction was quantified by first thresholding confocal images of cell nuclei. An ellipse was fit to each identified nucleus and the angle between the major axis of the ellipse and the groove direction was determined with the ImageJ Analyze Particles plugin. The second order Legendre polynomial was employed to quantify the average degree of alignment with the groove direction within the cell population. All values in the text are presented as the average s.e.m. A one-way ANOVA followed by a Tukey test for means comparison or two-sample t-tests were performed to assess significance ($p < 0.05$).

3.7 ACKNOWLEDGEMENTS

A.L. acknowledges support from the Natural Sciences and Engineering Research Council (NSERC) Undergraduate Student Research Award and the University of Ottawa Undergraduate Research Opportunities Program. D.T. thanks the Fond de recherche du Québec: Nature et Technologie (FQRNT) and Mitacs Elevate Program. A.E.P. acknowledges generous support from a Province of Ontario Early Researcher Award and a Canada Research Chair (CRC). This work was made possible by funding from the Canadian Foundation for Innovation (M.G. and A.E.P.), NSERC Discovery Grants (M.G. and A.E.P), an NSERC Discovery Accelerator Supplement (A.E.P.) and a CRC Operating Grant (A.E.P.). The authors wish to thank Dr. Yun Liu for assistance with SEM imaging.

Chapter 4 | Manuscript

Exploiting contact guidance to trap cells in three-dimensions

Sebastian V. Hadjiantoniou[1], Radin Tahvildari[2], Maxime Ignacio[2], Ryan Hickey, Ali Najafi Sohi[2], Michel Godin[2,3,4], Andrew E. Pelling[1,2,5]

[1]*Department of Biology, Gendron Hall, 30 Marie Curie*
[2]*Department of Physics, MacDonald Hall, 150 Louis Pasteur*
[3]*Department of Mechanical Engineering, Site Building, 800 King Edward Avenue*
[4]*Ottawa-Carleton Institute for Biomedical Engineering*
[6]*Institute for Science, Society and Policy, Desmarais Building, 55 Laurier Ave. East*

In preparation *for Biomaterials* Aug 2017

Motivation & Objectives |

A climbing phenomenon by which fibroblast cells migrated out and onto the ridges in response to distinct levels of confinement was previously observed in Chapter 3. We seek to identify the mechanisms by which cells sense the channeled geometry and preferentially pattern onto the ridges. We systematically eliminate all known form of guided migration to reveal the mechanism at play.

4 | EXPLOITING CONTACT GUIDANCE TO TRAP CELLS IN THREE-DIMENSIONS

4.1 INTRODUCTION

The physical and biochemical properties of the microenvironment have become well recognized as key modulators of cell biology[5,186,211,212]. This environment, also known as the extracellular matrix (ECM), is composed of proteoglycans and fibrous proteins, which together, formalize the physical and biochemical properties of the cellular milieu[4,5,101]. Each distinctive material property impacts major signaling pathways inside the cell, influencing a wide array of processes such as morphogenesis[66,191,213], proliferation[201] and differentiation[103,106,214]. During regeneration, fibroblast cells are responsible for remodeling damaged tissue by reconstructing a scaffolding matrix permitting cell invasion[215]. For this successful remodeling to occur, fibroblasts must collect new geometric information from their microenvironment in addition to synchronously communicating cell-cell interactions[215]. Numerous studies have explored the mechanisms by which cells achieve these appropriate physiological responses[215,216].

The cell is sensitive to an extensive list of external stimuli, any of which can influence morphology and cell migration[24,217]. Gradients of dissolved (chemotaxis) or surface-attached chemicals (haptotaxis) have been extensively studied [218–221] and has been the basis for morphogen guided embryogenesis[121] and immune response[222]. Other stimuli originate from the mechanical properties of the substrate such as its deformability. Fibroblast demonstrate a preferential adhesion to stiffer substrates, a process described as durotaxis [34,223–225]. However, they are capable of adjusting their internal mechanical properties to mimic their surrounding substrate stiffness, a phenomenon which has been suggested as a mechanism to promote migration towards skin defects to accelerate wound healing[226]. With the advent of microfabricated topographies, engineered substrates have been able to reveal the effects of surface topography on cell behaviour. In two dimensions, varying the widths and depths of

nanosized grooves display higher adhesive interactions by means of recruited integrin clustering[227,228]. Similar results are shown when plating cells on pillars or pitted substrates arranged in spatial gradients[209,229,230]. Other phenomena have been observed such as ridge walking, whereby cells will migrate along edge surfaces rather than across, actively guiding the polarity in neurons[65], fibroblasts[71] and smooth muscle cells[76,84]. This is known as contact guidance and extensive research has been performed which has led to understanding of the modular effects of groove width[68,70,72,74,84], ridge width[67,68,70–72,85] and ridge height[67,69,74,85] on cell behavior.

We have previously reported that co-cultured cells will spatially separate in response to their three dimensional microtopography[231]. NIH3T3 fibroblasts and MDCK epithelial cells were seeded onto microfabricated channels measuring 100µm wide by 100µm high. After settling at the bottom of the grooves due to their higher mass density than the surrounding media, the cells quickly adhered to the substrate. After 12 hours incubation time, NIH3T3 fibroblasts migrated up the channel walls and specifically localized to the top ridges. In contrast, MDCK cells remained strongly adhered at the bottom of the grooves and remained there throughout the study. The effect of geometric confinement was sufficient to control cell migration and subsequent proliferation. Even in a co-culture, we found that this topographical cue was strong enough to cause the spontaneous separation and spatial patterning of a mixture of cell types in three dimensions. Although the phenomenon was well documented in our previous work, and work of others [66,74,229,232] the exact physical and biochemical mechanisms by which NIH3T3 fibroblasts actively migrated and patterned on top of the groove ridges remains to be elucidated.

Here, we utilize a series of specifically designed microfabricated topographies to explore the potential mechanisms driving the spontaneous patterning of fibroblast cells in 3D. To elucidate the guiding forces at play, we systematically tested each mechanism known to influence directional cell migration. Here, we show that the geometric properties of channeled topographies alone can induce three-dimensional patterning in

fibroblasts. At a 20µm high threshold, cells no longer randomly disperse on the substrate but actively migrate and align along the channel ridges. A microfabrication reflow technique was subsequently utilized to create an elliptical topography in the effort to eliminate the 90° degree contact angle at the edges of the channels. Removal of this contact angle resulted in the inhibition of the active migration phenomenon previously observed. The traditional paradigm of contact guidance has revolved around the cell's local response to its underlying surface, which governs its re-orientation in two dimensions. We demonstrate that contact guidance is an important geometric cue that can trigger complex behavioural responses in three dimensional topographies. It is important that such geometric cues are carefully considered as behavioural triggers during three dimensional patterning and morphogenesis.

4.2 RESULTS

4.2.1 CHANNELED THREE DIMENSIONAL GEOMETRIES INDUCE CELL PATTERNING

In this study, we sought to elucidate the mechanisms by which NIH3T3 fibroblasts demonstrate patterning out of confined geometries and onto to channeled surfaces. This phenomenon was observed by microfabricating 100µm high by 100µm wide channeled topographies through soft photolithography techniques, consistent with our previous study (Fig 4.1) [231]. Cells were seeded on the PDMS substrate and were found to sink to the bottom of the groove because of their higher relative density compared to the surrounding media. Time-lapse imaging reveals (Fig 4.2A) that cells begin to demonstrate preferential adherence to the sidewall within 4hrs incubation time. At 12hrs, cells are no longer present at the bottom of the grooves. They have all migrated whereby most have settle on the ridges of the channels. After 48hrs incubation, cells demonstrate a clear patterning formation along the top of the ridges with a ridge to groove ratio of 3.91 ±0.66 (Fig 4.2B). The orthogonal view further reveals how although some cells are found within the grooves, they are constrained to the sidewalls. These cells may still be actively climbing or are being prevented to migrate further due to surface area limitations and increasing cell densities. Interestingly, after

48hrs incubation, cells become highly aligned 0.76 ±0.01 due to contact guidance cues, likely arising from the distinctive ridge edge.

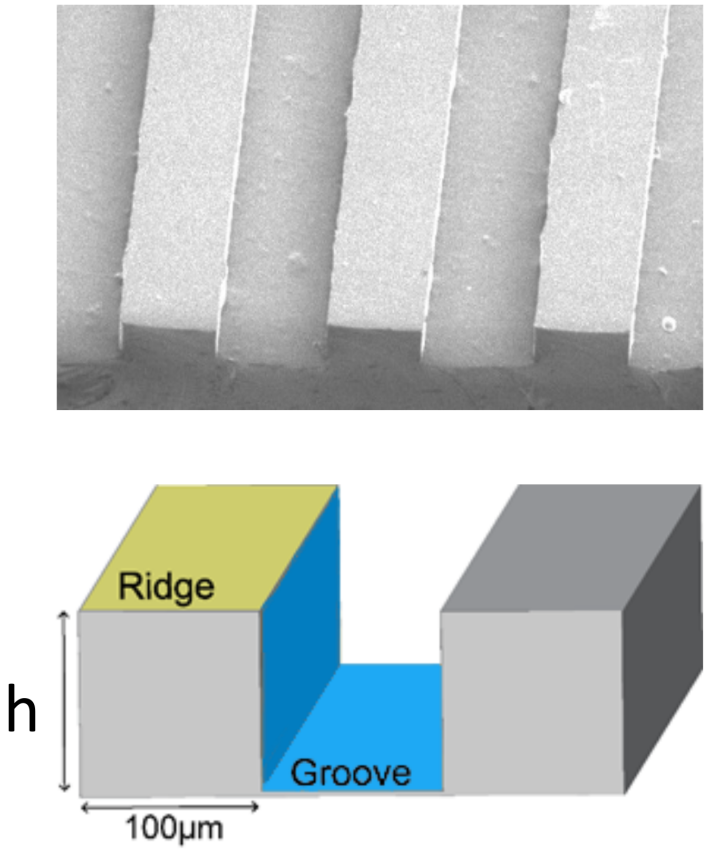

FIGURE 4.1 FABRICATION OF CHANNELED MICROTOPOGRAPHIC PDMS FEATURES.
Channels are fabricated through traditional soft lithography techniques. (A) SEM image (perspective view) of channeled PDMS substrate revealing the typical microtopography. Below, a diagrammatic representation describing the dimensions and the terminology utilized when discussing the positional location of cells in the channels. For the purpose of this study, we describe "Ridge" as the top of the channel and "Groove" as the bottom and sidewalls. The height (h) was varied at 100, 20 and 10µm whilst the width remained consistent at 100µm for all substrates.

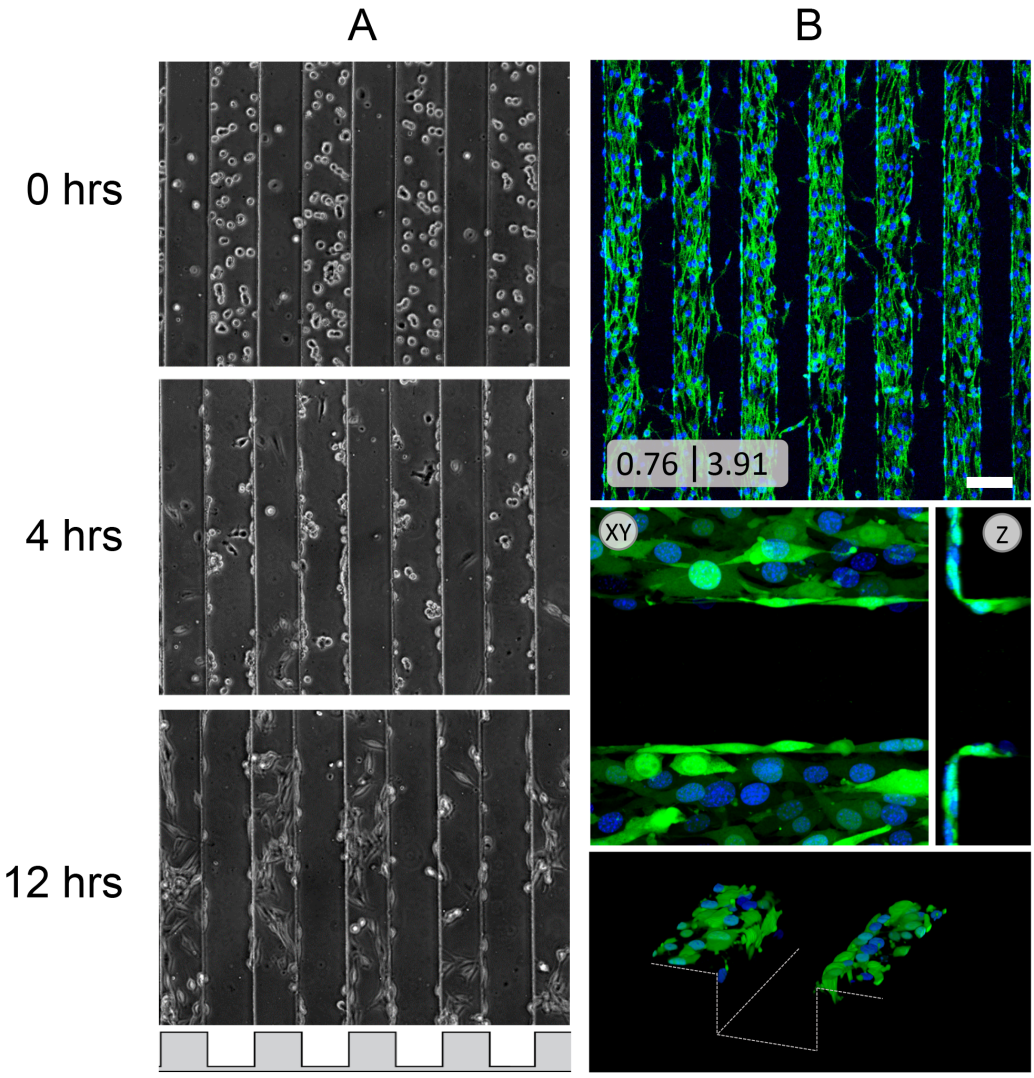

FIGURE 4.2 NIH3T3 CELLS MIGRATE ONTO SURFACE RIDGES WHEN CULTURED IN CHANNELED TOPOGRAPHIES.

(A) Timelapse of the preferential migration phenomenon observed in 100µm high PDMS channels. At T= 0hrs, fibroblasts sink at the bottom of the grooves and begin adhering to the substrate. By T= 4hrs, cells have already begun migrating displaying preferential adhesion towards the sidewalls of the topography. At T= 12hrs, cells have fully migrated to the ridges of the substrate and begin proliferating. (B) Actin (green) and nucleus (blue) confocal image at T=48hrs displaying the distinct patterning phenomenon of NIH3T3 cells. The average order parameter & ridge/groove ratio are shown respectively (bottom left corner). Scale bar = 100µm. Orthogonal views reveal alignment along the ridges and the presence of cells within the side walls and ridge surfaces. Dotted lines are used in the perspective view to overlap the presence of the PDMS topography with respect to the position of the cells.

4.2.2 THE INFLUENCE OF CONTACT GUIDANCE IN CHANNELED TOPOGRAPHIES

Contact guidance describes the phenomenon by which cells align their stress fiber formations relative to one another and the surface topography[197]. It has long been shown that on two dimensional surfaces, fibroblasts are sensitive to grooved geometries ranging from nanometer to micrometer features [233]. This patterning not only affects their morphology but their behaviour as a cellular collective. To analyze the potential effects of contact guidance on NIH3T3 cell migration in three dimensions, we systematically microfabricated channeled topographies of varying heights to identify a threshold at which point the phenomenon subsides.

Figure 4.3A,B,C demonstrates the resulting effects of a 10µm high channel on fibroblast patterning. The results show a well dispersed mesh with no clear preferential alignment along the groove ridges. Order parameter analysis shows 0.40±0.01. Compared to our control experiments, these results are significantly different ($p<0.05$, $n=3$) and indicate a more stochastic angle distribution, which is in accordance with non-contact guided cells. The ridge to groove ratio is 1.16±0.13, suggesting that the number of cells in the grooves is similar to those found on the ridges and that the topography has little effect on patterning. This observation is once again statistically different ($p<0.05$, $n=3$) than that observed in the 100µm channels. Having identified the threshold at which preferential patterning due to channeled topography no longer occurs, we then sought to reveal the minimum height required to induce the patterning effect.

Figure 4.3D,E,F depicts the effects of a 20µm high channeled topography on NIH3T3 fibroblast growth. The patterning effect is clearly apparent as cells localize on top of the channels ridges. Interestingly, cells appear to be at extremely high densities on top of the ridges, with a ridge to groove ratio of 9.40±1.20. This is significantly different ($p<0.05$, $n=3$) when compared to the 20µm high channels. They prefer to minimize their occupying surface area to maintain their position rather than climb back down into the groove. This is contrary to NIH3T3 behaviour on flat surfaces, as they will

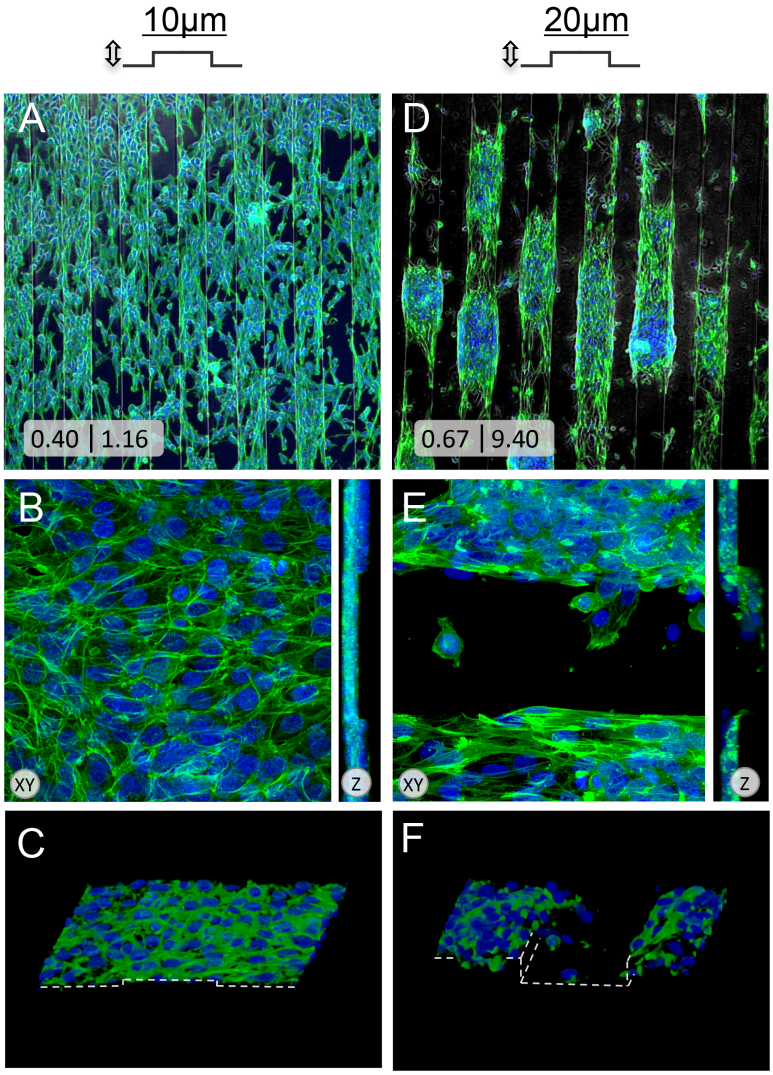

FIGURE 4.3 VARYING THE TOPOGRAPHY HEIGHT AND SHAPE MODULATES FIBROBLASTS MIGRATION IN THREE DIMENSIONS.

Images are of actin (green) and nuclei (blue) for (A,B) at 10x (scale bar = 100µm) and 60x (orthogonal/perspective, scale bar = 25µm) of NIH3T3 cells cultured for 48hrs in vitro on; (A) A 10µm high channeled substrate demonstrating no migrational guidance as cells acquire a typical equidistant cell dispersion morphology; (B) A 20µm high channeled substrate presenting a clear patterning effect suggesting a threshold height inducing migrational guidance. The average order parameter (S) & ridge/groove ratio are shown respectively (bottom left corner). At S= 1, cells are parallel with the groove whilst S=0 indicates a perpendicular alignment. Preferential parallel alignment is shown in 20µm channels topographies. On 20µm channels, cells had significantly ($p < 0.001$, n=3) migrated to the top of the ridge compared to the 10µm channel topography.

spread out to maximize contact surface area. This would suggest that the edge is, in some form, locking them onto the ridge. Alignment analysis also demonstrates their preferential orientation parallel to the groove with an order parameter of 0.67±0.01.

To further elucidate NIH3T3 behaviour over time, we performed a time-lapse imaging analysis of NIH3T3 cells seeded on a 20μm channeled topography at 4-24hrs and 48-68hrs. This revealed the behavioral characteristics over time of cells responding to their topography at early and late stages of the experiment. Fig 4A is a heat map of the migrational distribution of cells over time. Analyzed via the HeatMap imageJ plugin, every colorized pixel is converted into a grey scale value for each frame over time. The total values for each pixel are then colorized on a scale, with red signifying the high presence of cells and black signifying no cells at all. At 4-24 hours, the heat map reveals that cells migrated from the groove to the ridges of the channels. Over time (48-68hrs), with increased cell density, cells appear to be locked in within the confines of the ridges. Despite spatial limitations, cells maintain their position on top of the ridges, rather than spreading out to occupy any available free surface. Displacement analysis (Fig 4.4B) indicates high levels of cell migration during early time points following seeding. However, as cells climb and begin to reside on the ridges, displacement due to migration decreases. The influence of contact guidance is particularly shown in Fig 4C as the orientation of cells slowly align along the axis of the channel over time. At the initial 4hr stage, the average order parameter displayed by the cells was 0.19±0.06, which is in accordance with a random distribution. After 68hrs, average cell alignment reaches 0.86.±0.03 demonstrating how contact guidance influences the patterning of NIH3T3 cells in three dimensional topographies.

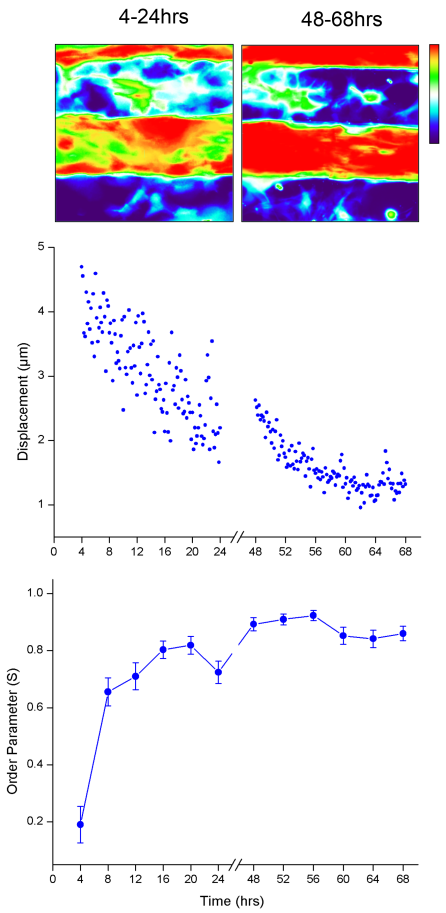

FIGURE 4.4 TIMELAPSE IMAGE ANALYSIS OF CELLS CLIMBING IN CHANNELED TOPOGRAPHIES.
Samples were prepared by seeding NIH3T3 cells onto a 20µm high PDMS channeled topogaphy. For 4-24hr timelapses, cells were allowed to adhere for 4hrs and subsequently inverted and imaged on the LSCM. Samples undergoing the 48-68hrs timelapse were incubated for the entire duration until imaging. A) Heat map analysis indicating the presence of cells in X, Y coordinates over the entire timelapse. At 4-24hrs, initial preliminary movement occurs within the grooves (white and green colour) but migration quickly migrates to the top of the channels as the presence of cells over 20hrs resides on the ridges (green and red). At 48-68hrs, cells are locked onto the ridges (red) and permanently reside there for the entire timelapse. B) Scatter plot analysis of the level of displacement(µm) over time. At initial time points, cells display higher variability and movement as they begin to climb the channels. At 48hrs, cells are uniformly locked and display no movement. C) Average order parameter(S) with respect to the channels at given time intervals. An order parameter of 1 indicates perfect parallel alignment along the channels whilst 0 indicates perpendicularity. At initial time points, alignment is random but begins to align along the channels over time.

To isolate and remove the effect of edge-induced contact guidance whilst maintaining a three-dimensional topography for cell migration we created 20µm high elliptical channels (Fig 4.5). We removed the 90° edge at the ridges by melting and resetting our channeled molds which gave rise to rounded grooves. Figure 4.6A,B,C demonstrates NIH3T3s seeded onto elliptically channeled topographies for 48hrs. The result is a complete absence of patterning along the ridges with cell dispersion resembling the 10µm high channeled conditions. Interestingly, although alignment is more evenly distributed as compared to the 20µm rectangular channels, a slight preference for order parameters between 0.70 - 0.98 was present. This may suggest that the cells are sensing and responding to the presence of grooved topographies by modifying their orientation but that it is insufficient to induce clear patterning. The ridge to groove ratio of 0.48±0.04 clearly indicates that the cells are not patterning significantly along the channels. Both the ridge to groove ratio and order parameter (0.67±0.01) are statistically different ($p<0.05$, $n=3$) when compared to 20µm channeled topographies. This indicates that the contact angle found at the edge of the ridges is highly responsible for the observed phenomenon under investigation.

Having identified that the contact angle at the edge of the ridges plays a pivotal role in fibroblast patterning on top of the channels, we sought to modulate it through reflowing 100µm channels. By doing so, we could control the eccentricity value that is determined by the ratio of the semi-major over the semi-minor axis. A value of 0 corresponds to a circle whilst a value of 1 indicates a parabola. Melting our 100µm channeled molds created an elliptically shaped channel with an eccentricity value of 0.46±0.02. Figure 4.6 shows NIH3T3s seeded on a 100µm high rounded channel for 48hrs. The result of reintroducing a lower eccentricity value caused cells to display preferential patterned formation on the channels. Interestingly, despite the clear overall patterning effect, instances of cell spreading beyond the contact angle of the groove were more frequent than 20µm channeled topographies. The perspective view reveals how cells appear to distance themselves from the contact angle of the lower channel (dotted line), suggesting an outward proliferation originating from the apex. The order

parameter of 0.56±0.01 reveals cells preferentially aligning parallel to the channel axis. The ridge to groove ratio of 2.82±1.01 also suggests high levels of actively guided migration compared to the 20µm wave topographies. In both measurements, the 100µm topography was statistically different ($p<0.05$, $n=3$) when compared to the 20µm elliptical channels.

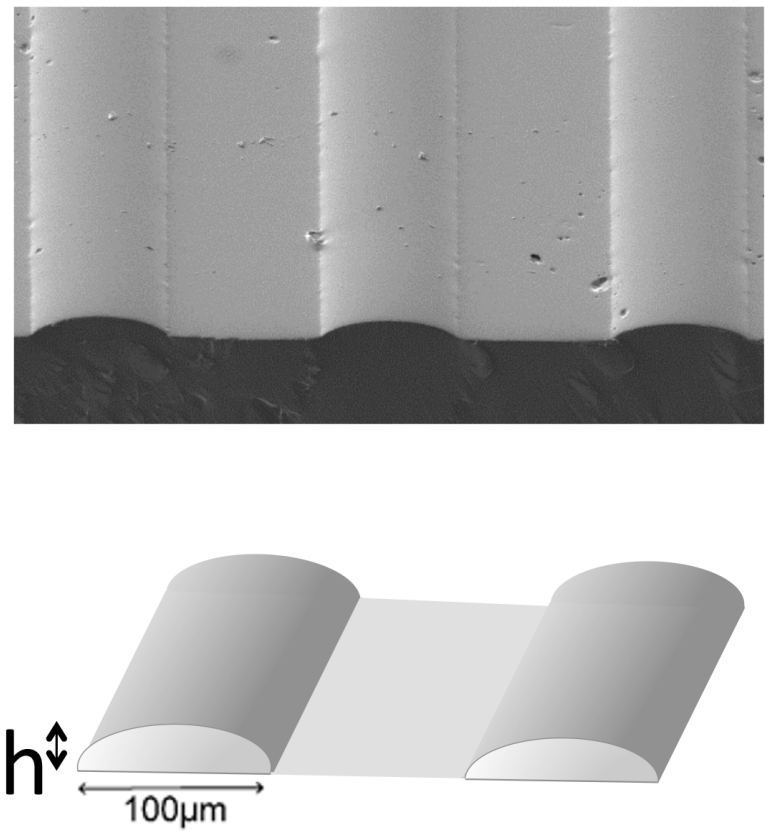

FIGURE 4.5 FABRICATION OF ELLIPTICAL MICROTOPOGRAHIC PDMS FEATURES.
Ellipses are fabricated by means of a two phase fabrication process. Traditional soft lithography is used to create channeled topographies that are then subsequently reflowed to soften contact angles. SEM image of elliptical PDMS substrate revealing the typical microtopography. A diagrammatic representation describing the dimensions is shown below indicating a varying height (h) of 20µm and 100µm whilst the width remained consistent at 100µm for all substrates.

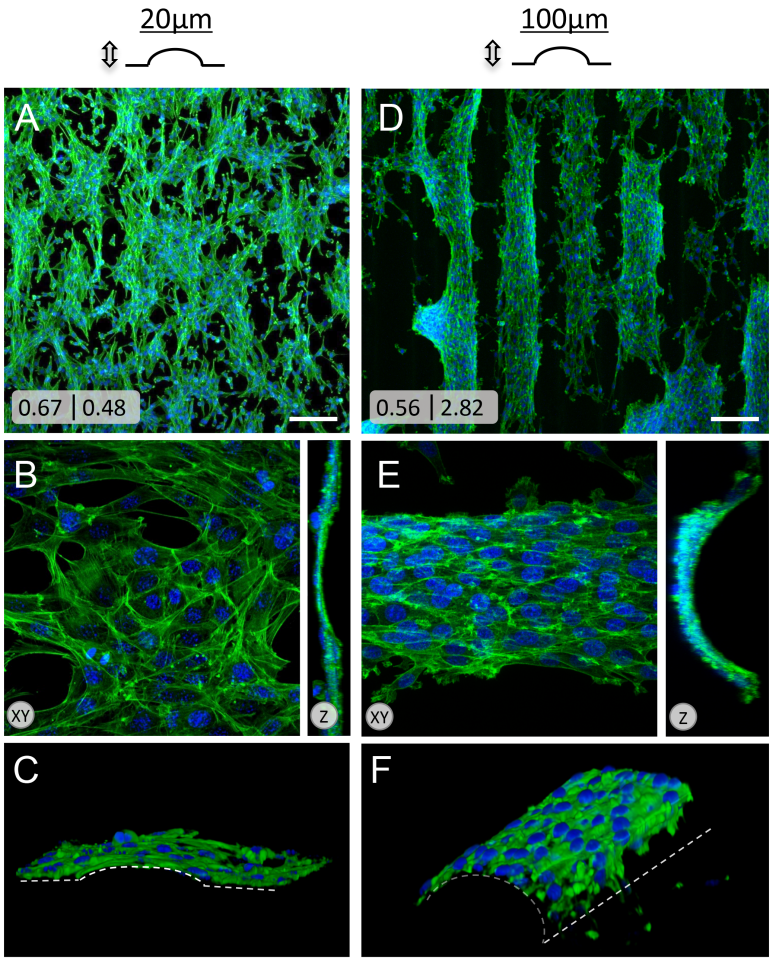

FIGURE 4.6 MODULATING THE CONTACT ANGLE OF CHANNELED TOPOGRAPHIES ALTERS THREE DIMENSIONAL MIGRATION

(A) Top down, (B) orthogonal and (C) perspective view of a 20µm high elliptical topography causes the stochastic dispersion of cells by removing the acute 90° contact angle found in channeled geometries. (D) Top down, (D) orthogonal and (E) perspective view of a 100µm high elliptical topography induces the original migrational phenomenon observed in channel substrates. After preliminary migration, cells centrally reside at the apex of the ellipse, align along the topography and subsequently proliferate outwards. The average order parameter(S) & ridge/groove ratio are shown respectively (bottom left corner). At S= 1, cells are parallel with the groove whilst S=-0.5 indicates a perpendicular alignment. Ridge to groove ratios demonstrate a significant difference ($p < 0.01$, n=3) in preferential migration of NIH3T3 cells between 20µm and 100µm elliptical topography. (Scale bar = 100µm). Topographies were created via traditional soft lithography of channeled substrates followed by a reflowing technique. This melting rounds the contact angles, creating an elliptical shape.

4.2.3 THE INFLUENCE OF CHEMOTAXIS AND GEOTAXIS IN CHANNELED CELL MIGRATION

In the attempt to rule out all other effects that may be driving cell patterning, we sought to systematically eliminate all known factors that influence cell guidance. Chemotaxis is the movement of a cell in a direction corresponding to a gradient of increasing or decreasing concentration of a particular molecule between the top and bottom of the channels. To investigate the potential role of growth factor gradients that may form as a result of cellular consumption, we performed time lapse imaging analysis at 5, 10 and 20% concentrations of FBS. By varying the concentrations of FBS, and thereby impacting any potential gradient, the rate of climbing should differ between experiments. As shown in Fig 4.7, the ridge to grove ratio over a 24 hour span shows no statistically significant ($p<0.05$, $n=3$) difference between any of the FBS concentrations. To explore other gradient formations such as paracrine signaling, we introduced a constant flow (Fig 4.7B) at a rate of 100µl/min of media in order to disturb any potential molecular gradients. As can be seen in Fig 4.7C, this had no effect on the migration and patterning of cells on top of the ridges with a ridge to groove ratio and order parameter of 3.91 ± 1.35 and 0.67 ± 0.01 respectively.

Geotaxis is the movement of a motile organism towards or away from a gravitational force. Organisms whose densities are higher than the surrounding mediums undergo negative geotaxis and migrate towards the surface at a steady rate[234]. To our knowledge, geotaxis has been reserved to microorganisms of specific morphological shapes in low viscous environments that migrate via forms of flagellar movements[235]. Its influence on complex multicellular organisms has yet to be shown and is only being considered here as an effort to explore any and all potential mechanisms. To investigate the potential role of negative geotaxis in NIH3T3 climbing, we seeded cells into the channels and allowed them to adhere for 4 hours. We then rotated the entire substrate 180° so that cells would be required to migrate in a positive

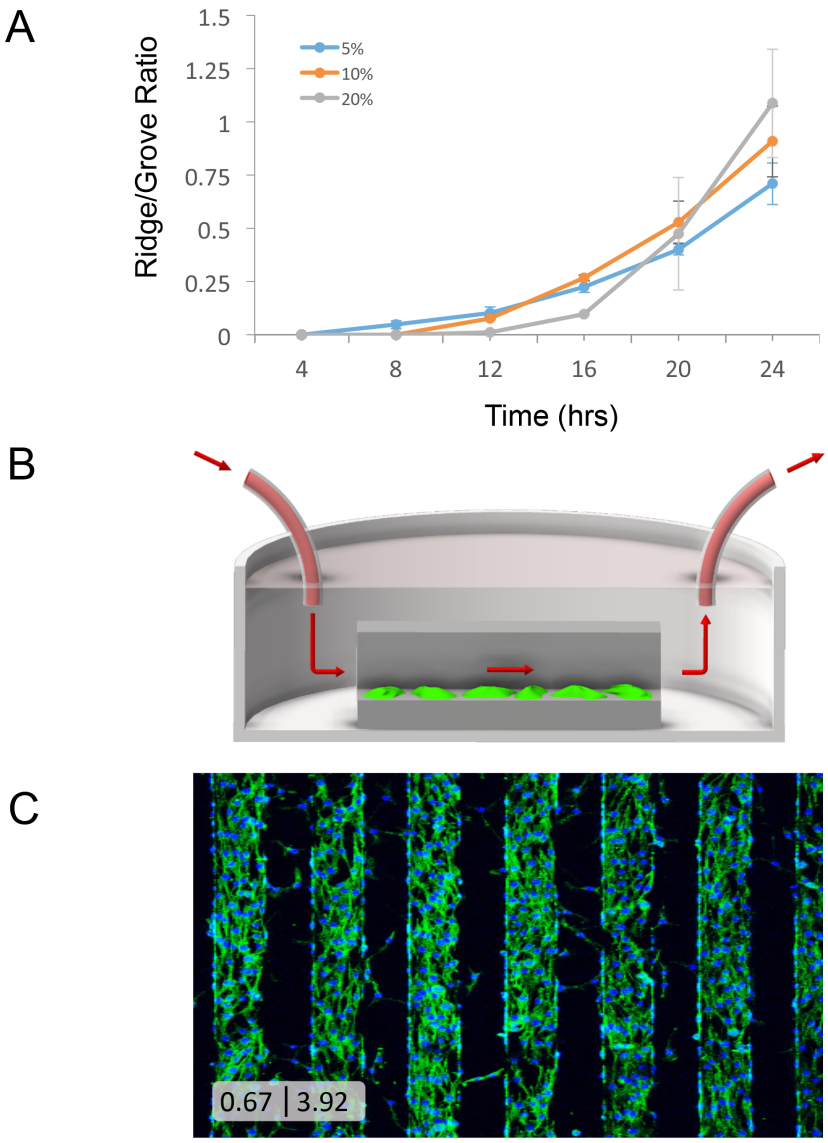

FIGURE 4.7 EFFECTS OF CHEMOTACTIC GRADIENTS IN CHANNELED TOPOGRAPHIES.
(A)Serum concentrations were modulated between 5, 10 and 20% during 24hrs to observe altered rates of migration due to a potential chemoattractant gradient formation. No statistically different ($P>0.05$, Anova, N=3) rates of climbing were observed between any of the of the varying serum concentrations. (B) NIH3T3s were seeded into 100µm channeled substrates for 4 hours to permit cell adhesion at the bottom of the grooves. A linear flow by means of a peristaltic pump was then introduced at a rate of 100µl/m flushing the entire 3 ml dish every 30 minutes (diagrammatic representation). (C) Actin (green) and Nuclei (blue) of fibroblasts after 48hrs of linear flow demonstrating unaffected migrational patterning at the top of the ridges. Scale bar= 100µm.

geotaxic form, travelling down and out of the channels. We also rotated the entire substrate 90° eliminating both positive and negative geotaxis, driving the cell to migrated horizontally out of the channel (Fig 4.8A,B). Alignment and ridge/groove ratios for 180° and 90° inversion indicate a clear patterning along the ridges (0.76±0.01 and 0.76±0.01) (2.98±0.23 and 2.01±0.91) respectively. This result is not statistically different ($p<0.05$, $n=3$) from our control experiments suggesting that geotaxis is involved in the patterning of NIH3T3s onto the ridges of channeled topographies.

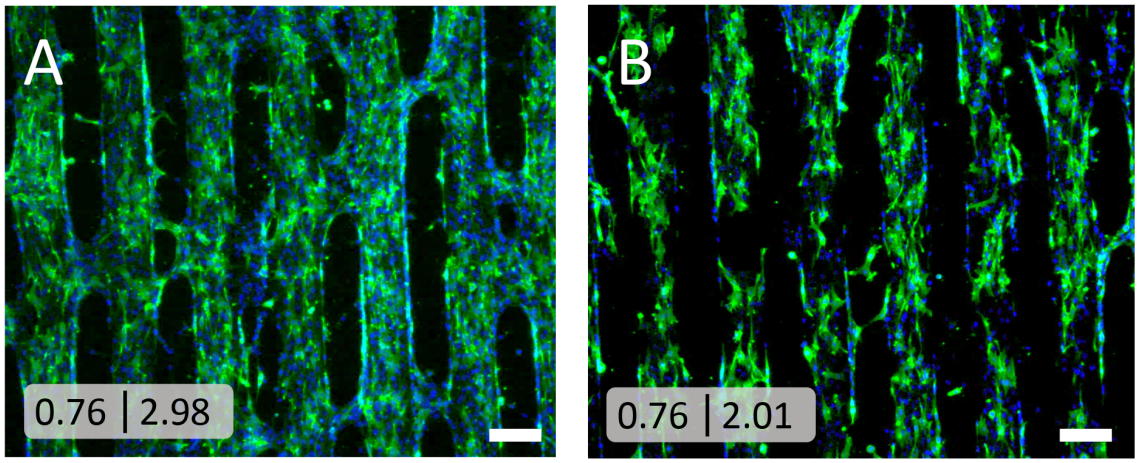

FIGURE 4.8 THE EFFECTS OF GEOTAXIS ON CHANNELED TOPOGRAPHIES.
Cells were plated and allowed to adhere onto channeled topographies for 4hrs. Two separate sets of experiments were performed in which the PDMS was turned upside down 180°(A) and on its side 90°(B). The cells were then subsequently allowed to incubate for the remaining 48hrs. Actin (green), Dapi (blue) images of (A) 180° and (B) 90° inverted channels demonstrating clear migrational patterning. The average order parameter & ridge/groove ratio are shown respectively (bottom left corner). No statistical differences ($p>0.05$, $n=3$) were observed. Scale bar = 100μm

4.2.4 THE INFLUENCE OF HAPTOTAXIS AND DUROTAXIS IN CHANNELED CELL MIGRATION.

We sought to further explore additional known factors that influence migration by elucidating the effects of collagen deposition gradients on channeled topographies. Haptotaxis is the directed movement of a cell in response to gradients of substrate-bound cues. When seeding cells onto microfabricated PDMS topographies, established protocols requires it to be plasma treated and functionalized via adherable fibrous proteins such as collagen or fibronectin [118,236,237]. These proteins further support cell-substrate binding in addition to the production of collagen that cells deposit during

adhesions. To observe whether different concentrations of collagen I were being deposited between the ridges and the groove during functionalization, we used a primary antibody bound to an alexa fluor 546 secondary antibody to fluorescently tag coated collagen I on our topography. Fig 4.9A demonstrates the clear difference in collagen I deposition between the grooves and the ridges. Average intensities for each sample were calculated with Image J indicating a concentration of almost 1.7 times higher on the ridges (1516 ±227) than the grooves (859±42.9). This statistically significant ($p<0.05$, $n=3$) result would suggest that a haptotactic gradient may potentially form during functionalizing and that cells are actively climbing because of increased adherable matrix toward the top of the ridges. To validate whether this was in fact guiding cell patterning, NIH3T3s were seeded on a 100µm high channeled topography with no pre-deposited collagen I deposition. Since cells sink at the bottom of the channels during seeding, the presence of collagen would solely originate from the cells and onto the grooves. The results show unaffected cellular migration out of the channel grooves and patterning onto of the ridges (Fig 4.9B). This clearly indicates that a haptotaxic gradient due to collagen surface concentration is not responsible for cell climbing and subsequent patterning.

Durotaxis is a form of cell migration in which the stiffness of a substrate that arises from different structural properties promotes the active guidance of cells. Most cells are sensitive to rigidity gradient and migrate towards stiffer areas. The inherent topographic shape of our channeled system whereby the ridge is 100µm high from the core PDMS base may create a substrate with a stiffness gradient. To analyze this, we utilized atomic force microscopy to measure the Young's modulus at the ridges and the grooves of the channels. The stiffness between the groove and the ridge are not significantly different, 0.26 ±0.08 MPa and 0.26 ±0.19 MPa respectively ($p> 0.05$, $n=5$).

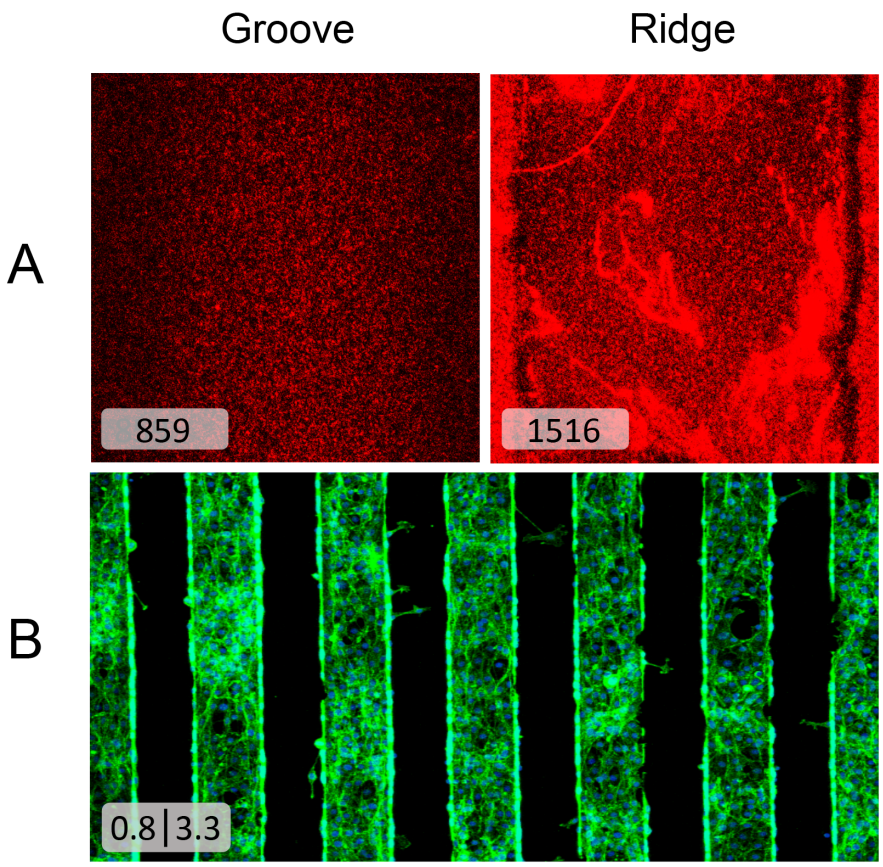

FIGURE 4.9. THE EFFECTS OF HAPTOTAXIS IN CHANNELED TOPOGRAPHIES.
A) Visualization of collagen I deposition within the groove vs ridge via antibody stain. Average Intensities measured in Arbitrary Unites (A.U) with Image J show a statistically significant difference in collagen I concentrations ($p<0.05$, $n = 3$). B) NIH 3T3 cells, actin (green), cultured on 100µm high channeled topographies for 48hrs with no collagen deposition prior to seeding. Cells display the same behavioral phenomenon of active migrational climbing onto the ridges

4.3 DISCUSSION

The use of microfabrication to create highly controlled topographies has led to a myriad of discoveries, all revealing the influential effects of the microenvironment on the cell[53,187,238]. We have previously published an example of such an effect [231], whereby 100x100µm channeled topographies were seeded with NIH3T3 fibroblast cells and left for 48hrs in incubation. The result was a climbing phenomenon in which cells migrated up the channel walls, proliferated into a dense mesh along the ridges and subsequently

formed bridges across the channel gaps. These observations revealed the cell's environmental awareness and preferential response to distinct three dimensional geometries. Despite discovering the effects of three dimensional channeled topographies on fibroblast behaviour, an explanation to the biological mechanisms through which cells were patterning was never proposed.

In this study, we examine the geometric properties of channeled topographies that induce a patterning response and the biological mechanisms responsible for it. Compared to the extensive research examining the effects of nano/microgrooves, our experiments are performed on macro scale topographies. Our 100x100µm microfabricated grooves create a microenvironment that subject cells not only to two-dimensional nano-scaled surface topographies but three-dimensional macro-scaled space. This space permits migration in three dimensions, and as such, opens the possibilities of other cell guiding mechanisms to influence cell behaviour. To elucidate the governing factor guiding fibroblast migration, we systematically tested every known mechanism that drives cell migration in three dimensions.

The most revealing experiments were performed by modulating the geometric properties of the topography. To establish a baseline whereby the migration phenomenon occurs, we microfabricated incremental channel heights to elucidate the threshold at which cells behaved differently. At 10µm (Fig 4.3), the channeled topography has no effect on cell behaviour. Cell dispersion and alignment resembled that of flat topographies. At 20µm (Fig 4.5D), phase separation between to ridge and the groove occurs suggesting that the governing influence on migration is formed at this geometric dimension. It has been proposed by Curtis et al.[232] that sharp discontinuities in the substrate can induce actin condensation resulting in the formation of focal adhesions along the edge of the microgroove. This promotes a phenomenon called " ridge-walking" where cells align and move along the sharp microgrooved drop, refraining from descending to the flat substrate below [239]. Time lapse imaging at both 24 and 48hrs (Supplementary Video 1&2) demonstrate this phenomenon clearly. At 24hrs,

numerous cells are observed to be ridge-walking along the 20µm groove, until finally climbing onto the ridge. At 48hrs, the zoomed inlet reveals the pseudopodial extension sensing and consistently retracting from the edges. This barrier is eventually overcome as proliferation on the ridges minimizes the available surface area and forces cells to move outwards. To further explore this discontinuity theory, we removed the 90° angle present at the edge of the microgroove by creating 20µm high ellipses. As a result, the discontinuity is replace with an eccentricity value of 0.88. Similarly to the 10µm channels, phase separation between the ridge and the grooves disappeared, and no significant preferential alignment was observed (Fig 4.6A). This is highly revealing as it suggests that the 90° contact angle is inducing a locking effect whereby cells are migrating onto the ridges and are then unwilling to climb down as a result of contact guided mechanisms. We further explored the effects of discontinuity by fabricating 100µm ellipses, creating an eccentricity value of 0.46±0.02 (Fig 4.6D). Interestingly, cells began to demonstrate preferential migration at the apex of the channels whilst aligning along the direction of the ridges. Lowering the eccentricity value induces similar effects to high contact angles. This is explained by the mechanical properties of cytoskeleton. During migration, the cell is dynamically remodeling the cytoskeleton through actin treadmilling. This permits the leading lamellipodia to rapidly interact and guide the cell forward[17]. It is proposed that oblique microfilament bundles located between the focal adhesions of the lamellipodia and the nuclear region of fibroblasts are relatively inflexible, so that any high contact angles or curvature would result in the shortening of the leading lamella[87,232,240,241]. This in turn promotes the orientation of the major axis of the cell to align along the edge through the tendency of focal adhesions to maximize their contact area, as described by the focal adhesion theory[88].

We propose that the observed phenomenon of preferential ridge migration occurs in three separate phases. The first is the “random walk” phase, whereby fibroblasts migrate in a stochastic fashion exploring their surroundings. Random walking has been shown extensively in fibroblasts on two dimensional substrates[239,242–244]. The second is the “multi-surface” phase, whereby cells, at some point within their migration, reach

the channel wall. It has been well established that cells display preferential adhesion to corners of microfabricated topographies [245]. They display this preference because surface adhesion is essential to their survival/proliferation and the vertical substrate enables additional focal adhesion binding. Once migrated onto the ridges, cells are submitted to the "locked in" phase. This phase is controlled by contact guidance, of which the theorems of discontinuity, focal adhesion and mechanical restriction all play influential roles. As fibroblasts settle onto the ridges, they continue to explore their surroundings. As they approach the edges they instinctively retract their lamellipodial extensions and continue to interact with other cells. As the density increases, the discontinuity of the edge forces cells to reorient along the channel and maximize focal adhesion binding. This cellular alignment is propagated through out the 100µm ridge to other cells and results in the unidirectional fibroblast network as observed in our experiments.

4.4 CONCLUSION

This study has revealed that contact guidance is capable of directing cell migration in three dimensional geometries. By seeding NIH3T3 fibroblasts in 100x100µm channels, we observed active migration out of the channels and on to the ridges. This occurred in three distinct phases that we have termed: random walk, multi-surface and locked in. Traditionally, contact guidance has been limited to two dimensional surfaces with grooves ranging between 75nm-3µm. Our study clearly demonstrates that large scale contact guidance can induce phase separation and manipulate cell morphology in large cell populations. Cell behavior to acute contact angles and radii of curvature are consistent with previous studies[232,239,246] and their proposed theorems. Understanding the mechanisms that cells utilize to interact with intricate geometries may have important implications in the future development of complex three dimensional biomaterials and the artificial tissue constructs that aim to be developed.

4.5 MATERIALS & METHODS

4.5.1 SUBSTRATE FABRICATION AND IMAGING

Master molds were fabricated by soft lithography[47]. Silicon wafers were cleaned through three cycles of isopropanol rinses, dried with purified nitrogen, and subsequently plasma treated for 5 minutes at 200W. Two layers of AZ P4620 were spin coated uniformly on the wafer. Spin speed and time were chosen based on final thickness. After each spin coat, the wafers prebaked at 80°C followed by. At least an hour of rehydration was required prior to UV exposure. The wafer was then immersed in AZ400K developer to remove uncross-linked residue of the photoresist. To obtain rounded microchannels, the wafer was required to be postbaked at 75°C, 105°C, 150°C and 200°C for 5 minutes each. Herein, the channels were first patterned with 20-µm thick features, which were then reflowed to obtain 20-µm thick rounded microchannels[48]. Microfluidic channels made of polydimethylsiloxane (PDMS) elastomer (Sylgrad 184, Dow Coring) were replicated from the master mold. Following the fabrication, the mold was treated with trichlorosilane (tridecafluoro-1, 1, 2, 2-tetrahydrooctyl, Sigma Aldrich) to facilitate PDMS removal. The PDMS base was mixed with curing agent (10:1 mixing ratio), then poured directly on the master mold. The mixture was degassed in a vacuum chamber for 30 minutes and baked at 80°C for 2 hours. Finally, the cured PDMS was peeled off and cut out to create the microchannel structures. Scanning electron microscope images were acquired on a JEOL JSM-7500F FESEM.

4.5.2 CELL CULTURE

NIH3T3 and NIH3T3 GFP mouse fibroblast cells (Cedarlane, #AKR-214) were cultured as per the recommended protocol[247] in Dulbecco's modified Eagle's medium. Unless otherwise stated, cells were grown in 10% fetal bovine serum and 1% Penicillin/Streptomycin (Hyclone). Before seeding, PDMS substrates were plasma treated at 50W for 30 seconds to functionalize the surface. They were subsequently coated with 5µg/cm2 collagen I rat tail (Gibco), incubated for 1 hour at room

temperature and rinsed with PBS. For seeding, a 100µl droplet containing 50 000 cells was pipetted onto the 10, 20 and 100µm microfabricated topographies and placed in the incubator (37°, 5% CO2) for 1 hour to allow adhesions. Once adhered, 3ml of media was added to the 35mm whereby the cells were then cultured for an additional 47hrs. Experiments analyzing the effects of geotaxis were performed by permitting cell adhesion for 4hrs and then inverting the entire topography 180° in the dish. For 90° inversions, a custom cut T-25 culture flask was used whereby the opening was removed to permit upright placement of the PDMS topography and subsequently covered with parafilm for 48hrs. Experiments inducing a linear flow were performed by introducing and inlet and outlet tubing routed to a peristaltic pump (Fisher Scientific 13-876-2) into the dish 4hrs after cell seeding. The flow rate was 100µl/m causing an entire fresh media cycle every 30mins for the entire 48hrs experiment.

4.5.3 Immunofluorescence staining, Time Lapse imaging and microscopy

Cells seeded on microfabricated substrates were fixed with 3.5% paraformaldehyde and permeabilized with Triton X-100 at 37°C. As previously published [50], actin was stained using an Alexa Fluor 546 Phalloidin (Invitrogen, #A22283) antibody for 1 hour followed by 5 mins of Dapi (Invitrogen, # D1306) for DNA staining. Cells were mounted with Vectashield (Vector Labs) and covered with a coverslip. The samples were then inverted and imaged with a Nikon Ti-E A1-R high-speed resonant laser scanning confocal microscope at 10x and 60x water immersion objective. Collagen staining was performed with a collagen I primary monoclonal antibody COL-1 (ThermoFisher Scientific) for 1 hour. The sample was then rinsed three times with PBS and a rabbit anti-mouse IgG CF546 mouse (Sigma, 1:500) was added for 1 hour. Samples were rinsed one last time with PBS and imaged on the confocal microscope.

Time Lapse imaging was performed on both a Nikon Ti-E inverted phase contrast microscope and the Nikon Ti-E A1-R confocal microscope. After cell seeding (as previously described), the dish was placed in a custom fabricated thermo regulated acrylic box maintained at 37°C. An inlet tube was place inside the box flowing 1ml/sec of

5% CO2/Air for the entire duration of the experiment to replicate incubator conditions. A small container containing 10mls of dH2O was also place inside the box to compensate for evaporation. Images were taken every 10 minutes capturing phase and fluorescence (488nm channel) for the 4-24hrs and 48-68hrs experiments.

4.5.4 Young's Modulus Measurements

To assess the stiffness of the tops and bottoms of the PDMS channels, a Nanowizard II atomic force microscope (AFM) (JPK Instruments, Germany) was used. A PNP-TR-TL cantilever with a 10µm bead attached with UV curable Norland optical adhesive glue (NOA 60) was used for each measurement and had an experimentally determined spring constant of 100.8 mN/m. Force-indentation curves were acquired on substrates with a set point of 1.0 nN. Substrate elasticity was calculated by fitting the force curves to the Sneddon-Hertz model for a spherical indenter for shallow 200 nm indentations, assuming a Poisson ratio of 0.5 (PUNIAS 3D Software). For each condition, 10 force curves were acquired at 3 different channels.

4.5.5 Image Analysis and Statistics

All image processing was performed in Image J (Fiji). Ridge to groove analysis was performed by manually counting cell nuclei within the max projected confocal stacks. Cells located within the bottom or side walls of the channels were designated as "groove", whilst all cells on top were tagged as "ridge"(Fig 4.1). The ridge to groove analysis is performed by calculating the ratio of cells on the ridges to those in the groove.

Alignment analysis was calculated by first thresholding max projected images to acquire the outline of each nucleus. We quantified cellular alignment by first determining the angle (θ) formed between the long axis of each elliptical nucleus and the groove direction [45]. We then calculated an order parameter [45] using:

$$S = \langle \frac{3cos^2\theta - 1}{2} \rangle$$

In a given population of cells, S will approach 0 if they are randomly oriented with respect to the groove direction. Conversely, S will approach 1 if there is a strong degree of alignment between the groove direction and the cells. Finally, if the cells are aligned perpendicular to the groove direction, S will approach -0.5.

Eccentricity measurements were performed by imaging cross-sectioned elliptical pdms topographies and analyzing them in Image J. The semi-major (a) and semi-minor (b) axes were measured and the eccentricity formula was used to calculate the values.

$$e = \sqrt{1 - \frac{b^2}{a^2}}$$

Cell tracking and analysis was performed through the TrackMate [248] plugin in image J. All values in the text are presented as the average ± s.e.m. A one-way ANOVA followed by a Tukey test for means comparison or two-sample t-tests were performed to assess significance ($p < 0.01$).

4.6 ACKNOWLEDGEMENTS

S.H. was supported by the Queen Elizabeth II Graduate Scholarship in Science and Technology. A.E.P. gratefully acknowledges generous support from the Canada Research Chairs program. This work was also supported by the Natural Sciences and Engineering Research Council of Canada (NSERC) Grant No. RGPIN/355535 to A.E.P. We would also like to acknowledge the University of Ottawa for their generous support.

Chapter 5 | Manuscript

Physical Confinement Signals Regulate the Organization of Stem Cells in Three Dimensions

Sebastian V. Hadjiantoniou[1], David Sean[2], Maxime Ignacio[2], Michel Godin[2,3,4], Gary W. Slater[2] and Andrew E. Pelling[1,2,6]

[1]*Department of Biology, Gendron Hall, 30 Marie Curie*
[2]*Department of Physics, MacDonald Hall, 150 Louis Pasteur*
[3]*Department of Mechanical Engineering, Site Building, 800 King Edward Avenue*
[4]*Ottawa-Carleton Institute for Biomedical Engineering*
[6]*Institute for Science, Society and Policy, Desmarais Building, 55 Laurier Ave. East*

Submitted Aug 3rd 2016 to The Royal Society Interface

Accepted September 20th 2016, V.13. (123)

Motivation & Objectives |

Previous studies have always grown embryonic stem cell in spherically engineered systems. We utilize anisotropic confinement to assess its effects on embryonic stem cell morphogenesis and assess the influence that physical binding interactions have on their growth. We further attempt to explain this by recreating the system in a Langevin dynamic simulation.

5 | PHYSICAL CONFINEMENT SIGNALS REGULATE THE ORGANIZATION OF STEM CELLS IN THREE DIMENSIONS

5.1 ABSTRACT

During embryogenesis, the spherical inner cell mass (ICM) proliferates in the confined environment of a blastocyst. Embryonic stem cells (ESCs) are derived from the ICM, and mimicking embryogenesis *in vitro*, mouse ESCs (mESCs) are often cultured in hanging droplets. This promotes the formation of a spheroid as the cells sediment and aggregate due to increased physical confinement and cell-cell interactions. In contrast, mESCs form 2D monolayers on flat substrates and it remains unclear if the difference in organization is due to a lack of physical confinement or increased cell-substrate vs cell-cell interactions. Employing microfabricated substrates we demonstrate that a single geometric degree of physical confinement on a surface can also initiate spherogenesis. Experiment and computation reveal that a balance between cell-cell and cell-substrate interactions finely controls the morphology and organization of mESC aggregates. Physical confinement is thus an important regulatory cue in the 3D organization and morphogenesis of developing cells.

5.2 INTRODUCTION

It is now well recognized that physical cues play an important role in the differentiation and fate of stem cells[249–252]. Mechanical forces, matrix topography, matrix mechanics and even cell shape have a profound influence on lineage commitment[249,251–253]. However, occurring well before commitment, the inner cell mass (ICM) must organize into a 3D spherical aggregate inside of the blastocyst, confined between a fluid filled cavity and the outer trophoblast membrane. These conditions permit the initiation of embryogenesis, whereby mESCs will subdivide into three germ layers and go on to differentiate into every cell type in the body.

It has been well established that during their pluripotent state, mESCs express high levels of cell adhesion proteins, most prominently E-cadherins[254–256]. This is unsurprising as preliminary formation of the ICM is heavily dependent on cell-cell

interactions that dynamically form the physical properties of their microenvironment. In turn, E-cadherin expression and regulation play a pivotal role in morphogenesis and development through biomechanical feedback events[257,258]. The spatiotemporal pattern of expression of E-cadherins is responsible for cell layer separation, recognition and rearrangement[171]. Furthermore, there is also an intimate association between intercellular adhesion sites, the actomyosin network and associated regulatory pathways[259,260]. It has been reported that cortical actin is responsible for promoting distinct patterns of cadherin migration and clustering along the rim of the contact plane between cells[261,262]. Clearly, there exist important regulatory mechanisms to control the adhesion and organization of mESCs during the early formation of the ICM.

In vitro, standard protocols have been devised to produce cell aggregates defined as embryoid bodies (EBs) in an effort to mimic the processes that give rise to the ICM. Widespread methodologies attempt to replicate the spherical aggregation and proliferation of the ICM by confining mESCs in a hanging drop, which forces cell-cell aggregation due to the lack of a substrate. In addition to hang drop cultures, microfabricated substrates containing spatially ordered arrays of semi-spherical wells have also been utilized to initiate the aggregation of mESCs into a spheroidal structure[118,119,263]. Cells seeded onto such substrates are passively confined within the wells that act as a mold for the developing EB. Microfabricated substrates have the advantage of allowing one to exert control over the size and geometry of the resulting EB, which ultimately influences downstream differentiation[119,263,264].

It is thought that semi-spherical microwells are simply acting as a geometric template for the resulting spherical EB. However, it is possible that the spherical formation of the EB is also finely controlled through distinct biochemical and biophysical regulatory mechanisms. Therefore, we hypothesized that spherical EBs would continue to form spontaneously even in the presence of anisotropic, non-circular physical confinement. Moreover, such aggregation and organization should be driven by both physical and biochemical mechanisms. Contrary to other studies that utilize isotropic

microwells[119], we've chosen to systematically examine this issue by fabricating substrates containing 1.5cm long, 100µm deep open-top grooves of varying widths (50-1000µm)[265]. On these substrates, cells quickly accumulate in the bottom of the grooves, as they possess a higher mass density than the surrounding medium. After accumulating in the bottom and adhering, cells are free to migrate out of the grooves and along their length. However cell migration is limited across the groove width. We demonstrate that this single axis of confinement (arising from the groove width) is all that is required to induce the spherical and isotropic aggregation of mESCs into an early EB. During the first ~6hrs after entering the grooves, physical confinement leads to an increase in cell-cell collisions which nucleate the formation of a spherical EB. Conversely, in the absence of any physical confinement (cells on planar surfaces) mESCs tended to form large, flat islands, even when seeded at high density. Finally, physical confinement alone is not enough to induce EB formation, as E-cadherin activity and actomyosin dynamics play a key regulatory role. The cytoskeleton constitutively exerts tension on E-cadherins at the plasma membrane capable of modulating E-cadherin expression and subsequent cell-cell binding[266–268]. Therefore, the molecular mechanisms that control cell-cell adhesion and aggregation are also important during the earliest stages of spherical EB formation. Although mechanical forces and material properties are clearly important during developmental processes [106,249], our work highlights the fact that physical confinement also plays an important role in early embryogenesis. One of the earliest stages of lineage specification occurs in a highly confined environment that itself imparts a regulatory role in the aggregation and organization of cells into the ICM. Our work suggests this physical separation of the ICM and the trophoblast is not only biochemically regulated, but also driven by physical signaling.

5.3 RESULTS

5.3.1 PHYSICAL CONFINEMENT PROMOTES THE SPONTANEOUS FORMATION OF 3D SPHEROIDS

Standard soft lithography techniques were employed to fabricate collagen coated PDMS substrates containing microfabricated grooves. Groove width was

systematically varied (50, 100, 200, 500, 1000μm) in order to alter the degree of physical confinement on scales 1-2 orders of magnitude larger than the average length of an individual cell (10μm). Importantly, such geometries act to confine cell movement across the groove width, yet permit movement along the length and out of the groove[265]. We have previously shown that this can have profound impacts on the organization and migration characteristics of epithelial and fibroblast cells, even in co-culture[265]. In the current study, SEM and phase contrast imaging 48hrs after plating reveals that the vast majority of mESCs were found to have spontaneously formed spherical aggregates resembling EBs (Fig 5.1B,C), including many that do not touch either vertical wall. Samples were also fixed and fluorescently labeled for actin and DNA, followed by imaging with laser scanning confocal microscopy (LSCM). Images reveal that physical confinement in the grooves clearly results in mESC aggregates that possess a 3D morphology (Fig 5.1D,E). On flat, collagen coated PDMS substrates, mESCs have essentially formed flat islands (1-2 cells thick), rather than a structure resembling a spheroid (Fig 5.1F,G).

To quantify the morphology of the mESC aggregates observed in this study, we calculated their planar (I_p) and globular (I_g) isotropy (Materials and Methods). After mESCs were allowed to proliferate on flat or grooved substrates for 48hrs, they were fixed and stained as described above and imaged with LSCM. For each substrate, 10 randomly chosen locations were imaged on both substrates. For each aggregate identified, the images were thresholded and for each image slice in the confocal stack, we determined the coordinates of the circumference of the aggregate using the 'analyze particles' ImageJ plugin. This approach provided the coordinates of the aggregates in 3D and allowed us to quantitatively assess the shape of the aggregates using our definitions of I_p and I_g. As the isotropy value approaches 1, I_p and I_g describe a perfect circle and sphere respectively. As expected, when one views the aggregates from above, regardless of substrate topography, all aggregates appear roughly circular with an I_p that varies between 0.66 ± 0.03 and 0.78 ± 0.03 depending on grove width. Importantly,

there was no statistically significant dependence of I_p on groove width or substrate topography ($p > 0.05$ in all cases).

In contrast, I_g analysis revealed that on flat substrates, cells proliferated in a planar fashion where $I_g = 0.27 \pm 0.02$. Conversely, in the grooves, globular isotropy was inversely proportional to groove width. In the 50 µm wide grooves, spheroids possessed an average I_g of 0.86 ± 0.03, which decreased to 0.32 ± 0.02 in the 1000µm wide grooves (Fig. 1H). Only the aggregates in the 50 and 100µm grooves possessed an I_g significantly larger than the aggregates on the flat substrates ($p<0.001$). Interestingly, the number of cells per aggregate (50 ± 7 cells) did not display any statistically significant dependence on groove width (Fig 5.1I).

An SEM image of a spheroid in a 100µm channel after 48hrs of proliferation (Fig 5.1B) clearly reveals that spheroids can form without contacting channel walls for support, consistent with LSCM data. However, spheroids can also be found in contact with groove walls if they become very large or happen to initiate immediately beside a wall. This presented a problem in the 50µm channels as the aggregates were often found in contact with both walls, potentially leading to the larger observed I_g values. Therefore, in the following sections, we performed all experiments in 100 µm wide channels in order to ensure that the observed morphology is not influenced by the aggregate coming into physical contact with both channel walls.

5.3.2 The role of actin dynamics on 3D aggregate formation

In order to investigate the role of actin dynamics in regulating aggregation and 3D morphology, mESCs were treated with a well-known Rho-kinase (ROCK) inhibitor (Y27632), a specific myosin-II (myoII) inhibitor (blebbistatin) and an mDia1/2 inhibitor (SMIFH2). In general, ROCK plays a major role in many aspects of actin organization, myo-II governs actin contractility and mDia1/2 belong to a family of formins that regulate actin nucleation and polymerization[238,269,270]. After 48hrs of culture, cells were fixed and stained to visualize the actin cytoskeleton and the nucleus with LSCM.

Inhibiting ROCK and mDia1 caused a statistically significant effect ($p<0.001$) on spheroid shape characteristics whilst blebbistatin had little effect. The ROCK inhibitor completely inhibited the 3D shape of the spheroid (Fig 5.2A), resulting in cells growing along the sides of the grooves. Cells could be found in isolation and small island-like aggregates that resembled growth on a flat substrate. The average I_g of the aggregates was determined to be 0.22±0.02, which is significantly less than untreated cells 0.49±0.04 ($p<0.001$). Blebbistatin treatments appeared to have no effect on I_g (0.54±0.05) compared to untreated cells in 100µm channels (Fig 5.2B). Conversely, inhibition of mDia resulted in the formation of more isotropic spheroids (I_g = 0.80±0.04, Fig 5.2C), significantly higher than the untreated cells in 100µm channels ($p<0.001$) (Fig 5.2D). Finally, on flat substrates, drug treatments had no statistically significant effect ($p>0.05$) on I_p or I_g compared to untreated cultures (Supplementary Fig 5.6.2). These results clearly demonstrate that the role of actomyosin dynamics in regulating cellular aggregation and organization in 3D spheroids is strongly dependent on the presence of physical confinement.

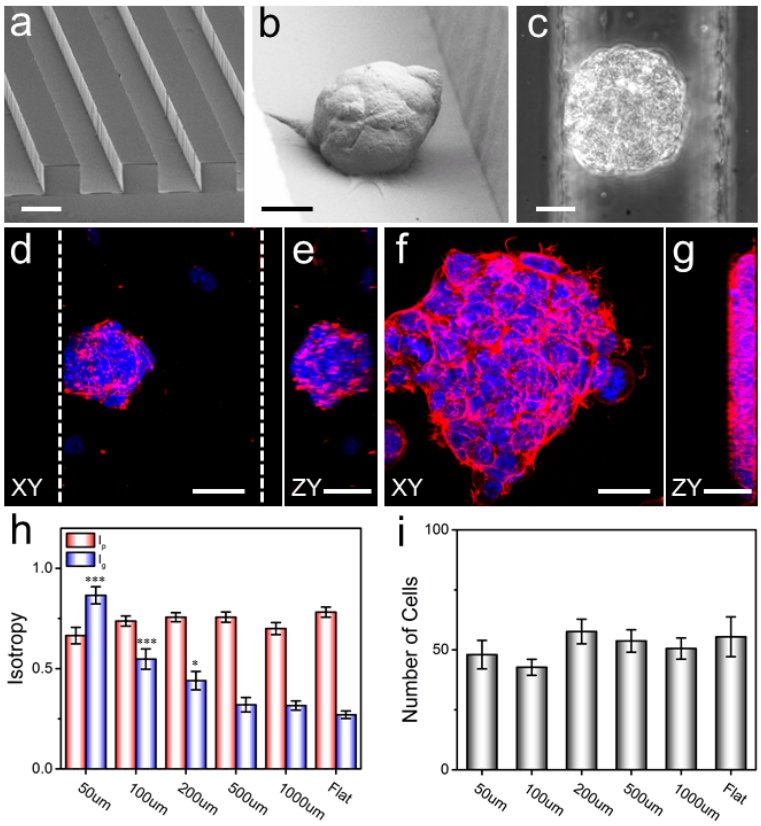

FIGURE 5.1 EFFECTS OF TOPOGRAPHICAL CONFINEMENT ON EMBRYONIC STEM CELL GROWTH.

(a) A perspective view of an SEM image of the PDMS substrate reveals the structure of a typical microtopography with 100 µm grooves and ridges. Embryonic stem cells are seeded on this 100µm groove topography for 48hrs, whereby spheroidal aggregates begin to form as a result of the confinement properties of the microenvironment (scale bar = 100 µm). SEM (b) and phase contrast (c) images display the spheroidal geometry of the aggregates in the 100 µm groove after 48hrs of growth (scale bars = 25 µm). Actin (red) and dapi (blue) in a top-down (d) and side (e) view further reveal the three dimensional geometry of the aggregate in a grooved space. Doted lines indicated the presence of the channel walls. Cells plated on a flat PDMS substrate demonstrated significantly different geometric shapes with their morphology resembling a circular (f, top-down) yet flat shape(g, side view) (all scale bars = 25 µm). (h) The globular isotropy Ig (blue) and planar isotropy Ip (red) which define the sphericity and circularity of the aggregate respectively revealed that at higher levels of confinement (50 µm, 100 µm, 200 µm), Ig is statistically different (*** $p<0.001$, * $p<0.05$, one way ANOVA, mean± s.e.m) to the flat substrate while Ip remains unaffected. The number of cells per aggregate (i) was also counted to ensure that the differences in morphology observed weren't the result of cell density. The results show no statistically significant difference across any of the channels and the flat substrate. (n=25)

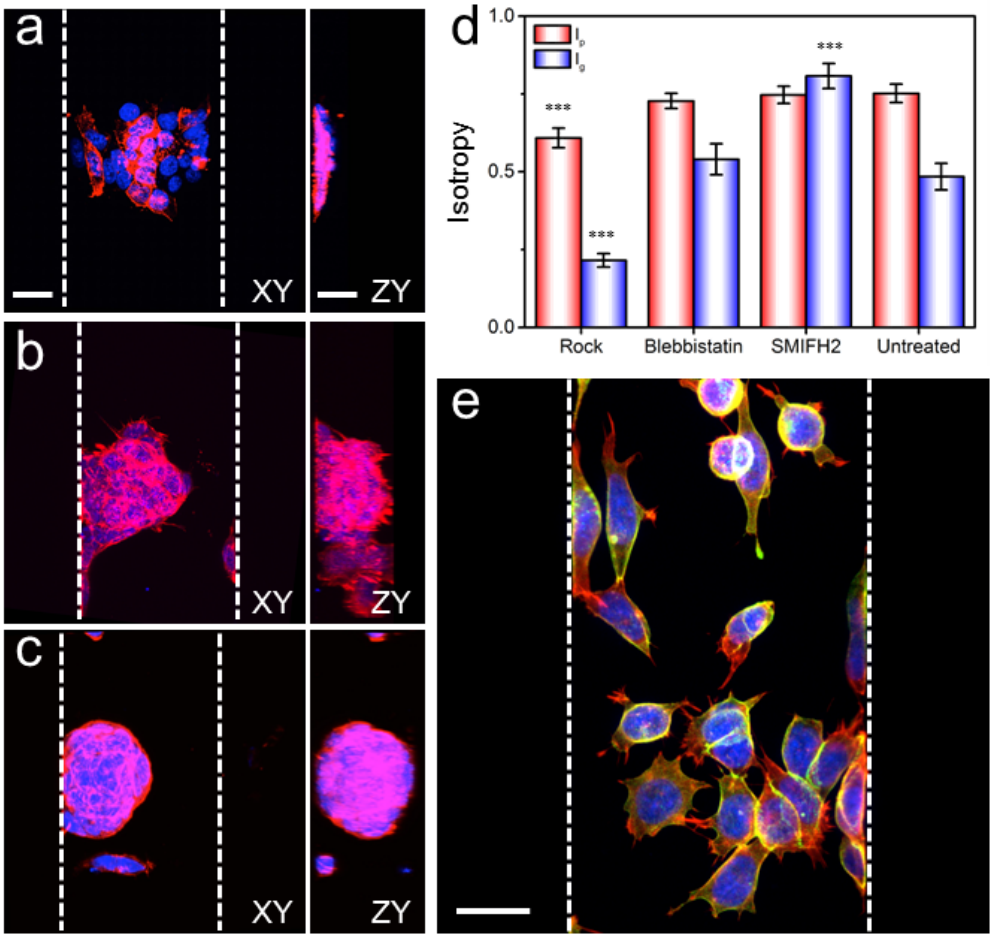

FIGURE 5.2 THE EFFECTS OF INHIBITING ACTOYMYOSIN DYNAMICS AND E-CADHERIN FUNCTION ON SPHEROID FORMATION.

Max projection images of actin (red) and dapi (blue) taken by confocal microscopy displaying the effects of the drugs Y-27632 (a)(n=20), blebbistatin (b)(n=24) and SMIFH2 (c)(n=28) on embryonic stem cells grown in 100um grooved channels (scale bars in (a) = 25 µm and apply to (b) and (c)). Dotted lines represent the presence of the wall. Inhibition studies were performed to elucidate the molecular mechanisms responsible for altered development in response to confinement. (d) With the exception of blebbistatin, both Y-27632 and SMIFH2 had a significant effect on the globular isotropy Ig (blue). Planar isotropy Ip (red) appears to be less affected by the selective inhibitions with only Y-27632 demonstrating a significant effect. E-cadherin, the cell surface protein responsible for cell-cell adhesions, was blocked by exposure to a primary E-cadherin antibody prior to sending. (e) Actin (red), dapi (blue) and e-cadherin (green) display the effects of blocking e-cadherin prior to seeding in the grooves, resulting in a complete breakdown of aggregation as cells aberrantly grew in a single cell manner (scale bar = 25 µm)(n=3).

5.3.3 Direct modification of cell-cell and cell-substrate adhesion

To investigate the importance of cell-cell and cell-substrate interactions during aggregate formation we designed two additional experiments. In the first case, we interfered with cell-cell interactions by treating mESCs in suspension with an E-cadherin primary antibody for 30 mins prior to culturing on flat and 100µm grooved surfaces. After 48hrs of culture, cells were stained and imaged for actin and DNA. As well, we also treated the cells with a fluorescently labeled secondary antibody to visualize the E-cadherin antibody that was introduced prior to plating. Applying the secondary antibody confirmed the presence of the primary antibody bound to E-cadherins even after 48hrs in culture. Imaging reveals that cell-cell aggregate formation was significantly impaired. Individual cells were clearly dispersed and sometimes found in isolation (Fig 5.2E). Spheroid formation was abolished and cells were found throughout the channels.

In a second experiment, we sought to manipulate cell-substrate adhesion. In this case, PDMS substrates were either left unfunctionalized or functionalized with fibronectin in addition to collagen. Bare PDMS channels or flat substrates completely lacked any significant cell proliferation after 48hrs confirming the importance of matrix proteins in promoting adhesion (Fig 5.8A,B). We then hypothesized that additional extracellular matrix proteins should provide an increased number of sites for cell-substrate binding via integrins and thereby enhance cell-substrate interactions. Interestingly, the altered adhesive properties of the substrate (collage + fibronectin) did not impede the formation of spheroids, which occurred in a manner consistent with previous data. However, the addition of fibronectin to the surface promoted cell growth on the groove ridges (Fig 5.8C). The morphology of the cells on the ridges was similar to cells growing on flat substrates. Cells found on ridges clearly lack the influence of physical confinement, indicating its importance in the formation of spheroids.

5.3.4 Effects of confinement on cell displacement and collision frequency

Thus far, we have reported on the appearance of spheroids in confined geometries after 48hrs of culture. In order to understand the initiation and progression

of spheroid formation at early times we performed live cell time-lapse phase contrast imaging of mESCs over a 24 hour period following plating on flat and grooved surfaces (3 replicates in both cases). On flat substrates (Fig 5.3A)(Supplementary Video 1), cells initially attach to the surface as single cells or in small groups and then proliferate into island shaped aggregates. In general we also observe that island growth occurs mainly through proliferation rather than through new cells joining the island through migration. Time lapse imaging of grooved surfaces reveals a very different series of events. Immediately after seeding, cells were found at the bottom of the grooves due to their higher mass density than the surrounding medium (Fig 5.3B). Within 12hrs incubation time, cell-cell aggregation nucleates the formation of the spheroids. By 24hrs, the spheroids have exhibited proliferative growth, expanding in 3D (Supplementary video 2). A more in depth analysis over a two hour period shortly after seeding (Fig 5.3C)(Supplementary Video 3), revealed that very early spheroid formation is driven by the collision and aggregation of a small number of cells. In the early spheroid, mitosis can be observed (Fig 5.3D). After cytokinesis occurs the newly divided cells remain adhered to the aggregate. This process continues as the initial nucleate develops into a 3D spheroid.

To quantify these observations, we measured the frequency of collision events between cells during the early formation of the spheroids (Fig 5.4A). Importantly, cells found in the grooves exhibited a collision frequency (22 ± 7 collisions/hr) ~4-fold higher than cells on flat surfaces (7 ± 2 collisions/hr). However, as the number of cells seeded onto each substrate was constant, the collection of cells into the grooves leads to a higher effective cell density as a result of physical confinement. To control for this effect, a series

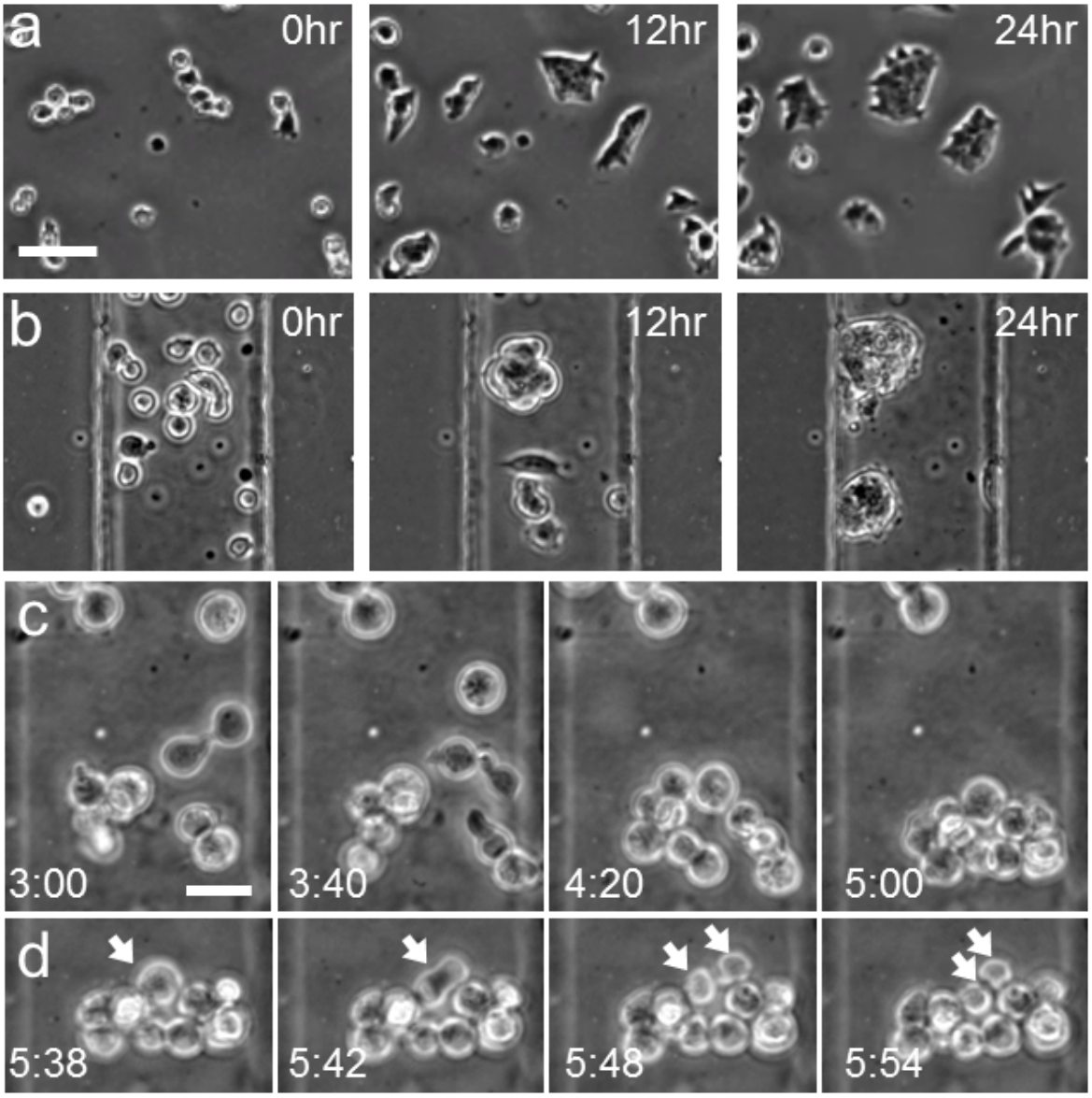

FIGURE 5.3 TIME LAPSE IMAGING OF MESC PROLIFERATION AND ORGANIZATION.
Embryonic stem cells were seeded on to a flat (a) and 100µm channeled (b) PDMS topography and imaged for a 24hr period. Scale bar = 50 µm. Aggregation between cells display distinctly different formation patterns as confined cells grow in a far more three dimensional manner. (c) A closer look at the preliminary cell-cell interactions of a developing aggregate in a 100µm channel. Scattered cells diffuse until they stochastically collide eventually forming a chain of cells. This is followed by an infolding, creating a preliminary spheroidal geometry. Once aggregated, (d) growth occurs through cycles of mitosis (white arrow) and cell re-organization. Scale bar = 25 µm.

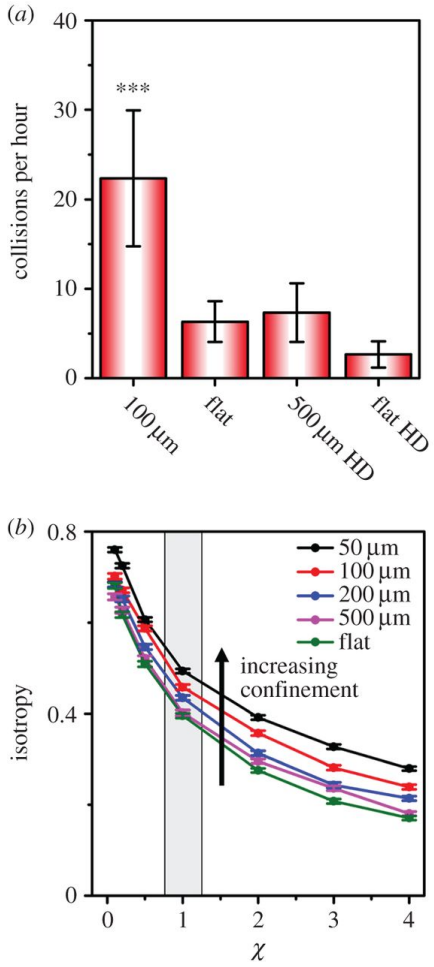

FIGURE 5.4 CELL-CELL COLLISION DYNAMICS AND COMPUTATIONAL MODELING OF CELLULAR ORGANIZATION AND MORPHOLOGY.

(a) The number of collision events between cells at varying levels of confinement. Cells were seeded onto PDMS topographies and recorded every 5 mins for 6hrs. To compensate for the difference in cell density due to confinement, a higher density (HD) seed matching the effective density of 100 µm channels (450 cells/mm^2) was performed for the 500 µm and flat conditions. The collision frequency of cells in 100µm channels was the only condition displaying a statistically significant difference (*** $p < 0.001$) compared to the flat PDMS control. (b) The globular isotropy I_g of simulated spheroids at varying levels of χ (cell-substrate/cell-cell energy). Channel widths: 50 µm (black), 100 µm (red), 500 µm (blue), 1000 µm (green), flat (pink). Simulations were performed replicating experimental conditions, with a preliminary cell density of ~ 450 cells/mm^2 at varying channel widths. Cells undergo a preliminary phase of diffusion followed by cycles of duplication and relaxation. The average (n=100) I_g of aggregates demonstrates that as cell-substrate energies increase, aggregate geometry becomes flatter. At $\chi = 1$, the simulation displays very similar results to those acquired experimentally.

of experiments were performed in which the number of cells added to the flat substrate matched the effective density observed in the 100µm channels (~450 cells/mm^2). Importantly, even at this higher seeding density the observed collision frequency (3 ± 1 collisions/hr) remained significantly lower than observed within the 100µm channels ($p<0.001$). Interestingly, when comparing the effect of cell density on flat substrates, there appears to be a two fold drop in cell collision frequency within high density conditions. Statistical analysis shows no significant difference ($p<0.05$) between these conditions, which suggests that the discrepancy is attributed to the inherent variability between experiments. Although islands were still observed to form at higher seeding density, they tended to be much larger, as expected (Fig. 5.8D,F). In our initial experiments, cell aggregates in 500µm channels were geometrically indistinguishable from aggregates on flat substrates (Fig 5.1H). Therefore, we also conducted an experiment where the higher seeding density was applied to the 500µm channels as well. In this case, we observed a significantly lower collision frequency (7 ± 4 collisions/hr) than in the 100µm channels ($p<0.001$). This suggests that increased cell density alone is not responsible for the observed changes in collision frequency and that physical confinement is playing an influential role in promoting cell-cell interactions.

5.3.5 Simulation of Spheroid Formation

Depending on their respective adhesion affinities, cell-cell and cell-substrate interactions can significantly alter cell morphology and behaviour[255,271–273]. To assess the relative importance of cell-cell and cell-substrate binding in spheroid formation, we developed a simulation model that recreates the confinement conditions of our experiments (Fig 5.4B). It is important to note that this model does not reproduce all the biological complexities of the system but presents complementary information that provides insight into the physical interaction between cell and substrate. In either 100µm channels or flat substrates, cells are allowed to diffuse, interact with each other and the substrate, and undergo mitosis. Through the utilization of a coarse-grain Langevin Dynamic model, we altered the binding energies between cells ($\in_{cc}$) and

substrate ($\in_{cs}$) and quantitatively analyzed the effect on the development of spheroid formations. The relative change in selective binding is denoted by chi ($\chi = \in_{cs}/\in_{cc}$), whereby $\in_{cc}$ is kept constant and $\in_{cs}$ is increased. As the value of χ increases, cell-substrate attraction becomes stronger. With an initial cell density of 450 cells/mm^2, the simulation initiates the diffusion phase, whereby cells explore the surrounding space. Random cells are then chosen periodically to duplicate followed by a relaxation phase whereby newly formed cells can move to a lower energy position. This sequence is repeated until each cell has undergone three generations of duplications.

As can be expected, under extreme χ values of 0 and 4, cell aggregation was extremely spheroidal or flat respectively (Fig. 5.6). Interestingly however, changing the channel width within any condition of χ displayed significant ($p<0.001$) changes in the I_g of the aggregates. At $\chi = 1$, the simulation represents similar I_p and I_g values acquired experimentally. In a non-confined system (flat), the simulation displayed aggregates with an average I_g of 0.39±0.005, negligibly higher ($p<0.01$) than the value of 0.27±0.02 acquired experimentally. Similarly, under the 100μm confinement condition, the simulated and experimental I_g values were 0.46±0.005 and 0.55±0.05 respectively. These results suggest that a relatively balanced $\in_{cc}$ and $\in_{cs}$ is required to induce spherogenesis.

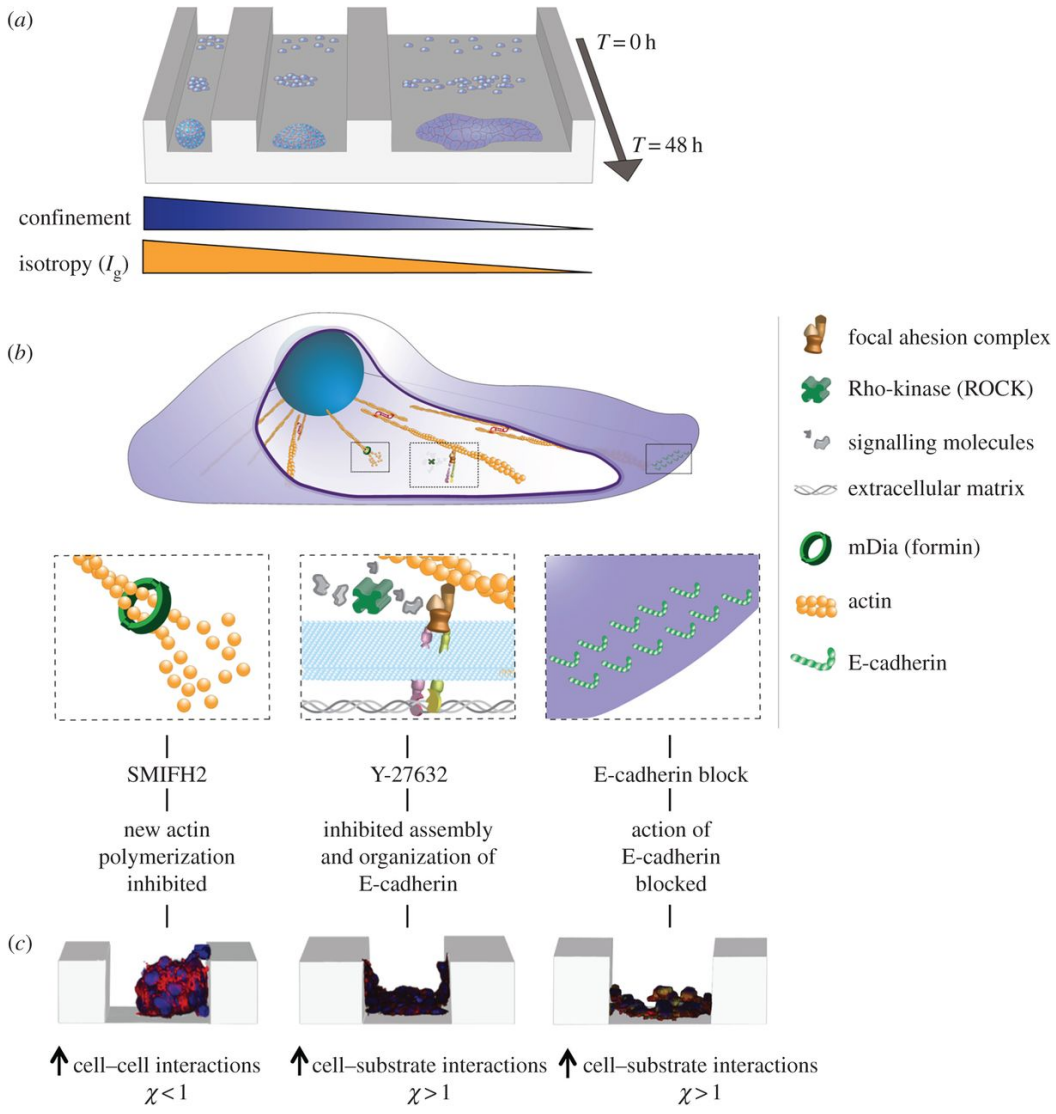

FIGURE 5.5 EFFECTS OF CONFINEMENT AND SELECTIVE PROTEIN INHIBITION IN EMBRYONIC STEM CELL FORMATION.

(A) At T = 0hrs, cells begin to adhere to the substrate. With time, stochastic collisions induce cell-cell interactions and promote aggregate formation. Although this formation occurs in all conditions, its globular isotropy is dependent on the level of confinement imposed on the cells, with higher levels promoting spheroidal formations. (B) Cell movement and growth is dictated by multiple key proteins that regulate actin formation, contraction and cell-cell adhesion. Inhibiting mDia, and consequently actin polymerization, (C) resulted in a spheroidal formation with higher I_g values. Inhibiting Rock, and hence E-cadherin assembly, completely prevented three-dimensional development, causing cells to be highly dependent on cell-substrate adhesion. Similarly, blocking E-cadherins, the cell-cell adhering junctions, prevented cell-cell interactions and prevented any aggregation after 48hrs.

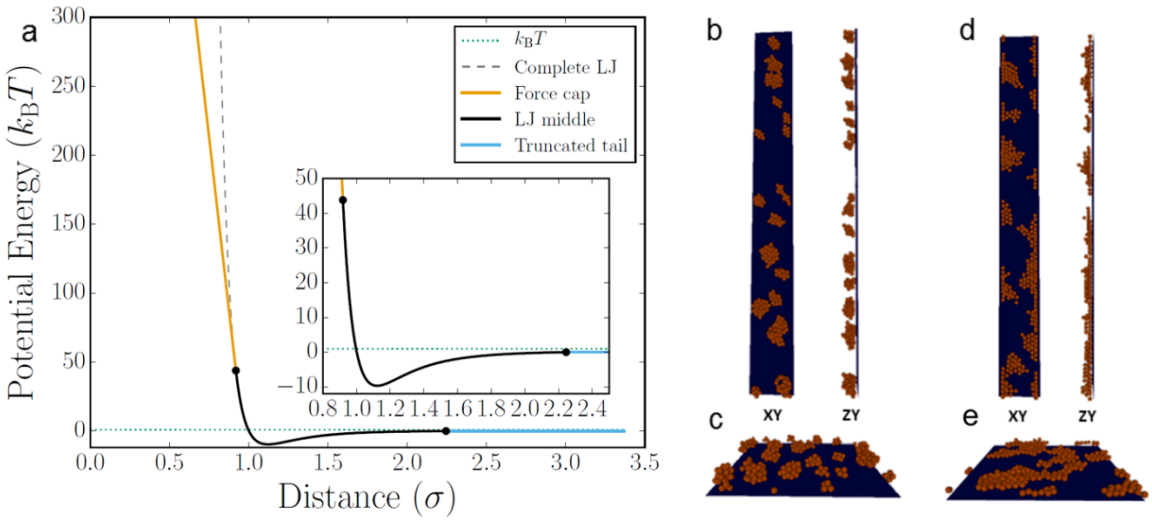

FIGURE 5.6 BEAD INTERACTION POTENTIAL.

a) The piece-wise interaction potential (in units of the effective thermal energy) is shown as a function of separation (in units of the bead diameter). For short distances, a constant force is used which yields a softer repulsion than the full Lennard-Jones interaction (shown as a dashed line). For intermediate distances, the Lennard-Jones potential is used which contains both a repulsive and an attractive component. At large distances the potential is truncated such that the beads have a finite attraction range. Simulations were carried out to understand the influence of cell-substrate (εcs) and cell-cell (εcc) interactions on embryonic stem cells growing within different levels of confinement. A simulation rendered with a χ (εcs/εcc) value of 0.1 (b) in 100 µm channels and (d) on a flat surface, revealing that with a low cell-substrate adhesion, cells are capable of aggregating in a spheroidal manner through purely diffusive means. When generated with a χ of 4, under (c) 100 µm and (e) flat conditions, cells demonstrate typical flat island morphology irrespective of the confinement.

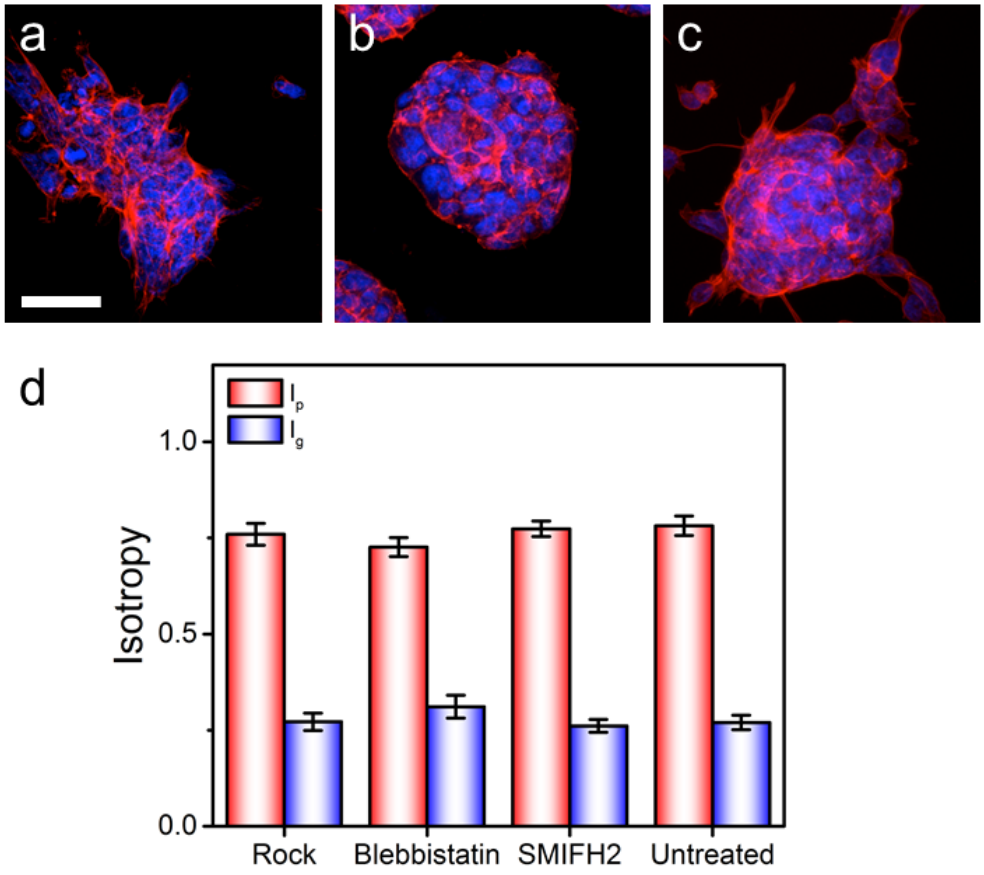

FIGURE 5.7 THE EFFECTS OF INHIBITING ACTOMYOSIN DYNAMICS AND E-CADHERIN FUNCTION ON MESC ORGANIZATION ON FLAT SUBSTRATES.

Embryonic stem cells were seeded onto a flat PDMS surface with inhibitory drugs (a) blebbistatin (2μM)(n=24) , (b) Y27632 (10μM)(n=20) and (c) SMIFH2 (10μM)(n=28) for a 48hr incubation period (Scale bar = 50 μm and applies to all). Contrary to cells grown in a confined microenvironment, inhibition of actin contractility, mechanotransduction signalling and actin polimerization respectively had no effect on aggregate morphology whilst on a two dimensional surface. (d) No significant difference was found with regards to the planar Isotropy (I_p, black) or globular isotropy (I_g, red) when we used any of the inhibitory conditions.

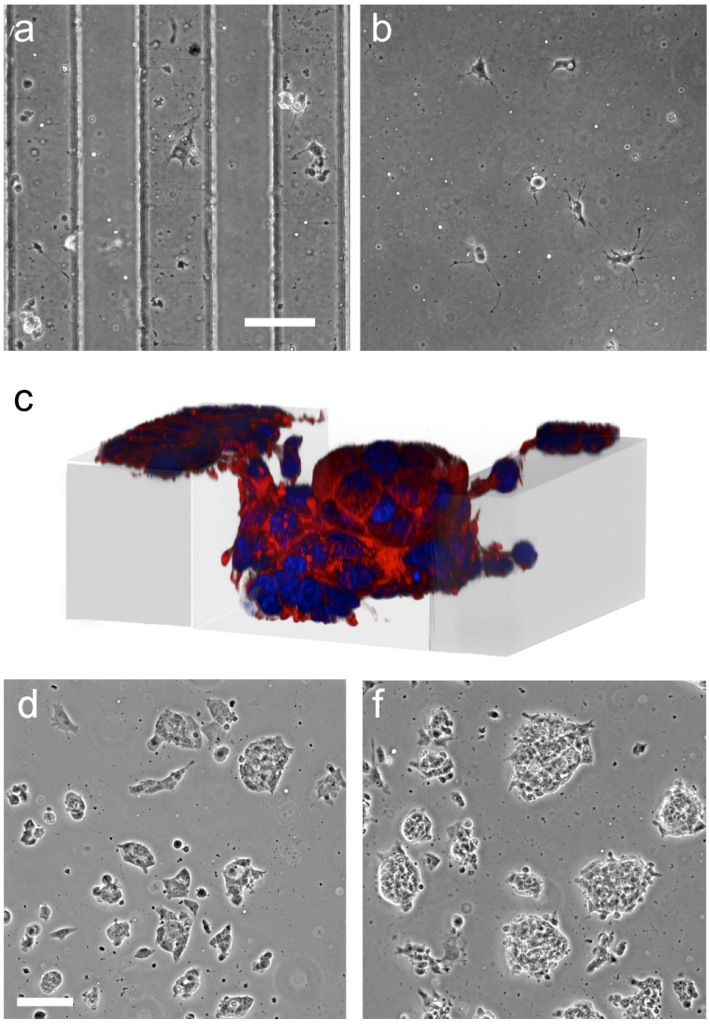

FIGURE 5.8 MANIPULATING CELL-SUBSTRATE INTERACTIONS THROUGH MATRIX PROTEIN DEPOSITION.

To confirm that collagen is responsible for the cell-substrate adhesion on PDMS channels, cells were seeded without collagen and incubated for 48hrs. Whether on the (a) 100 µm channel or the (b) flat substrate, no cells had successfully adhered (Scale bar = 100 µm and applies to (b) as well). (c) In an attempt to reverse the spheroidal geometry observed in the channels, we increased cell-substrate adhesion by depositing fibronectin in addition to collagen. Increased cell substrate adhesion appeared to have no effect of embryonic stem cells growth, as the aggregate still formed a highly three dimensional geometry. Interestingly, the increased substrate interaction promoted cell adhesion at the top of the channels; however, these cells formed typical two dimensional flat aggregates. To ascertain whether the observed changes in geometry are the result of a higher cell density, cells were seeded to match the density of 100 µm channels (~450 cells/mm^2). Shown are cells at (d) 12hrs and (e) 48 hours after seeding, displaying a typical island shaped morphology. Scale bar = 100 µm.

TABLE 5.9 MONTE CARLO SIMULATION PARAMETER

Description	ESPResSo variable	Numerical value
Gravitational force ($\boldsymbol{F}_{\mathrm{grav}}$)	ext_force (constant force vector)	(0, 0, -0.1)
Integration time step	time_step	0.01
Fluctuation energy	temperature (Langevin thermostsat)	0.1
Bead friction coefficient	gamma (Langevin thermostsat)	50
Cell-cell well depth (ε_{CC})	epsilon (Lennard-Jones)	1.0
Cell-substrate well depth (ε_{CS})	epsilon (Lennard-Jones)	(0.1- 4.0)
Effective cell diameter (σ)	sigma (Lennard-Jones)	1.0
V_{LJ} cutoff radius (r_{cut})	rcut (Lennard-Jones)	1.12246
Force cap (F_{cap})	fmax (ljforcecap)	100.0

5.4 DISCUSSION

In this study we examined the influence of physical confinement on the three-dimensional spatial organization and growth of mESCs. To investigate this, we fabricated grooved, collagen-functionalized, PDMS substrates of varying widths (50, 100, 200, 500, 1000µm) and constant depth (100µm). Interestingly, after 48hrs of incubation, cells grown on substrates with 50-200µm grooves displayed clear spheroidal growth. This differs from the traditional flat two-dimensional cultures in which cells display flat, island-shaped aggregates. Importantly, in the absence of collagen-functionalization, cells did not adhere or proliferate on the PDMS substrates. Contrary to previous strategies utilizing concave microwells[119] to form spheroids, this experiment reveals that spontaneous 3D growth can occur as a result of a single axis of physical confinement. Quantitative globular isotropy analysis revealed how 3D growth decreased with decreasing physical confinement (Fig 5.1H). It is interesting to note that the I_p within flat conditions was <0.8, suggesting an intrinsic level of anisotropy. Although speculative, this intrinsic level of anisotropy may potentially arise from actin stress fiber polarization

in individual cells in the aggregate. Furthermore, spheroid formation did not appear to be dependent on the proximity to channel walls, displaying 3D growth without a surrounding matrix. The aggregation was also not the result of a higher cell density, as there was no statistical difference ($p>0.05$) in the collision frequency of highly seeded (450 cells/mm^2) flat PDMS surfaces.

To examine whether increased substrate adhesion could alter spheroid formation in the channel, we increased cell-substrate interaction by depositing both collagen and fibronectin before cellular plating. Within the confines of the grooves, spheroid formation was not obviously altered**.** Interestingly, cells adhered and grew at the top of the ridges as well, in a flat island like shape, a completely different morphology to the cells below. This occurrence, in which all sets of conditions are the same, isolates confinement as the influencing factor inducing three dimensional growth.

In our previous work, mouse NIH3T3 fibroblasts and Madin-Darby Canine Kidney (MDCK) epithelial cells grown in similar channeled conditions favored substrate adhesion and eventual monolayer formation[265]. The preferential affinity displayed by in vitro mESCs for globular formation vs substrate adhesion mimics in vivo development at the blastocyst stage. Confined within the inner cell mass, E-Cadherins play a pivotal role in cell rearrangement, tissue morphogenesis, establishing cell polarity and tissue architecture maintenance[274,275]. It is also highly associated with the actomysin network, as they possess a regulatory feedback loop which can modulate cadherin expression during embryogenesis[255,257,262,276]. Expression of E-Cadherin significantly lowers immediately after differentiation, which has made it a pluripotency marker for undifferentiated cells[275,277,278]. To examine its influence on spheroid formation within a confined channel, cells were pre-loaded with a primary E-Cadherin antibody to block cell-cell adhesion that caused the abolition of spheroid formation (Fig 5.2E). This observation is consistent with the notion that E-cadherin operates within a positive feedback loop, that if perturbed, disrupts colony formation and impairs long-term survival of ESCs[279].

ROCK and myo-II are also known to play a role in regulating the stability of newly formed cell-cell junctions[156,169]. Here, ROCK inhibition disrupted spheroid formation, producing results consistent with the E-Cadherin blocking experiments. This is also consistent with our understanding of actin dynamics as inhibiting Rho subsequently effects E-cadherin binding. Surprisingly, myo-II did not have any clear effect on spheroid formation or shape characteristics. In this study we were forced to use a relatively low concentration of blebbistatin (2μM) as higher concentrations (5 and 10μM) resulted in the complete loss of all cells from the substrate. Myosin-II inhibition will destabilize E-cadherin cell-cell contacts [156,169] and disrupt cell-substrate contacts (Fig 5.5) [280]. We speculate there exists a sharp threshold level of myo-II activity that is required to maintain cell-substrate and cell-cell adhesion. Finally, inhibition of formins via SMIFH2 allowed us to directly inhibit actin nucleation, migration and cell-substrate adhesion pathways. As an actin regulator, mDia1/2 accelerates actin polymerization, focal adhesion dynamics, cell-substrate attachment and migration[163,270,281,282]. It mediates this through its interactions with the c-Src pathway and focal adhesion kinase (FAK) pathway. Both c-Src and FAK are key proteins responsible for the formation and dynamic reorganization of focal adhesion complexes[163,283]. Formin inhibition resulted in spheroids with significantly larger I_g. As decreased cell-substrate adhesion and inhibited migratory processes tend to promote cell-cell adhesion through cadherin binding, subsequently leading to a more spherical morphology as shown by their globular isotropy values. Finally, in the channels, the number of cell-cell collisions per hour was about 3-fold higher compared to cells on flat substrates. This leads to an increased probability of experiencing a cell-cell collision and adhesion event in the channels.

Taken together, the picture that emerges from the experimental data is that a balance between physical and biochemical factors are influencing the early formation of embryoid bodies. The developmental pathway of the cells depends upon their dynamic interaction with the physical properties that surround them rather than their static position at any moment in development, as suggested by Beloussov et al.[284–286]. To explore this idea further, we developed a simulation that could reproduce the

organization of cells we observed during experiments. Specific cellular organization could arise from cells allowed to diffuse and collide while undergoing energetically favorable movements during relaxation phases. A parameter χ ($\frac{\epsilon_{cs}}{\epsilon_{cc}}$), was developed to explore this phenomenon by simply changing the relative balance between cell-substrate and cell-cell adhesion strength. At χ = 1.0, whereby the strength of cell-cell adhesion is equal to that of cell-substrate, simulated aggregates resemble the aggregates observed experimentally. Importantly, experimental observations were reproduced under situations in which cell-cell and cell-substrate strength becomes unbalanced. In cases where $\chi < 1.0$, spheroids are formed with much higher I_g than the case where χ = 1.0. This reflects the experimental results obtained with formin inhibition where cell-substrate interaction is impaired significantly. Alternatively, when $\chi > 1.0$, cellular aggregates possessed a low I_g compared to the scenario in which χ = 1.0. In this case, inhibiting cell-cell interactions promotes the likelihood of cell-substrate interactions and the formation of islands, or dispersed groups of cells that do not resemble spheroids.

It is well appreciated that soluble signals (growth factors, cytokines) are highly involved in the self-regulating microenvironment designated the stem cell niche[101,272,287]. However, recent evidence also suggests that stem cell development is strongly influenced by coexisting insoluble adhesive, topological and mechanical cues inherently contained in the niche[113,288–292]. Manipulating these physical cues via patterned ECM protein or altered substrate topography has been shown to induce morphological, orientational and proliferative changes in a wide array of cell types[131,193,201,206,209]. In this study, we have demonstrated that physical confinement characteristics can also be exploited to control the 3D organization of mESC aggregates. Contrary to flat substrates, mESCs were observed to grow spherically in confined grooves, through initial phases of cellular aggregation followed by proliferative expansion. In recent years, considerable interest has grown in the role physical cues in the microenvironment play in stem cell regulation[106,186,250,293,294], such as matrix

elasticity, nanotopography and stretch. The objective of this work has been to demonstrate that physical confinement also plays an important role in the regulation of stem cell organization in 3D. Therefore, physical confinement can be considered yet another physical cue that stem cells are able to sense and respond to, although its full significance is still being fully elucidated.

Here, we have revealed that topographical confinement can promote 3D spheroidal formation of embryonic stem cells. Cell proliferation in confined space was clearly altered compared to traditional flat 2D cultures. Importantly, confinement is a major factor influencing cell-type dependent response to microtopographies [251,295]. This is in line with other recent studies that have manipulated the confinement properties of hydrogels to direct stem cell growth and differentiation[251]. Much like the recent elucidation of the importance of substrate stiffness in stem cell fate[106], the evidence of confinement as a critical factor in controlling cell growth is becoming more prominent. With the advent of three dimensional tissue engineering and stem cell regeneration, the phenomenon demonstrated here may further help develop new scaffolds that can direct cell growth and behavior.

5.5 MATERIALS AND METHODS

5.5.1 SUBSTRATE FABRICATION

Master substrates were fabricated by means of standard soft photolithography techniques on polished silicon wafers (Unicersitywafers.com, USA). Impurities on the wafer were removed with a Piranha solution (3:1 sulphuric acid: hydrogen peroxide) followed by a rinsing in de-ionized water and finally baked at 200°C for 30 mins. A 100µm uniform thickness of SU-8 2050 photoresists (Microchip, USA) was then spin-coated onto the wafer. Photomask patterns were subsequently transferred to the photoresist via UV exposure for 10 sec as per the manufacturer protocol. The photomask consisted of separate 2.25cm^2 square regions each containing 1.5cm long black lines, with 100µm spacing. The widths of the lines varied among square regions from 50, 100, 200, 500 to 1000 µm. Polydimethylsiloxane (PDMS) molds with channeled

topographies were formed by pouring a 1:10 (curing agent: elastomer) (Sylgard 184, Ellsworth Adhesives) over the photoresist master mold. The PDMS was allowed to crosslink in a convection oven at 80°C for 3hrs. Functionalization of the PDMS to permit collagen coating was achieved through air plasma treatment at 50w for 30 sec. Rat-tail collagen I (5 μg/cm^2, Gibco) was then deposited onto the PDMS at room temperature for 30 mins to allow adhesion followed by a phosphate buffered saline (PBS) rinse.

5.5.2 CELL CULTURE AND DRUG STUDIES

D3 mouse embryonic stem cells (mESC) (ATTC, #CRL-1934) were cultured as per ATTC's protocol[296], in Dulbeco's modified Eagle's medium (DMEM) supplemented with 12.5% Fetal Bovine Serum, 0.1μm non-essential amino acids, 30μg/ml Gentamicin (Gibco), 0.1μm 2-mercaptoenthanol (Sigma) and 1000U/ml leukemia inhibitory Factor (LIF) (Millipore, Catalogue # ESG1106). Cells were passaged every 48hrs to prevent differentiation. Cells were seeded onto the PDMS topographies immediately after passaging at 50 000 cells/dish. Inhibition studies of Rho-kinase (Y-27632; 10μM, Sigma, Catalogue #Y0503), Myo II (Blebbistatin; 10μM, Sigma, Catalogue #B0560) and mDia (SMIFH2; 10μM, Sigma, Catalogue #S4826) were all performed by exposing mESC for the 48hrs incubation time period.

5.5.3 E-CADHERIN BLOCKING

Prior to seeding, monoclonal DECMA-1 anti-uromodulin/e-cadherin antibody (Sigma; 1:1600, Catalogue # U3254) was added to cells in free suspension for 30 min. This antibody binds directly to uvomorulin/E-Cadherin, which has been characterized as a 120kDa cell surface glycoprotein. Due to their protein structure similarities, the antibody also binds to L-CAM and Cell CAM 80/120, additional transmembrane proteins involved in cell adhesion. Cells were then centrifuged and re-suspended in fresh media and plated as described in section 2.2. Verification of primary antibody binding was performed with an anti-rat IgG CF488A secondary antibody (Sigma, 1:500) during immunofluorescent staining [214,297].

5.5.4 IMMUNOFLUORESCENCE STAINING, QUANTIFICATION, TIME LAPSE IMAGING AND MICROSCOPY

Cells cultured on PDMS substrates were fixed with 3.5% paraformaldehyde and permeabilized with Triton X-100 at 37°C. Cells were stained for: vinculin, using monoclonal anti Vinculin (Sigma, Catalogue # V9131), actin, using phalloidin conjugated to Alexa Fluor 546 (Invitrogen, Catalogue #A22283) and DNA using DAPI (Invitrogen, Catalogue #D1306). A full protocol has been published previously [175]. Samples were then mounted using Vectashield (Vector Labs) and a #1 coverslip placed on top of the PDMS substrate. Samples were then inverted and imaged with a Nikon Ti-E A1-R high-speed resonant laser scanning confocal microscope (LSCM) with a phase contrast 10x NA0.3 objective or a DIC 60x NA1.2 water immersion objective. Immunofluorescence quantification of vinculin was performed by uniformly staining all samples concurrently and image capturing at set parameters. Images were then processed in Image J whereby the integrated density is relatively compared to background fluorescence using the measure tool. [298] For time-lapse imaging, cells were seeded onto the PDMS substrate with an additional 3 ml of media. Time-lapse phase contrast imaging was carried out on an AE30 Motic microscope with a 10x objective, which was enclosed in a temperature regulated (37°C) box. Samples were imaged every 10 mins for up to 48hrs. Scanning Electron Microscope images were acquired on a JEOL JSM-7500F FESEM.

5.5.5 IMAGE AND STATISTICAL ANALYSIS

To obtain a quantitative description of the changes in aggregate morphology, we developed two metrics defined as planar isotropy (I_p) and globular isotropy (I_g). The planar isotropy describes the circularity of the aggregate in the *xy* plane, whereas globular isotropy describes its sphericity by comparing its vertical growth (*z*-direction) to its effective *xy* size. A three-dimensional mesh representation of the cell surface is generated in ImageJ [299] from the confocal image slices using a marching cube algorithm[300]. The mesh vertices $\vec{r} = (r_x, r_y, r_z)$ are used to define the object's position $(\langle r_x \rangle, \langle r_y \rangle, \langle r_z \rangle)$, where $\langle\ \rangle$ denotes an unweighted mean over the vertices. The root

mean square distance of all the points to this center position is then used as a metric describing the extent of the aggregate in the three Cartesian directions. Thus $R_x = \sqrt{\sigma_{xx}}$, $R_y = \sqrt{\sigma_{yy}}$ and $R_z = \sqrt{\sigma_{zz}}$ where

$$(1)\ \sigma_{ij} = \langle\ (r_i - \langle r_i \rangle)\big(r_j - \langle r_j \rangle\big)\ \rangle,$$

for $i, j = \{x, y, z\}$. To calculate the planar isotropy, we first project the points onto the bottom surface (the *xy*-plane) and calculate the principal components of the resulting data set. This requires finding the eigenvalues and eigenvectors of the covariance matrix

$$(2)\ \begin{bmatrix} \sigma_{xx} & \sigma_{xy} \\ \sigma_{yx} & \sigma_{yy} \end{bmatrix}.$$

The ratio between the effective length along the major ($R_{max} = \sqrt{\sigma_{max}}$) and minor ($R_{min} = \sqrt{\sigma_{min}}$) axes (from the eigenvalues σ_{max} and σ_{min} respectively) then defines the dimensionless parameter

$$(3)\ planar\ isotropy = \ I_p = \frac{R_{min}}{R_{max}}.$$

Note that a value of $I_p \approx 1$ is expected for an isotropic sample (with a roughly circular footprint) while $I_p < 1$ is indicative of an elongated profile.

In addition, we define the dimensionless *globular isotropy* as a measure of the effective height R_z relative to its effective planar size $R_p = \sqrt{\frac{1}{2}({R_{max}}^2 + {R_{min}}^2)}$. This is calculated using the formula

$$(4)\ \ globular\ isotropy = I_g = \frac{R_z}{R_p} = \sqrt{\frac{2\sigma_{zz}}{(\lambda_{max} + \lambda_{min})}}.$$

With this definition, we expect $I_g < 1$ for the usual 'flat' (two-dimensional growth) profile and $I_g \approx 1$ for a spherical (three-dimensional growth) profile.

5.5.6 STATISTICS

All statistical analyses were performed using a one-way ANOVA followed by a Tukey test for mean comparison. Unless otherwise stated, all data is presented as mean ± s.e.m. Each condition, consisting of the various drugs and channel widths were duplicated 3 times.

5.5.7 SIMULATIONS

In order to elucidate the dependence of the cluster morphology upon both geometrical confinement and cell-cell/cell-substrate interactions, a simple simulation model is used where these factors can be independently controlled. Additional factors that can possibly influence morphology, such as cell interaction range, initial cell surface density, and initial cell seed amount are held constant. This simulation model is used as a tool to reveal the potential influencing physical factors observed in aggregate formation and does not attempt to fully represent the complexities of dynamic biological systems.

We thus use coarse-grained Langevin-Dynamics simulations where cells are described as single spherical beads. Individual cells are subject to forces arising from gravity, the solvent, the substrate, as well as other cells in the system. The equation of motion for the simulation beads is given by the Langevin equation [301]

$$m\frac{d^2\boldsymbol{r}_i(t)}{dt^2} = -\nabla V + \boldsymbol{F}_{\mathrm{grav}} + \boldsymbol{F}_f + \boldsymbol{F}_B \quad (1)$$

where m is the mass of the cells, $\boldsymbol{r}_i$ is the position of the i^{th} cell, V is the net interaction potential, and $\boldsymbol{F}_{\mathrm{grav}}$ is the gravitational force. The last two terms are used to implicitly model the solvent as contributing to a dissipative friction $\boldsymbol{F}_f$, and an effective Brownian force $\boldsymbol{F}_B$ [301]

For simplicity, the cell-cell and cell-substrate interaction potentials have an identical form so that they can be controlled via a single parameter. This is achieved using the modified Lennard-Jones potential:

$$V_{\mathrm{LJ}} = \begin{cases} -F_{\mathrm{cap}} r + A_1 & \text{if } r < r_{\mathrm{cap}}, \\ 4\,\varepsilon \left(\left(\frac{\sigma}{r}\right)^{12} - \left(\frac{\sigma}{r}\right)^{6} \right) + A_2 & \text{if } r_{\mathrm{cap}} < r < r_{\mathrm{cut}}, \\ 0 & \text{if } r_{\mathrm{cut}} < r, \end{cases} \qquad (2)$$

with *r* being the distance between a cell and an object (either another cell or a substrate surface), ε is the depth of the potential well, and σ is the effective size of the cell (see Fig 5.7). First, for short distances ($r < r_{\mathrm{cap}}$) we define a maximum repulsive force of F_{cap}. This force cap is needed due to our chosen duplication method that places overlapping daughter cells unto mother cells. The constant A_1 is chosen such that the potential is continuous at $r = r_{\mathrm{cap}}$. The Lennard-Jones potential is used for intermediate distances $\left(r_{\mathrm{cap}} < r < r_{\mathrm{cut}}\right)$ and has a well minimum at $r_{\mathrm{m}} = 2^{1/6}\sigma$. The A_2 offset is chosen such that the potential is continuous at r_{cut}.

We use different well-depths ε_{CC} and ε_{CS} for the cell-cell and cell-substrate interactions, respectively. A finite interaction range is enforced by using a cut-off distance of $r_{\mathrm{cut}} = 2r_{\mathrm{m}}$. Using these three components in the interaction potential maintains a repulsive behavior at short distances and an attractive component over a finite distance (see Fig 5.7).

A single channel is constructed using three mathematical surfaces placed as a bottom plate at *z*=0 surrounded by two walls positioned at y = ±*w/2*, where *w* is the channel width. Periodic boundary conditions (Fig 5.7) are used in the *x*-direction with the channel nominal length l_x chosen such that we achieve a constant cell number density $\rho = N_{\mathrm{init}}/wl_x$ (to match a selected experimental value *C*= 450 *cell/mm²)* for all widths. This implies that with an initial seed of $N_{\mathrm{init}} = 45$ cells, the simulation system has an area corresponding to 100μ*m²*. Under this construction, all the simulation results are taken from systems that have the same cell count and the same cell density despite having varying channel widths. Thus, by only changing the channel aspect-ratio (while keeping the area of the channel floor the same), these simulations allows us to de-couple growth effects arising from different cell numbers and densities inside the channels.

The simulation is structured into two distinct phases, i) initial cell diffusion; and ii) cell duplication. After the cells are initialized randomly unto the bottom surface, they are allowed to diffuse and explore the channel during an initial period of time (10^5 timesteps), during which they are allowed to coalesce into small clusters and / or fall into low-energy regions such as along the edges of the channels. Since cell diffusion is observed to be suppressed after approximately 6 hours due to integrin binding, the duration of this phase was chosen when the bead configurations were found to be similar to those obtained from the experimental images of freshly attached cells.

At the end of this diffusion stage, daughter cells are added into the simulation until a total population of $N_{\mathrm{tot}} = 352$ cells is reached. This corresponds to doubling the initial population of N_{init}=44 cells three times (which is thus equivalent to 45 hours of incubation time). Duplication is conducted by selecting a random mother cell from the simulation and inserting an overlapping daughter cell at the same location. We find that a short lapse is sufficient to allow the mother-daughter cell duo to relax and move away from one another. During this short time period, the cells are still allowed to diffuse. This sequence is repeated until all potential mother cells have duplicated once, which marks the end of a doubling phase.

The described simulation is implemented with the ESPResSO package [302] and visualized with VMD [303]. Supplementary Table 1 contains the ESPResSO numerical values for the parameters described herein. We find that these values yield stable integration in the over-damped limit and provide simulated trajectories that are qualitatively in agreement with those observed in the laboratory. Given the generic nature of this model, we nevertheless find the dependence of the cluster morphology upon the channel width (Fig 5.4). A systematic study of these parameters remains to be conducted, as it is out of the scope of the current study.

5.6 ACKNOWLEDGEMENTS

This work was supported by individual Natural Sciences and Engineering Research Council (NSERC) Discovery Grants to M.G., G.S. and A.E.P. S.H. was supported by the Queen Elizabeth II Graduate Scholarship in Science and Technology. A.E.P. gratefully acknowledges generous support from the Canada Research Chairs (CRC) program. A.E.P and M.G also acknowledge the support of the Canadian Foundation for Innovation.

6 | CONCLUSION

It has become well established that the physical properties of the extracellular microenvironment impose their influence on cell behavior[2,20,31,304]. Great strides have been made in revealing the interaction between surface topography and cell morphology, but these have remained mostly constricted to the canonical paradigm of contact guidance in single cell type systems. Since initially proposed, contact guidance describes the phenomenon by which the cell aligns along geometric patterns of nano/micron scaled grooves. This definition has been the staple of our understanding and has given rise to an extensive body of scientific literature. What happens however, when the geometric properties of the cellular milieu reach larger scales, beyond that of an individual cell? Where the influence of contact guidance is no longer imposed on a single cell but drives a collective behaviour. How does the element of confinement influence behaviour and at what point do physically driven interactions transition to biologically guided mechanisms? And lastly, what effects does incorporating an entirely different cell population into the system have on all these parameters?

We have revealed that a fine balance between physical interactions and biologically driven morphogenesis exists and that it can be modulated through the levels of confinement within a system. These levels of confinement ultimately tip the interplay and promote cell-cell interactions, inducing cell type dependent responses. This has major implications in embryonic stem cell research as cell-cell binding and preliminary aggregate formations are capable of dictating future differentiation lineages. Future work will lie in systematically analyzing the effects of confinement through the modulation of porosity. Some work has already begun in this field by seeding stem cells in digestible and non digestible biogels, leading to altered levels of confinement and subsequently altered differentiation[2]. Furthermore, it will be crucial to identify the relevance of individual and combined components of the sensing pathway for controlling cell interactions. Among the most effective techniques will be knock-out models of key acto-myosin and Rock associated proteins. Selective inhibition of

mechanosensing proteins has already been demonstrated to promote survival in embryonic stem cell culture. Further revealing their interplay in more complex three dimensional environments will be pivotal to harnessing their regenerative therapeutic potential.

It has been well established that contact guidance imposes its influence at the nanoscale on two dimensional surfaces. Our results from introducing 100μm channels demonstrated the large-scale effect of contact guidance on large populations of cells through what we describe as a "locked in" phenomenon. Despite being able to migrate out of the channels and overcome the acute 90°edge onto the ridge, cells are subsequently locked and align within the channel. This is the first time that contact guidance has been shown to influence cells in complex three-dimensional geometries leading to collective cell patterning. Furthermore, it's also the first demonstration of phase separating two different cell types purely through topography. This phenomenon raises numerous questions as to how cells acquire a spatial understanding of their environment and through what means do they communicate a unified response (e.g. fibroblast bridging). Their selective overcoming of specific edges over others within the channel also indicates a preferential orientation or migration. Future studies will focus on engineering three dimensional geometries whereby contact guidance is utilized to manipulate cell patterning on a larger three dimensional scale. It will also expand to incorporate cocultured systems so as to drive the reorganization of multicellular tissues. Amongst the most promising future applications of this work resides in tissue regeneration. Although the body has become incredibly efficient at reconstructing damaged tissue and wound healing, the residing scar possesses an altered cellular organization, which is non-homologous to its original state. Having demonstrated the potential of higher order cellular organization in large geometric topographies, future biomaterials will focus on incorporating these guiding parameters into their design. Fine tuning spatial confinement and substrate geometry, which in turn alters the binding dynamics between cells and substrate, which may further help guide the regeneration of tissues to their original state.

Our results however have paved the way for new unsolved questions. Although the alignment of single cells along the apex of a curved channel has been shown before, to our knowledge, the collective patterned behaviour of a monolayer reacting similarly has never been demonstrated[232,305]. The dynamics of this result presents a new confounding understanding of how and why cells respond in certain ways to topography. Based on our current understanding of contact guidance, the high contact angle would promote their alignment along the bottom of the grooves, yet our results demonstrate otherwise. In what way do high levels of curvature contact guide in the same manner as discontinued edges? Do the cells feel this difference and respond accordingly or is the resulting mechanotransductive input merely identical?

It will be in the systematic characterization of different substrate geometries and their resulting effect on the behaviour of large cell populations that we will continue to reveal the gaps in knowledge in the field. Whilst in conjunction, taking a bottom up approach to further elucidating the function of downstream mechanosensing proteins, we will continue to chisel away at the mysteries of mechanosensing and it's ability to drive the cell's dynamic response to its surroundings.

REFERENCES

1. Albert, B. *et al. Molecular Biology of the cell*. (Garland Science, 2008).

2. Baker, B. M. & Chen, C. S. Deconstructing the third dimension: how 3D culture microenvironments alter cellular cues. *J. Cell Sci.* **125,** 3015–24 (2012).

3. Fletcher, D. a & Mullins, R. D. Cell mechanics and the cytoskeleton. *Nature* **463,** 485–92 (2010).

4. Fletcher, D. A. & Mullins, R. D. Cell mechanics and the cytoskeleton. *Nature* **463,** 485–492 (2010).

5. Bukoreshtliev, N. V, Haase, K. & Pelling, A. E. Mechanical cues in cellular signalling and communication. *Cell Tissue Res.* **352,** 77–94 (2013).

6. Hunt, A. J., Gittes, F. & Howard, J. The force exerted by a single kinesin molecule against a viscous load. *Biophys. J.* **67,** 766–781 (1994).

7. Howard, J. & Clark, R. Mechanics of Motor Proteins and the Cytoskeleton. *Appl. Mech. Rev.* **55,** B39 (2002).

8. Lau, A. W. C., Lacoste, D. & Mallick, K. Nonequilibrium Fluctuations and Mechanochemical Couplings of a Molecular Motor. *Phys. Rev. Lett.* **99,** 158102 (2007).

9. Lammerding, J. *et al.* Lamins A and C but not lamin B1 regulate nuclear mechanics. *J. Biol. Chem.* **281,** 25768–80 (2006).

10. Ho, C. Y. & Lammerding, J. Lamins at a glance. *J. Cell Sci.* **125,** (2012).

11. Versaevel, M., Grevesse, T. & Gabriele, S. Regulation of Nuclear Shape and Function with Cell Elongation. *Biophys. J.* **104,** 151a (2013).

12. Crisp, M. *et al.* Coupling of the nucleus and cytoplasm: Role of the LINC complex.

J. Cell Biol. **172,** (2006).

13. Pekovic, V. *et al.* Conserved cysteine residues in the mammalian lamin A tail are essential for cellular responses to ROS generation. *Aging Cell* **10,** 1067–79 (2011).

14. Gonzalez-Suarez, I., Redwood, A. B. & Gonzalo, S. Loss of A-type lamins and genomic instability. *Cell Cycle* **8,** 3860–3865 (2009).

15. Dechat, T. *et al.* Nuclear lamins: major factors in the structural organization and function of the nucleus and chromatin. *Genes Dev.* **22,** 832–53 (2008).

16. Simon, D. N. & Wilson, K. L. The nucleoskeleton as a genome-associated dynamic 'network of networks'. *Nat. Rev. Mol. Cell Biol.* **12,** 695–708 (2011).

17. Stricker, J., Falzone, T. & Gardel, M. L. Mechanics of the F-actin cytoskeleton. *J. Biomech.* **43,** 9–14 (2010).

18. Goode, B. L. & Eck, M. J. Mechanism and function of formins in the control of actin assembly. *Annu. Rev. Biochem.* **76,** 593–627 (2007).

19. Shemesh, T., Geiger, B., Bershadsky, A. D. & Kozlov, M. M. Focal adhesions as mechanosensors: a physical mechanism. *Proc. Natl. Acad. Sci. U. S. A.* **102,** 12383–8 (2005).

20. Geiger, B., Spatz, J. P. & Bershadsky, A. D. Environmental sensing through focal adhesions. *Nat. Rev. Mol. Cell Biol.* **10,** 21–33 (2009).

21. Mammoto, A., Mammoto, T. & Ingber, D. E. Mechanosensitive mechanisms in transcriptional regulation. *J. Cell Sci.* **125,** 3061–73 (2012).

22. Kovács, M., Tóth, J., Hetényi, C., Málnási-Csizmadia, A. & Sellers, J. R. Mechanism of blebbistatin inhibition of myosin II. *J. Biol. Chem.* **279,** 35557–63 (2004).

23. Frey, M. T., Tsai, I. Y., Russell, T. P., Hanks, S. K. & Wang, Y.-L. Cellular responses

to substrate topography: role of myosin II and focal adhesion kinase. *Biophys. J.* **90,** 3774–82 (2006).

24. DuFort, C. C., Paszek, M. J. & Weaver, V. M. Balancing forces: architectural control of mechanotransduction. *Nat. Rev. Mol. Cell Biol.* **12,** 308–319 (2011).

25. Holle, A. W. & Engler, A. J. More than a feeling: discovering, understanding, and influencing mechanosensing pathways. *Curr. Opin. Biotechnol.* **22,** 648–654 (2011).

26. Li, Y.-S. J. *et al.* Molecular basis of the effects of shear stress on vascular endothelial cells. *J. Biomech.* **38,** 1949–71 (2005).

27. Vincent, J.-P., Fletcher, A. G. & Baena-Lopez, L. Al. Mechanisms and mechanics of cell competition in epithelia. *Nat. Rev. Mol. Cell Biol.* **14,** 581–591 (2013).

28. Wang, N., Butler, J. P. & Ingber, D. E. Mechanotransduction across the cell surface and through the cytoskeleton. *Science* **260,** 1124–7 (1993).

29. Booth-Gauthier, E. A., Alcoser, T. A., Yang, G. & Dahl, K. N. Force-Induced Changes in Subnuclear Movement and Rheology. *Biophys. J.* **103,** 2423–2431 (2012).

30. Dahl, K. N. & Kalinowski, A. Nucleoskeleton mechanics at a glance. *J. Cell Sci.* **124,** (2011).

31. Fletcher, D. A. & Mullins, R. D. Cell mechanics and the cytoskeleton. *Nature* **463,** 485–492 (2010).

32. Ananthakrishnan, R. & Ehrlicher, A. The forces behind cell movement. *Int. J. Biol. Sci.* **3,** 303–17 (2007).

33. Moore, J. K. & Cooper, J. A. Coordinating mitosis with cell polarity: Molecular motors at the cell cortex. *Semin. Cell Dev. Biol.* **21,** 283–289 (2010).

34. Harris, A. K., Wild, P. & Stopak, D. Silicone Rubber Substrata : A New Wrinkle in the Study of Cell Locomotion. *Science (80-.).* **208,** 177–179 (1980).

35. Oliver, T., Jacobson, K. & Dembo, M. Traction forces in locomoting cells. *Cell Motil. Cytoskeleton* **31,** 225–240 (1995).

36. Singhvi, R. *et al.* Engineering cell shape and function. *Science* **264,** 696–8 (1994).

37. Geiger, B., Spatz, J. P. & Bershadsky, A. D. Environmental sensing through focal adhesions. *Nat. Rev. Mol. Cell Biol.* **10,** 21–33 (2009).

38. Brown, N. H. *et al.* Talin is essential for integrin function in Drosophila. *Dev. Cell* **3,** 569–79 (2002).

39. Torgler, C. N. *et al.* Tensin stabilizes integrin adhesive contacts in Drosophila. *Dev. Cell* **6,** 357–69 (2004).

40. Pasapera, A. M., Schneider, I. C., Rericha, E., Schlaepfer, D. D. & Waterman, C. M. Myosin II activity regulates vinculin recruitment to focal adhesions through FAK-mediated paxillin phosphorylation. *J. Cell Biol.* **188,** 877 (2010).

41. Humphries, J. D. *et al.* Vinculin controls focal adhesion formation by direct interactions with talin and actin. *J. Cell Biol.* **179,** (2007).

42. Hytnen, V. P., Vogel, V., Bhandarkar, M., Brunner, R. & Gursoy, A. How Force Might Activate Talin's Vinculin Binding Sites: SMD Reveals a Structural Mechanism. *PLoS Comput. Biol.* **4,** e24 (2008).

43. Lee, S. E., Kamm, R. D. & Mofrad, M. R. K. Force-induced activation of Talin and its possible role in focal adhesion mechanotransduction. *J. Biomech.* **40,** 2096–2106 (2007).

44. Cluzel, C. *et al.* The mechanisms and dynamics of αvβ3 integrin clustering in living cells. *J. Cell Biol.* **171,** (2005).

45. Zamir, E. *et al.* Quantitative Multicolor Compositional Imaging Resolves Molecular Domains in Cell-Matrix Adhesions. *PLoS One* **3,** e1901 (2008).

46. Ballestrem, C. *et al.* Molecular mapping of tyrosine-phosphorylated proteins in focal adhesions using fluorescence resonance energy transfer. *J. Cell Sci.* **119,** (2006).

47. Zaidel-Bar, R., Milo, R., Kam, Z. & Geiger, B. A paxillin tyrosine phosphorylation switch regulates the assembly and form of cell-matrix adhesions. *J. Cell Sci.* **120,** (2006).

48. Zaidel-Bar, R., Ballestrem, C., Kam, Z. & Geiger, B. Early molecular events in the assembly of matrix adhesions at the leading edge of migrating cells. *J. Cell Sci.* **116,** (2003).

49. Katoh, K. *et al.* Rho-Kinase–Mediated Contraction of Isolated Stress Fibers. *J. Cell Biol.* **153,** (2001).

50. Peterson, L. J. *et al.* Simultaneous stretching and contraction of stress fibers in vivo. *Mol. Biol. Cell* **15,** 3497–508 (2004).

51. Girish Kumar, †, Jin-Jun Meng, ‡, Wallace Ip, ‡, Carlos C. Co, † and & Chia-Chi Ho*, †. Cell Motility Assays on Tissue Culture Dishes via Non-Invasive Confinement and Release of Cells. (2005).

52. Balaban, N. Q. *et al.* Force and focal adhesion assembly: a close relationship studied using elastic micropatterned substrates. *Nat. Cell Biol.* **3,** 466–472 (2001).

53. Geiger, B., Spatz, J. P. & Bershadsky, A. D. Environmental sensing through focal adhesions. *Nat. Rev. Mol. Cell Biol.* **10,** 21–33 (2009).

54. Hill, T. *Linear aggregation theory in cell biology.* (Springer Science & Business Media, 2012).

55. Burridge, K. & Wennerberg, K. Rho and Rac Take Center Stage. *Cell* **116,** 167–179 (2004).

56. Brock, J., Midwinter, K., Lewis, J. & Martin, P. Healing of incisional wounds in the embryonic chick wing bud: characterization of the actin purse-string and demonstration of a requirement for Rho activation. *J. Cell Biol.* **135,** (1996).

57. Clark, E. A., King, W. G., Brugge, J. S., Symons, M. & Hynes, R. O. Integrin-mediated signals regulated by members of the rho family of GTPases. *J. Cell Biol.* **142,** 573–86 (1998).

58. Rossman, K. L., Der, C. J. & Sondek, J. GEF means go: turning on RHO GTPases with guanine nucleotide-exchange factors. *Nat. Rev. Mol. Cell Biol.* **6,** 167–180 (2005).

59. Hodge, R. G. & Ridley, A. J. Regulating Rho GTPases and their regulators. *Nat. Rev. Mol. Cell Biol.* **17,** 496–510 (2016).

60. Tilghman, R. W. & Parsons, J. T. Focal adhesion kinase as a regulator of cell tension in the progression of cancer. *Semin. Cancer Biol.* **18,** 45–52 (2008).

61. Amano, M., Nakayama, M. & Kaibuchi, K. Rho-kinase/ROCK: A key regulator of the cytoskeleton and cell polarity. *Cytoskeleton (Hoboken).* **67,** 545–54 (2010).

62. Seo, C. H., Furukawa, K., Montagne, K., Jeong, H. & Ushida, T. The effect of substrate microtopography on focal adhesion maturation and actin organization via the RhoA/ROCK pathway. *Biomaterials* **32,** 9568–9575 (2011).

63. Narumiya, S., Ishizaki, T. & Ufhata, M. Use and properties of ROCK-specific inhibitor Y-27632. *Methods Enzymol.* **325,** 273–284 (2000).

64. Harrison, R. G. The reaction of embryonic cells to solid structures. *J. Exp. Zool.* **17,** 521–544 (1914).

65. Weiss, P. Experiments on cell and axon orientation in vitro: The role of colloidal exudates in tissue organization. *J. Exp. Zool.* **100,** 353–386 (1945).

66. Clark, P., Connolly, P., Curtis, a S., Dow, J. a & Wilkinson, C. D. Topographical control of cell behaviour: II. Multiple grooved substrata. *Development* **108,** 635–44 (1990).

67. Teixeira, A. I., Abrams, G. A., Bertics, P. J., Murphy, C. J. & Nealey, P. F. Epithelial contact guidance on well-defined micro- and nanostructured substrates. *J. Cell Sci.* **116,** 1881–92 (2003).

68. Dreier, B. *et al.* Early responses of vascular endothelial cells to topographic cues. *Am. J. Physiol. Cell Physiol.* **305,** C290-8 (2013).

69. Uttayarat, P., Toworfe, G. K., Dietrich, F., Lelkes, P. I. & Composto, R. J. Topographic guidance of endothelial cells on silicone surfaces with micro- to nanogrooves: orientation of actin filaments and focal adhesions. *J. Biomed. Mater. Res. A* **75,** 668–80 (2005).

70. van Kooten, T. G. & von Recum, a F. Cell adhesion to textured silicone surfaces: the influence of time of adhesion and texture on focal contact and fibronectin fibril formation. *Tissue Eng.* **5,** 223–240 (1999).

71. DENBRABER, E., DERUIJTER, J., GINSEL, L., VONRECUM, A. & JANSEN, J. Quantitative analysis of fibroblast morphology on microgrooved surfaces with various groove and ridge dimensions. *Biomaterials* **17,** 2037–2044 (1996).

72. Dunn, G. a & Brown, a F. Alignment of fibroblasts on grooved surfaces described by a simple geometric transformation. *J. Cell Sci.* **83,** 313–40 (1986).

73. Oakley, C. & Brunette, D. M. The sequence of alignment of microtubules, focal contacts and actin filaments in fibroblasts spreading on smooth and grooved titanium substrata. *J. Cell Sci.* **106,** (1993).

74. Walboomers, X. F., Monaghan, W., Curtis, A. S. G. & Jansen, J. A. Attachment of fibroblasts on smooth and microgrooved polystyrene. *J. Biomed. Mater. Res.* **46,** 212–220 (1999).

75. Walboomers, X. F., Ginsel, L. A. & Jansen, J. A. Early spreading events of fibroblasts on microgrooved substrates. *J. Biomed. Mater. Res.* **51,** 529–534 (2000).

76. Saito, A. C., Matsui, T. S., Ohishi, T., Sato, M. & Deguchi, S. Contact guidance of smooth muscle cells is associated with tension-mediated adhesion maturation. *Exp. Cell Res.* **327,** 1–11 (2014).

77. Rajnicek, A., Britland, S. & McCaig, C. Contact guidance of CNS neurites on grooved quartz: influence of groove dimensions, neuronal age and cell type. *J. Cell Sci.* **110,** (1997).

78. Rajnicek, A. & McCaig, C. Guidance of CNS growth cones by substratum grooves and ridges: effects of inhibitors of the cytoskeleton, calcium channels and signal transduction pathways. *J. Cell Sci.* **110,** (1997).

79. Karuri, N. W. *et al.* Biological length scale topography enhances cell-substratum adhesion of human corneal epithelial cells. *J. Cell Sci.* **117,** (2004).

80. Teixeira, A. I., Nealey, P. F. & Murphy, C. J. Responses of human keratocytes to micro- and nanostructured substrates. *J. Biomed. Mater. Res.* **71A,** 369–376 (2004).

81. Diehl, K. A., Foley, J. D., Nealey, P. F. & Murphy, C. J. Nanoscale topography modulates corneal epithelial cell migration. *J. Biomed. Mater. Res. Part A* **75A,** 603–611 (2005).

82. YIM, E. *et al.* Nanopattern-induced changes in morphology and motility of smooth muscle cells. *Biomaterials* **26,** 5405–5413 (2005).

83. Biela, S. A., Su, Y., Spatz, J. P. & Kemkemer, R. Different sensitivity of human endothelial cells, smooth muscle cells and fibroblasts to topography in the nano–micro range. *Acta Biomater.* **5,** 2460–2466 (2009).

84. Sarkar, S., Dadhania, M., Rourke, P., Desai, T. A. & Wong, J. Y. Vascular tissue engineering: Microtextured scaffold templates to control organization of vascular smooth muscle cells and extracellular matrix. *Acta Biomater.* **1,** 93–100 (2005).

85. Britland, S. *et al.* Synergistic and hierarchical adhesive and topographic guidance of BHK cells. *Exp. Cell Res.* **228,** 313–325 (1996).

86. DENBRABER, E., DERUIJTER, J., GINSEL, L., VONRECUM, A. & JANSEN, J. Quantitative analysis of fibroblast morphology on microgrooved surfaces with various groove and ridge dimensions. *Biomaterials* **17,** 2037–2044 (1996).

87. Dunn, G. A. & Heath, J. P. A new hypothesis of contact guidance in tissue cells. *Exp. Cell Res.* **101,** 1–14 (1976).

88. Ohara, P. T. & Buck, R. C. Contact guidance in vitro. A light, transmission, and scanning electron microscopic study. *Exp. Cell Res.* **121,** 235–249 (1979).

89. Petrie, R. J., Doyle, A. D. & Yamada, K. M. Random versus directionally persistent cell migration. *Nat. Rev. Mol. Cell Biol. Publ. online 15 July 2009; | doi10.1038/nrm2729* **10,** 538 (2009).

90. Ranucci, C. S. & Moghe, P. V. Substrate microtopography can enhance cell adhesive and migratory responsiveness to matrix ligand density. *J. Biomed. Mater. Res.* **54,** 149–161 (2001).

91. Prina Mello, A., Volkov, Y., Kelleher, D. & Prendergast, P. J. Comparative Locomotory Behavior of T Lymphocytes versus T Lymphoma Cells on Flat and Grooved Surfaces. *Ann. Biomed. Eng.* **31,** 1106–1113 (2003).

92. Brammer, K. S., Oh, S., Gallagher, J. O. & Jin, S. Enhanced Cellular Mobility Guided by TiO2 Nanotube Surfaces. *Nano Lett.* **8,** 786–793 (2008).

93. Tan, J. & Saltzman, W. M. Topographical control of human neutrophil motility on micropatterned materials with various surface chemistry. *Biomaterials* **23,** 3215–3225 (2002).

94. Paszek, M. J. *et al.* Tensional homeostasis and the malignant phenotype. *Cancer Cell* **8,** 241–254 (2005).

95. Liliensiek, S. J., Campbell, S., Nealey, P. F. & Murphy, C. J. The scale of substratum topographic features modulates proliferation of corneal epithelial cells and corneal fibroblasts. *J. Biomed. Mater. Res. Part A* **79A,** 185–192 (2006).

96. Bettinger, C. J., Langer, R. & Borenstein, J. T. Engineering substrate topography at the micro- and nanoscale to control cell function. *Angew. Chem. Int. Ed. Engl.* **48,** 5406–15 (2009).

97. Dulgar-Tulloch, A. J., Bizios, R. & Siegel, R. W. Human mesenchymal stem cell adhesion and proliferation in response to ceramic chemistry and nanoscale topography. *J. Biomed. Mater. Res. Part A* **90A,** 586–594 (2009).

98. Brunetti, V. *et al.* Neurons sense nanoscale roughness with nanometer sensitivity. *Proc. Natl. Acad. Sci. U. S. A.* **107,** 6264–9 (2010).

99. Washburn, N. R., Yamada, K. M., Simon, C. G., Kennedy, S. B. & Amis, E. J. High-throughput investigation of osteoblast response to polymer crystallinity: influence of nanometer-scale roughness on proliferation. *Biomaterials* **25,** 1215–24

100. Kim, D.-H., Provenzano, P. P., Smith, C. L. & Levchenko, A. Matrix nanotopography as a regulator of cell function. *J. Cell Biol.* **197,** 351–60 (2012).

101. Discher, D. E., Mooney, D. J. & Zandstra, P. W. Growth factors, matrices, and forces combine and control stem cells. *Science* **324,** 1673–7 (2009).

102. Human, S. *et al.* Nanotopography In fl uences Adhesion , Embryonic Stem Cells. 4094–4103 (2012).

103. Teo, B. K. K. *et al.* Nanotopography Modulates Mechanotransduction of Stem Cells and Induces Differentiation through Focal Adhesion Kinase. *ACS Nano* **7,** 4785–98 (2013).

104. Bettinger Cj, Langer R, B. J. The effect of actin disrupting agents on contact guidance of human embryonic stem cells. *Angew Chem Int Ed Engl* **48,** 5406–5415 (2009).

105. Kulangara, K., Yang, Y., Yang, J. & Leong, K. W. Nanotopography as modulator of human mesenchymal stem cell function. *Biomaterials* **33,** 4998–5003 (2012).

106. Engler, A. J., Sen, S., Sweeney, H. L. & Discher, D. E. Matrix Elasticity Directs Stem Cell Lineage Specification. *Cell* **126,** 677–689 (2006).

107. Pauklin, S., Pedersen, R. a & Vallier, L. Mouse pluripotent stem cells at a glance. *J. Cell Sci.* **124,** 3727–32 (2011).

108. Thomson, J. A. Embryonic Stem Cell Lines Derived from Human Blastocysts. *Science (80-.).* **282,** 1145–1147 (1998).

109. Bratt-leal, M., Carpenedo, R. L. & Mcdevitt, T. C. Engineering the Embryoid Body Microenvironment to Direct Embryonic Stem Cell Differentiation. 43–51 (2009). doi:10.1021/bp.139

110. Dinsmore, J. *et al.* Embryonic stem cells differentiated in vitro as a novel source of cells for transplantation. *Cell Transplant.* **5,** 131–143 (1996).

111. Keller, G. Embryonic stem cell differentiation: emergence of a new era in biology

and medicine. *Genes Dev.* **19,** 1129–55 (2005).

112. Lanza, R. Cell Biology Essentials of Stem Cell Biology. *Zyw. Czlowieka I Metab.* **48,** 148–212 (2011).

113. Khang, I. *et al.* Expression of epithin in mouse preimplantation development: its functional role in compaction. *Dev. Biol.* **281,** 134–144 (2005).

114. Peerani, R. *et al.* Niche-mediated control of human embryonic stem cell self-renewal and differentiation. *EMBO J.* **26,** 4744–55 (2007).

115. Www.humanphysiology.com. HumanPhysiology2011 - 15. Reproductive Physiology. Available at: http://humanphysiology2011.wikispaces.com/15.+Reproductive+Physiology.

116. Kurosawa, H. Methods for inducing embryoid body formation: in vitro differentiation system of embryonic stem cells. *J. Biosci. Bioeng.* **103,** 389–98 (2007).

117. Rungarunlert, S., Techakumphu, M., Pirity, M. K. & Dinnyes, A. Embryoid body formation from embryonic and induced pluripotent stem cells: Benefits of bioreactors. *World J. Stem Cells* **1,** 11–21 (2009).

118. Karp, J. M. *et al.* Controlling size, shape and homogeneity of embryoid bodies using poly(ethylene glycol) microwells. *Lab Chip* **7,** 786–94 (2007).

119. Choi, Y. Y. *et al.* Controlled-size embryoid body formation in concave microwell arrays. *Biomaterials* **31,** 4296–303 (2010).

120. Morgan, T. Regeneration Macmillan. *New York* (1901).

121. Turing, A. M. The chemical basis of morphogenesis. *Bull. Math. Biol.* **52,** 153–197 (1990).

122. Wartlick, O., Kicheva, A. & González-Gaitán, M. Morphogen gradient formation. *Cold Spring Harbor perspectives in biology* **1,** (2009).

123. Wang, X., Brouillette, M. J., Ayati, B. P. & Martin, J. A. A validated model of the pro- and anti-inflammatory cytokine balancing act in articular cartilage lesion formation. *Front. Bioeng. Biotechnol.* **3,** 25 (2015).

124. El Khatib, N., Genieys, S., Kazmierczak, B. & Volpert, V. Reaction-diffusion model of atherosclerosis development. *J. Math. Biol.* **65,** 349–74 (2012).

125. Adam, J. a & Bellomo, N. A Survey of Models for Tumor-Immune System Dynamics. *Sherratt. 1997. A Surv. Model. Tumor-Immune Syst. Dyn. Bull. Math. Biol. 59 1023-1024.* **5,** 1023–1024 (1997).

126. Ferreira, S. C., Martins, M. L. & Vilela, M. J. Reaction-diffusion model for the growth of avascular tumor. *Phys. Rev. E. Stat. Nonlin. Soft Matter Phys.* **65,** 21907 (2002).

127. Altrock, P. M., Liu, L. L. & Michor, F. The mathematics of cancer: integrating quantitative models. *Nat. Rev. Cancer* **15,** 730–745 (2015).

128. Painter, K. J. & Hillen, T. Mathematical modelling of glioma growth: the use of Diffusion Tensor Imaging (DTI) data to predict the anisotropic pathways of cancer invasion. *J. Theor. Biol.* **323,** 25–39 (2013).

129. Gan, Q. Exponential synchronization of stochastic neural networks with leakage delay and reaction-diffusion terms via periodically intermittent control. *Chaos* **22,** 13124 (2012).

130. Wang, L. & Zhao, H. Synchronized stability in a reaction–diffusion neural network model. *Phys. Lett. A* **378,** 3586–3599 (2014).

131. Zatti, S. *et al.* Micropatterning topology on soft substrates affects myoblast

proliferation and differentiation. *Langmuir* **28,** 2718–26 (2012).

132. Yates, P. A., Holub, A. D., McLaughlin, T., Sejnowski, T. J. & O'Leary, D. D. M. Computational modeling of retinotopic map development to define contributions of EphA-ephrinA gradients, axon-axon interactions, and patterned activity. *J. Neurobiol.* **59,** 95–113 (2004).

133. Camci-Unal, G., Newsome, D., Eustace, B. K. & Whitesides, G. M. Fibroblasts Enhance Migration of Human Lung Cancer Cells in a Paper-Based Coculture System. *Adv. Healthc. Mater.* **5,** 641–647 (2016).

134. Hu, H. Chemorepulsion of Neuronal Migration by Slit2 in the Developing Mammalian Forebrain. *Neuron* **23,** 703–711 (1999).

135. Nehls, V., Herrmann, R. & Hühnken, M. Guided migration as a novel mechanism of capillary network remodeling is regulated by basic fibroblast growth factor. *Histochem. Cell Biol.* **109,** 319–29 (1998).

136. Novozhilova, E., Olivius, P., Siratirakun, P., Lundberg, C. & Englund-Johansson, U. Neuronal Differentiation and Extensive Migration of Human Neural Precursor Cells following Co-Culture with Rat Auditory Brainstem Slices. *PLoS One* **8,** e57301 (2013).

137. Steinberg, M. S. Mechanism of tissue reconstruction by dissociated cells. II. Time-course of events. *Science* **137,** 762–763 (1962).

138. Steinberg, M. S. Reconstruction of Tissues by Dissociated Cells. *Science (80-.).* **141,** 401–408 (1963).

139. Foty, R. A. & Steinberg, M. S. The differential adhesion hypothesis: a direct evaluation. *Dev. Biol.* **278,** 255–263 (2005).

140. Foty, R. A. & Steinberg, M. S. Differential adhesion in model systems. *Wiley*

Interdiscip. Rev. Dev. Biol. **2,** 631–45

141. Chen, L., Wang, D., Wu, Z., Ma, L. & Daley, G. Q. Molecular basis of the first cell fate determination in mouse embryogenesis. *Cell Res.* **20,** 982–93 (2010).

142. Hadjiantoniou, S. V. *et al.* Physical confinement signals regulate the organization of stem cells in three dimensions. *J. R. Soc. Interface* **13,** (2016).

143. Miki, Y. *et al.* The advantages of co-culture over mono cell culture in simulating in vivo environment. *J. Steroid Biochem. Mol. Biol.* **131,** 68–75 (2012).

144. Qian, X., Karpova, T., Sheppard, A. M., McNally, J. & Lowy, D. R. E-cadherin-mediated adhesion inhibits ligand-dependent activation of diverse receptor tyrosine kinases. *EMBO J.* **23,** 1739–48 (2004).

145. Nicolaidou, V. *et al.* Monocytes Induce STAT3 Activation in Human Mesenchymal Stem Cells to Promote Osteoblast Formation. *PLoS One* **7,** e39871 (2012).

146. Gracz, A. D. *et al.* A high-throughput platform for stem cell niche co-cultures and downstream gene expression analysis. *Nat. Cell Biol.* **17,** 340–349 (2015).

147. Horie, M., Saito, A., Yamaguchi, Y., Ohshima, M. & Nagase, T. Three-dimensional Co-culture model for tumor-stromal interaction. *J. Vis. Exp.* (2015). doi:10.3791/52469

148. Fang, X., Sittadjody, S., Gyabaah, K., Opara, E. C. & Balaji, K. C. Novel 3D co-culture model for epithelial-stromal cells interaction in prostate cancer. *PLoS One* **8,** e75187 (2013).

149. Jaganathan, H. *et al.* Three-dimensional in vitro co-culture model of breast tumor using magnetic levitation. *Sci. Rep.* **4,** 6468 (2014).

150. Steinberg, M. S. & Takeichi, M. Experimental specification of cell sorting, tissue spreading, and specific spatial patterning by quantitative differences in cadherin

expression. *Proc. Natl. Acad. Sci. U. S. A.* **91,** 206–9 (1994).

151. Cachat, E. *et al.* 2- and 3-dimensional synthetic large-scale de novo patterning by mammalian cells through phase separation. *Sci. Rep.* **6,** 20664 (2016).

152. Rabito, C. A., Tchao, R., Valentich, J. & Leighton, J. Distribution and characteristics of the occluding junctions in a monolayer of a cell line (MDCK) derived from canine kidney. *J. Membr. Biol.* **43,** 351–365 (1978).

153. Modulevsky, D. J. *et al.* The physical interaction of myoblasts with the microenvironment during remodeling of the cytoarchitecture. *PLoS One* **7,** e45329 (2012).

154. Gumbiner, B. M. Regulation of cadherin-mediated adhesion in morphogenesis. *Nat. Rev. Mol. Cell Biol.* **6,** 622–634 (2005).

155. Gumbiner, B. M. Cell Adhesion: The Molecular Basis of Tissue Architecture and Morphogenesis. *Cell* **84,** 345–357 (1996).

156. Weber, G. F., Bjerke, M. A. & DeSimone, D. W. Integrins and cadherins join forces to form adhesive networks. *J. Cell Sci.* **124,** 1183–93 (2011).

157. Halbleib, J. M. & Nelson, W. J. Cadherins in development: cell adhesion, sorting, and tissue morphogenesis. *Genes Dev.* **20,** 3199–214 (2006).

158. Gumbiner, B. M. Regulation of cadherin-mediated adhesion in morphogenesis. *Nat. Rev. Mol. Cell Biol.* **6,** 622–634 (2005).

159. Rosner, M., Schipany, K. & Hengstschläger, M. Merging high-quality biochemical fractionation with a refined flow cytometry approach to monitor nucleocytoplasmic protein expression throughout the unperturbed mammalian cell cycle. *Nat. Protoc.* **8,** 602–26 (2013).

160. Moore, R., Tao, W., Meng, Y., Smith, E. R. & Xu, X.-X. Cell adhesion and sorting in

embryoid bodies derived from N- or E-cadherin deficient murine embryonic stem cells. *Biol. Open* **3,** 121–8 (2014).

161. Doyle, A. D. *et al.* Micro-environmental control of cell migration--myosin IIA is required for efficient migration in fibrillar environments through control of cell adhesion dynamics. *J. Cell Sci.* **125,** 2244–56 (2012).

162. Even-Ram, S. *et al.* Myosin IIA regulates cell motility and actomyosin-microtubule crosstalk. *Nat. Cell Biol.* **9,** 299–309 (2007).

163. Yamana, N. *et al.* The Rho-mDia1 pathway regulates cell polarity and focal adhesion turnover in migrating cells through mobilizing Apc and c-Src. *Mol. Cell. Biol.* **26,** 6844–6858 (2006).

164. Logue, J. S. & Morrison, D. K. Complexity in the signaling network: insights from the use of targeted inhibitors in cancer therapy. *Genes Dev.* **26,** 641–50 (2012).

165. Kaibuchi, K., Kuroda, S. & Amano, M. Regulation of the Cytoskeleton and Cell Adhesion by the Rho Family GTPases in Mammalian Cells. *Annu. Rev. Biochem.* **68,** 459–486 (1999).

166. Hall, A. Rho GTPases and the control of cell behaviour. *Biochem. Soc. Trans.* **33,** 891 (2005).

167. Zaidel-Bar, R., Cohen, M., Addadi, L. & Geiger, B. Hierarchical assembly of cell–matrix adhesion complexes. *Biochem. Soc. Trans.* **32,** 416–421 (2004).

168. Wozniak, M. A., Modzelewska, K., Kwong, L. & Keely, P. J. Focal adhesion regulation of cell behavior. *Biochim. Biophys. Acta - Mol. Cell Res.* **1692,** 103–119 (2004).

169. Shewan, A. M. *et al.* Myosin 2 is a key Rho kinase target necessary for the local concentration of E-cadherin at cell-cell contacts. *Mol. Biol. Cell* **16,** 4531–42

(2005).

170. Van Roy, F. & Berx, G. The cell-cell adhesion molecule E-cadherin. *Cellular and Molecular Life Sciences* **65,** 3756–3788 (2008).

171. Gumbiner, B. M. Regulation of cadherin-mediated adhesion in morphogenesis. *Nat. Rev. Mol. Cell Biol.* **6,** 622–34 (2005).

172. Charrasse, S., Meriane, M., Comunale, F., Blangy, A. & Gauthier-Rouvière, C. N-cadherin-dependent cell-cell contact regulates Rho GTPases and beta-catenin localization in mouse C2C12 myoblasts. *J. Cell Biol.* **158,** 953–65 (2002).

173. Braga, V. M., Machesky, L. M., Hall, A. & Hotchin, N. A. The small GTPases Rho and Rac are required for the establishment of cadherin-dependent cell-cell contacts. *J. Cell Biol.* **137,** 1421–31 (1997).

174. Omelchenko, T. *et al.* Contact interactions between epitheliocytes and fibroblasts: formation of heterotypic cadherin-containing adhesion sites is accompanied by local cytoskeletal reorganization. *Proc. Natl. Acad. Sci. U. S. A.* **98,** 8632–8637 (2001).

175. Guolla, L., Bertrand, M., Haase, K. & Pelling, A. E. Force transduction and strain dynamics in actin stress fibres in response to nanonewton forces. *J. Cell Sci.* **125,** 603–13 (2012).

176. Cachat, E. *et al.* 2- and 3-dimensional synthetic large-scale de novo patterning by mammalian cells through phase separation. *Sci. Rep.* **6,** 20664 (2016).

177. Bortz, A. B., Kalos, M. H. & Lebowitz, J. L. A new algorithm for Monte Carlo simulation of Ising spin systems. *J. Comput. Phys.* **17,** 10–18 (1975).

178. Kotrla, M. Numerical simulations in the theory of crystal growth. *Comput. Phys. Commun.* **97,** 82–100 (1996).

179. Mombach, J. & Glazier, J. Single Cell Motion in Aggregates of Embryonic Cells. *Phys. Rev. Lett.* **76,** 3032–3035 (1996).

180. Neagu, A. *et al.* in *Cell and Tissue Engineering* **9783642219,** 251–272 (2012).

181. Beysens, D. a, Forgacs, G. & Glazier, J. a. Cell sorting is analogous to phase ordering in fluids. *Proc. Natl. Acad. Sci. U. S. A.* **97,** 9467–9471 (2000).

182. Flenner, E. *et al.* Kinetic Monte Carlo and cellular particle dynamics simulations of multicellular systems. *Phys. Rev. E - Stat. Nonlinear, Soft Matter Phys.* **85,** (2012).

183. Glazier, J. A. & Graner, F. Simulation of the differential adhesion driven rearrangement of biological cells. *Phys. Rev. E* **47,** 2128–2154 (1993).

184. Janmey, P. a & Miller, R. T. Mechanisms of mechanical signaling in development and disease. *J. Cell Sci.* **124,** 9–18 (2011).

185. Buxboim, A., Ivanovska, I. L. & Discher, D. E. Matrix elasticity, cytoskeletal forces and physics of the nucleus: how deeply do cells 'feel' outside and in? *J. Cell Sci.* **123,** 297–308 (2010).

186. Holle, A. W. & Engler, A. J. More than a feeling: discovering, understanding, and influencing mechanosensing pathways. *Curr. Opin. Biotechnol.* **22,** 648–54 (2011).

187. Hynes, R. O. The extracellular matrix: not just pretty fibrils. *Science* **326,** 1216–9 (2009).

188. Janmey, P. A. & Miller, R. T. Mechanisms of mechanical signaling in development and disease. *J. Cell Sci.* **124,** (2010).

189. Bettinger, C. J., Langer, R. & Borenstein, J. T. Engineering Substrate Topography at the Micro- and Nanoscale to Control Cell Function. *Angew. Chemie Int. Ed.* **48,** 5406–5415 (2009).

190. Curtis, a & Wilkinson, C. Topographical control of cells. *Biomaterials* **18,** 1573–83 (1997).

191. Clark, P., Connolly, P., Curtis, a S., Dow, J. a & Wilkinson, C. D. Cell guidance by ultrafine topography in vitro. *J. Cell Sci.* **99 (Pt 1),** 73–7 (1991).

192. Kulangara, K. & Leong, K. W. Substrate topography shapes cell function. *Soft Matter* **5,** 4072 (2009).

193. Wong, J. Y., Leach, J. B. & Brown, X. Q. Balance of chemistry, topography, and mechanics at the cell–biomaterial interface: Issues and challenges for assessing the role of substrate mechanics on cell response. *Surf. Sci.* **570,** 119–133 (2004).

194. Lim, J. Y. & Donahue, H. J. Cell sensing and response to micro- and nanostructured surfaces produced by chemical and topographic patterning. *Tissue Eng.* **13,** 1879–91 (2007).

195. Cornelissen, K. *et al.* Correction for Unadkat et al., An algorithm-based topographical biomaterials library to instruct cell fate. *Proc. Natl. Acad. Sci.* **109,** 5905–5905 (2012).

196. Yang, Y., Kulangara, K., Lam, R. T. S., Dharmawan, R. & Leong, K. W. Effects of topographical and mechanical property alterations induced by oxygen plasma modification on stem cell behavior. *ACS Nano* **6,** 8591–8 (2012).

197. Weiss, P. in 391–423 (1958). doi:10.1016/S0074-7696(08)62692-3

198. Seo, C. H., Furukawa, K., Montagne, K., Jeong, H. & Ushida, T. The effect of substrate microtopography on focal adhesion maturation and actin organization via the RhoA/ROCK pathway. *Biomaterials* **32,** 9568–75 (2011).

199. Gerecht, S. *et al.* The effect of actin disrupting agents on contact guidance of human embryonic stem cells. *Biomaterials* **28,** 4068–77 (2007).

200. Greco, F. *et al.* Microwrinkled conducting polymer interface for anisotropic multicellular alignment. *ACS Appl. Mater. Interfaces* **5,** 573–84 (2013).

201. Chen, C. S., Mrksich, M., Huang, S., Whitesides, G. M. & Ingber, D. E. Geometric control of cell life and death. *Science (80-.).* **276,** 1425–1428 (1997).

202. Lim, J. Y., Hansen, J. C., Siedlecki, C. A., Runt, J. & Donahue, H. J. Human foetal osteoblastic cell response to polymer-demixed nanotopographic interfaces. *J. R. Soc. Interface* **2,** (2005).

203. Milner, K. R. & Siedlecki, C. A. Fibroblast response is enhanced by poly(L-lactic acid) nanotopography edge density and proximity. *Int. J. Nanomedicine* **2,** 201–211 (2007).

204. Su, W.-T., Liao, Y.-F. & Chu, I.-M. Observation of fibroblast motility on a micro-grooved hydrophobic elastomer substrate with different geometric characteristics. *Micron* **38,** 278–85 (2007).

205. Stevenson, P. M. & Donald, A. M. Identification of three regimes of behavior for cell attachment on topographically patterned substrates. *Langmuir* **25,** 367–76 (2009).

206. Charest, J. L., Eliason, M. T., García, A. J. & King, W. P. Combined microscale mechanical topography and chemical patterns on polymer cell culture substrates. *Biomaterials* **27,** 2487–94 (2006).

207. Gaush, C. R., Hard, W. L. & Smith, T. F. Characterization of an Established Line of Canine Kidney Cells (MDCK). *Exp. Biol. Med.* **122,** 931–935 (1966).

208. Gonzalez-Mariscal, L., Ch?vez de Ram?rez, B. & Cereijido, M. Tight junction formation in cultured epithelial cells (MDCK). *J. Membr. Biol.* **86,** 113–125 (1985).

209. Bettinger, C. J., Langer, R. & Borenstein, J. T. Engineering substrate topography at

the micro- and nanoscale to control cell function. *Angew. Chemie Int. Ed.* **48,** 5406–5415 (2009).

210. Izumi, Y. *et al.* An Atypical PKC Directly Associates and Colocalizes at the Epithelial Tight Junction with ASIP, a Mammalian Homologue of Caenorhabditis elegans Polarity Protein PAR-3. *J. Cell Biol.* **143,** (1998).

211. Vogel, V. & Sheetz, M. Local force and geometry sensing regulate cell functions. *Nat. Rev. Mol. Cell Biol.* **7,** 265–275 (2006).

212. Humphrey, J. D., Dufresne, E. R. & Schwartz, M. A. Mechanotransduction and extracellular matrix homeostasis. *Nat. Rev. Mol. Cell Biol.* **15,** 802–812 (2014).

213. Kim, D.-H., Provenzano, P. P., Smith, C. L. & Levchenko, A. Matrix nanotopography as a regulator of cell function. *J. Cell Biol.* **197,** (2012).

214. Dang, S. M., Gerecht-Nir, S., Chen, J., Itskovitz-Eldor, J. & Zandstra, P. W. Controlled, scalable embryonic stem cell differentiation culture. *Stem Cells* **22,** 275–82 (2004).

215. Klingberg, F., Hinz, B. & White, E. S. The myofibroblast matrix: implications for tissue repair and fibrosis. *J. Pathol.* **229,** 298–309 (2013).

216. Hinz, B. *et al.* Recent Developments in Myofibroblast Biology. *Am. J. Pathol.* **180,** 1340–1355 (2012).

217. Lara Rodriguez, L. *et al.* Directed cell migration in multi-cue environments. *Integr. Biol.* **5,** 1306 (2013).

218. Harris, A. K., Stopak, D. & Wild, P. Fibroblast traction as a mechanism for collagen morphogenesis. *Nature* **290,** 249–251 (1981).

219. Carter, S. Principles of cell motility: the direction of cell movement and cancer invasion. *Nature* **208,** 1183 (1965).

220. Carter, S. Haptotaxis and the mechanism of cell motility. *Nature* **213,** 256–260 (1967).

221. Van Haastert, P. J. M. & Devreotes, P. N. Chemotaxis: signalling the way forward. *Nat. Rev. Mol. Cell Biol.* **5,** 626–634 (2004).

222. Balkwill, F. Cancer and the chemokine network. *Nat. Rev. Cancer* **4,** 540–550 (2004).

223. Isenberg, B. C., DiMilla, P. A., Walker, M., Kim, S. & Wong, J. Y. Vascular smooth muscle cell durotaxis depends on substrate stiffness gradient strength. *Biophys. J.* **97,** 1313–1322 (2009).

224. Liu, F. *et al.* Feedback amplification of fibrosis through matrix stiffening and COX-2 suppression. *J. Cell Biol.* **190,** 693–706 (2010).

225. Raab, M. *et al.* Crawling from soft to stiff matrix polarizes the cytoskeleton and phosphoregulates myosin-II heavy chain. *J. Cell Biol.* **199,** 669–683 (2012).

226. Li, Y., Xiao, Y. & Liu, C. The Horizon of Materiobiology: A Perspective on Material-Guided Cell Behaviors and Tissue Engineering. *Chem. Rev.* acs.chemrev.6b00654 (2017). doi:10.1021/acs.chemrev.6b00654

227. Deeg, J. A. *et al.* Impact of local versus global ligand density on cellular adhesion. *Nano Lett.* **11,** 1469–76 (2011).

228. Schvartzman, M. *et al.* Nanolithographic Control of the Spatial Organization of Cellular Adhesion Receptors at the Single-Molecule Level. *Nano Lett.* **11,** 1306–1312 (2011).

229. Hu, J. *et al.* Enhanced Cell Adhesion and Alignment on Micro-Wavy Patterned Surfaces. *PLoS One* **9,** e104502 (2014).

230. Kulangara, K. & Leong, K. W. Substrate topography shapes cell function. *Soft*

Matter **5,** 4072 (2009).

231. Leclerc, A. *et al.* Three dimensional spatial separation of cells in response to microtopography. *Biomaterials* **34,** (2013).

232. CURTIS, A. S. G. & CLARK, P. THE EFFECTS OF TOPOGRAPHIC AND MECHANICAL PROPERTIES OF MATERIALS ON CELL BEHAVIOR. *Crit. Rev. Biocompat.* **5,** 343–363 (1986).

233. Loesberg, W. a *et al.* The threshold at which substrate nanogroove dimensions may influence fibroblast alignment and adhesion. *Biomaterials* **28,** 3944–51 (2007).

234. Colombetti, G. & Lenci, F. *Membranes and Sensory Transduction* -. (Springer Science & Business Media, 2012).

235. Roberts, a M. Geotaxis in motile micro-organisms. *J. Exp. Biol.* **53,** 687–699 (1970).

236. Hadjiantoniou, S. V *et al.* Physical confinement signals regulate the organization of stem cells in three dimensions. *J. R. Soc. Interface* **16,** (2016).

237. Qin, D., Xia, Y. & Whitesides, G. M. Soft lithography for micro- and nanoscale patterning. *Nat. Protoc.* **5,** 491–502 (2010).

238. Jaalouk, D. E. & Lammerding, J. Mechanotransduction gone awry. *Nat. Rev. Mol. Cell Biol.* **10,** 63–73 (2009).

239. Curtis, A. & Wilkinson, C. Topographical control of cells. *Biomaterials* **18,** 1573–1583 (1997).

240. Tamiello, C. Heading in the Right Direction: Understanding Cellular Orientation Responses to Complex Biophysical Environments. *Cell. Mol. Bioeng.* **9,** (2016).

241. Zimerman, B. *et al.* Formation of focal adhesion-stress fibre complexes coordinated by adhesive and non-adhesive surface domains. *IEEE Proc. nanobiotechnology* **151,** 207–211 (2004).

242. Ghibaudo, M. *et al.* Substrate Topography Induces a Crossover from 2D to 3D Behavior in Fibroblast Migration. *Biophys. J.* **97,** 357–368 (2009).

243. Ascione, F. *et al.* Comparison between fibroblast wound healing and cell random migration assays in vitro. *Exp. Cell Res.* **347,** 123–132 (2016).

244. Petrie, R. J., Gavara, N., Chadwick, R. S. & Yamada, K. M. Nonpolarized signaling reveals two distinct modes of 3D cell migration. *J. Cell Biol.* **197,** 439–455 (2012).

245. Hamilton, D. W. & Brunette, D. M. 'Gap guidance' of fibroblasts and epithelial cells by discontinuous edged surfaces. *Exp. Cell Res.* **309,** 429–437 (2005).

246. Clark, P., Connolly, P., Curtis, a S., Dow, J. a & Wilkinson, C. D. Topographical control of cell behaviour. I. Simple step cues. *Development* **99,** 439–48 (1987).

247. Uttayarat, P., Toworfe, G. K., Dietrich, F., Lelkes, P. I. & Composto, R. J. Topographic guidance of endothelial cells on silicone surfaces with micro- to nanogrooves: Orientation of actin filaments and focal adhesions. *J. Biomed. Mater. Res. Part A* **75A,** 668–680 (2005).

248. Tinevez, J.-Y. *et al.* TrackMate: An open and extensible platform for single-particle tracking. *Methods* **115,** 80–90 (2017).

249. Lee, J., Abdeen, A. A., Zhang, D. & Kilian, K. A. Directing stem cell fate on hydrogel substrates by controlling cell geometry, matrix mechanics and adhesion ligand composition. *Biomaterials* **34,** 8140–8148 (2013).

250. Dalby, M. J., Gadegaard, N. & Oreffo, R. O. C. Harnessing nanotopography and integrin-matrix interactions to influence stem cell fate. *Nat. Mater.* **13,** 558–69

(2014).

251. Khetan, S. *et al.* Degradation-mediated cellular traction directs stem cell fate in covalently crosslinked three-dimensional hydrogels. *Nat. Mater.* **12,** 458–65 (2013).

252. Poh, Y.-C. *et al.* Generation of organized germ layers from a single mouse embryonic stem cell. *Nat. Commun.* **5,** 4000 (2014).

253. Dalby, M. J., Gadegaard, N. & Oreffo, R. O. C. Harnessing nanotopography and integrin-matrix interactions to influence stem cell fate. *Nat. Mater.* **13,** 558–69 (2014).

254. Soncin, F. & Ward, C. M. The function of E-cadherin in stem cell pluripotency and self-renewal. *Genes (Basel).* **2,** 229–259 (2011).

255. Li, L., Bennett, S. A. L. & Wang, L. Role of E-cadherin and other cell adhesion molecules in survival and differentiation of human pluripotent stem cells. *Cell Adh. Migr.* **6,** 59–70 (2012).

256. Kim, Y.-S., Yi, B.-R., Kim, N.-H. & Choi, K.-C. Role of the epithelial-mesenchymal transition and its effects on embryonic stem cells. *Exp. Mol. Med.* **46,** 1–5 (2014).

257. Redmer, T. *et al.* E-cadherin is crucial for embryonic stem cell pluripotency and can replace OCT4 during somatic cell reprogramming. *EMBO Rep.* **12,** 720–6 (2011).

258. Chou, L., Firth, J. D., Uitto, V. J. & Brunette, D. M. Substratum surface topography alters cell shape and regulates fibronectin mRNA level, mRNA stability, secretion and assembly in human fibroblasts. *J. Cell Sci.* **108 (Pt 4,** 1563–73 (1995).

259. Miller, C. J. & Davidson, L. A. The interplay between cell signalling and mechanics in developmental processes. *Nat. Rev. Genet.* **14,** 733–744 (2013).

260. Fernandez-Gonzalez, R. & Zallen, J. A. Cell mechanics and feedback regulation of actomyosin networks. *Sci. Signal.* **2,** pe78 (2009).

261. de Rooij, J. Cadherin adhesion controlled by cortical actin dynamics. *Nat. Cell Biol.* **16,** 508–510 (2014).

262. Engl, W., Arasi, B., Yap, L. L., Thiery, J. P. & Viasnoff, V. Actin dynamics modulate mechanosensitive immobilization of E-cadherin at adherens junctions. *Nat. Cell Biol.* **16,** 587–594 (2014).

263. Hwang, Y.-S. *et al.* Microwell-mediated control of embryoid body size regulates embryonic stem cell fate via differential expression of WNT5a and WNT11. *Proc. Natl. Acad. Sci. U. S. A.* **106,** 16978–83 (2009).

264. Discher, D. E., Mooney, D. J. & Zandstra, P. W. Growth factors, matrices, and forces combine and control stem cells. *Science (80-.).* **324,** 1673–1677 (2009).

265. Leclerc, A. *et al.* Three dimensional spatial separation of cells in response to microtopography. *Biomaterials* **34,** 8097–8104 (2013).

266. Mammoto, T., Mammoto, A. & Ingber, D. E. Mechanobiology and Developmental Control. *http://dx.doi.org/10.1146/annurev-cellbio-101512-122340* (2013).

267. Strzyz, P. Cell adhesion: SUMO controls a tug of war at junctions. *Nat. Rev. Mol. Cell Biol.* **16,** 641–641 (2015).

268. Leckband, D. E. & Rooij, J. de. Cadherin Adhesion and Mechanotransduction. *http://dx.doi.org/10.1146/annurev-cellbio-100913-013212* (2014).

269. Gardel, M. L., Schneider, I. C., Aratyn-Schaus, Y. & Waterman, C. M. Mechanical integration of actin and adhesion dynamics in cell migration. *Annu. Rev. Cell Dev. Biol.* **26,** 315–33 (2010).

270. Gupton, S. L., Eisenmann, K., Alberts, A. S. & Waterman-Storer, C. M. mDia2

regulates actin and focal adhesion dynamics and organization in the lamella for efficient epithelial cell migration. *J. Cell Sci.* **120,** 3475–87 (2007).

271. Yang, Y., Kulangara, K., Lam, R. T. S., Dharmawan, R. & Leong, K. W. Effects of topographical and mechanical property alterations induced by oxygen plasma modification on stem cell behavior. *ACS Nano* **6,** 8591–8 (2012).

272. Guilak, F. *et al.* Control of stem cell fate by physical interactions with the extracellular matrix. *Cell Stem Cell* **5,** 17–26 (2009).

273. Kim, D.-H., Provenzano, P. P., Smith, C. L. & Levchenko, A. Matrix nanotopography as a regulator of cell function. *J. Cell Biol.* **197,** 351–60 (2012).

274. Oda, H. & Takeichi, M. Evolution: structural and functional diversity of cadherin at the adherens junction. *J. Cell Biol.* **193,** 1137–46 (2011).

275. Li, L., Bennett, S. A. L. & Wang, L. © 2012 Landes Bioscience . Do not distribute . Do not distribute . 59–70 (2012).

276. Borghi, N. *et al.* E-cadherin is under constitutive actomyosin-generated tension that is increased at cell-cell contacts upon externally applied stretch. *Proc. Natl. Acad. Sci. U. S. A.* **109,** 12568–73 (2012).

277. D'Amour, K. a *et al.* Efficient differentiation of human embryonic stem cells to definitive endoderm. *Nat. Biotechnol.* **23,** 1534–41 (2005).

278. Eastham, A. M. *et al.* Epithelial-mesenchymal transition events during human embryonic stem cell differentiation. *Cancer Res.* **67,** 11254–62 (2007).

279. Li, D. *et al.* Integrated biochemical and mechanical signals regulate multifaceted human embryonic stem cell functions. *J. Cell Biol.* **191,** 631–644 (2010).

280. Stricker, J., Beckham, Y., Davidson, M. W. & Gardel, M. L. Myosin II-mediated focal adhesion maturation is tension insensitive. *PLoS One* **8,** e70652 (2013).

281. Li, F. & Higgs, H. N. The mouse formin mDia1 is a potent actin nucleation factor regulated by autoinhibition. *Curr. Biol.* **13,** 1335–1340 (2003).

282. Maekawa, M. *et al.* Signaling from Rho to the actin cytoskeleton through protein kinases ROCK and LIM-kinase. *Science* **285,** 895–898 (1999).

283. Chaudhary, A., Brugge, J. S. & Cooper, J. A. Direct phosphorylation of focal adhesion kinase by c-Src: Evidence using a modified nucleotide pocket kinase and ATP analog. *Biochem. Biophys. Res. Commun.* **294,** 293–300 (2002).

284. Beloussov, L. V, Luchinskaya, N. N., Ermakov, A. S. & Glagoleva, N. S. Gastrulation in amphibian embryos, regarded as a succession of biomechanical feedback events. *Int. J. Dev. Biol.* **50,** 113–22 (2006).

285. Beloussov, L. V. Mechano-geometric generative rules of morphogenesis. *Biol. Bull.* **39,** 119–126 (2012).

286. Beloussov, L. V. Integrating self-organization theory into an advanced course on morphogenesis at Moscow State University. *International Journal of Developmental Biology* **47,** 177–181 (2003).

287. Wang, J. H.-C. & Thampatty, B. P. Mechanobiology of adult and stem cells. *Int. Rev. Cell Mol. Biol.* **271,** 301–46 (2008).

288. Dard, N., Louvet-Vallée, S., Santa-Maria, A. & Maro, B. Phosphorylation of ezrin on threonine T567 plays a crucial role during compaction in the mouse early embryo. *Dev. Biol.* **271,** 87–97 (2004).

289. Eckert, J. J. *et al.* Specific PKC isoforms regulate blastocoel formation during mouse preimplantation development preimplantation development. *Peptides* **274,** 384–401 (2004).

290. Fleming, T. P., McConnell, J., Johnson, M. H. & Stevenson, B. R. Development of

tight junctions de novo in the mouse early embryo: control of assembly of the tight junction-specific protein, ZO-1. *J. Cell Biol.* **108,** 1407–18 (1989).

291. Guilak, F. *et al.* Control of stem cell fate by physical interactions with the extracellular matrix. *Cell Stem Cell* **5,** 17–26 (2009).

292. Plusa, B. *et al.* Downregulation of Par3 and aPKC function directs cells towards the ICM in the preimplantation mouse embryo. *J. Cell Sci.* **118,** 505–515 (2005).

293. Chowdhury, F. *et al.* Material properties of the cell dictate stress-induced spreading and differentiation in embryonic stem cells. *Nat. Mater.* **9,** 82–88 (2010).

294. Arulmoli, J. *et al.* Static stretch affects neural stem cell differentiation in an extracellular matrix-dependent manner. *Sci. Rep.* **5,** 8499 (2015).

295. Irimia, D. & Toner, M. Spontaneous migration of cancer cells under conditions of mechanical confinement. *Integr. Biol. (Camb).* **1,** 506–12 (2009).

296. Doetschman, T. C., Eistetter, H., Katz, M., Schmidt, W. & Kemler, R. The in vitro development of blastocyst-derived embryonic stem cell lines: formation of visceral yolk sac, blood islands and myocardium. *J. Embryol. Exp. Morphol.* **87,** 27–45 (1985).

297. Mohamet, L., Lea, M. L. & Ward, C. M. Abrogation of E-cadherin-mediated cellular aggregation allows proliferation of pluripotent mouse embryonic stem cells in shake flask bioreactors. *PLoS One* **5,** e12921 (2010).

298. McCloy, R. A. *et al.* Partial inhibition of Cdk1 in G2 phase overrides the SAC and decouples mitotic events. *Cell Cycle* **13,** 1400–1412 (2014).

299. Schneider, C. a, Rasband, W. S. & Eliceiri, K. W. NIH Image to ImageJ: 25 years of image analysis. *Nat. Methods* **9,** 671–675 (2012).

300. Lewiner, T., Lopes, H., Vieira, A. W. & Tavares, G. Efficient Implementation of Marching Cubes' Cases with Topological Guarantees. *J. Graph. Tools* **8,** 1–15 (2003).

301. Slater, G. W. *et al.* Modeling the separation of macromolecules: a review of current computer simulation methods. *Electrophoresis* **30,** 792–818 (2009).

302. Limbach, H. J., Arnold, A., Mann, B. A. & Holm, C. ESPResSo—an extensible simulation package for research on soft matter systems. *Comput. Phys. Commun.* **174,** 704–727 (2006).

303. Humphrey, W., Dalke, A. & Schulten, K. VMD: Visual molecular dynamics. *J. Mol. Graph.* **14,** 33–38 (1996).

304. Tamiello, C., Buskermolen, A. B. C., Baaijens, F. P. T., Broers, J. L. V & Bouten, C. V. C. Heading in the Right Direction: Understanding Cellular Orientation Responses to Complex Biophysical Environments. *Cell. Mol. Bioeng.* **9,** 12–37 (2016).

305. Nikkhah, M., Edalat, F., Manoucheri, S. & Khademhosseini, A. Engineering microscale topographies to control the cell-substrate interface. *Biomaterials* **33,** 5230–5246 (2012).